AN ABSTRACT OF THE THESIS OF

TEDD LYNCH WRIGHT (Name of Student) for the degree of MASTER OF SCIENCE (Degree)

in OCEANOGRAPHY presented on 29 April 1976 (Date)

Title: A DESCRIPTION OF THE COASTAL UPWELLING REGION OFF OREGON DURING JULY - AUGUST 1973

Abstract approved: Redacted for Privacy
Dr. Robert L. Smith

Observations of the winds, sea level, currents, and hydrography off the Oregon coast during July and August, 1973, are described. For frequencies less than 0.6 cycles per day two time scales are identified: a "seasonal" time scale of several months and an "event" time scale of several days.

On the seasonal time scale wind stress is predominantly southeastward. Alongshore currents are geostrophic and baroclinic, with an equatorward surface current ($\simeq$ 20 cm sec^{-1}) and a poleward undercurrent ($\simeq$ 5 cm sec^{-1}). Onshore-offshore currents are largely onshore in the interior region and offshore in the upper 15 to 20 m. Mean vertical velocities on the order of 10^{-3} to 10^{-2} cm sec^{-1} are estimated for the nearshore region. The hydrographic regime is greatly influenced by the upwelling of cold, high salinity subsurface water and the presence of the relatively fresh Columbia River plume in the surface layer. Surfaces of constant temperature, salinity, and density slope upward toward the coast.

On the event time scale, highly correlated, barotropic fluctuations occur in the winds, sea level, and currents. Unidirectional

fluctuations of the wind stress with maxima of about 2 dynes cm^{-2} occur and generate "upwelling events" during periods of strong southward wind. The vertical shear in the alongshore component of the velocity persists and is relatively constant despite the variations in the currents. A reversal of the undercurrent is sometimes observed during events. The greatest changes in the hydrographic regime occur in the surface layer ($\simeq$ upper 20 m), the nearshore region ($\simeq$ innermost 20 km), and along the bottom. During events plume water is advected offshore, nearshore isopycnals rise to intersect the surface; after events a warm temperature inversion often occurs at the base of the permanent pycnocline (delineated by the 25.5 to 26.0 σ_t isopycnals).

A Description of the Coastal Upwelling Region off Oregon During July - August 1973

by

Tedd Lynch Wright

A THESIS

submitted to

Oregon State University

in partial fulfillment of
the requirements for the
degree of

Master of Science

June 1976

APPROVED:

Redacted for Privacy

Professor of Oceanography
in charge of major

Redacted for Privacy

Dean of School of Oceanography

Redacted for Privacy

Dean of Graduate School

Date thesis is presented 29 April 1976
(Date of Examination)

Typed by Karie Jean Tamura for Tedd Lynch Wright

ACKNOWLEDGMENTS

I would like to thank all those associated with the CUEA group who contributed to this thesis by helping to obtain and process the data. In particular, I would like to thank Drs. Eric D. Barton and Robert L. Smith for their supervisory assistance in the preparation of this thesis.

Special thanks are extended to Ms. Karie Tamura for typing and editorial assistance, and to Mr. William E. Gilbert for drafting some of the figures and patiently explaining how to perform much of the necessary computer processing.

Financial support for CUE-II and my graduate studies was provided by the Office for the International Decade of Ocean Exploration, National Science Foundation.

TABLE OF CONTENTS

LIST OF TABLES

LIST OF FIGURES

LIST OF FIGURES (CONTINUED)

A DESCRIPTION OF THE COASTAL UPWELLING REGION OFF OREGON DURING JULY - AUGUST 1973

I. INTRODUCTION

During recent years, upwelling has received considerable study, not only off Oregon but in other upwelling regions of the world as well. The reason for this interest is the importance of upwelling in influencing and altering oceanic and atmospheric conditions which affect the ecosystem.

In an extensive review of the subject, Smith (1968) has defined upwelling as "an ascending motion, of some minimum duration and extent, by which water from subsurface layers is brought into the surface layer and is removed from the area of upwelling by horizontal flow". The biological importance of this is that nutrients, which are generally limiting in the euphotic zone of the oceans, are brought to the surface where they may be utilized in increasing oceanic productivity.

Upwelling off the Oregon coast is seasonal in nature, occurring in a narrow coastal belt much less than 100 kilometers wide during the summer months from April to September, when the dominating North Pacific atmospheric high pressure system causes predominantly southward winds along the coast. According to the Ekman-Sverdrup model (Smith, 1968), coastal upwelling is caused by the action of the southward wind stress on the sea surface and the rotation of the earth, which result in an offshore transport in the surface layer; this 'Ekman' transport creates a divergence in the surface layer at the coast, and mass continuity then requires that water from subsurface layers be upwelled into the nearshore surface region.

Off Oregon, where the water temperature generally decreases with depth and the salinity increases with depth, the effects of upwelling are seen in the existence of colder, more saline, and hence, denser water inshore at the surface. This is a manifestation of the upward slope toward the coast of surfaces of constant temperature and salinity (as well as other physical and chemical parameters) as a result of upwelling. The characteristic pattern of these 'isoplanes' serves as a useful indicator of upwelling (Park, Pattullo and Wyatt, 1962).

A comprehensive overview of the coastal upwelling region off Oregon prior to 1972 has been given by Pillsbury (1972). During the upwelling season the permanent pycnocline (delineated by the 25.5 to 26.0 σ_t isopycnals) rises toward the coast from a depth of about 100 to 150 meters at 200 kilometers offshore, often intersecting the sea surface during intense upwelling and forming a front some five to ten kilometers from the coast (Collins, 1964). In addition, a seasonal pycnocline (24.5 to 25.0 σ_t isopycnals), which is probably due to summer heating and the presence at the surface of Columbia River plume water advected southward during summer, exists above the permanent pycnocline. Temperature inversions have been frequently observed in the vertical hydrographic structure during upwelling with anomalously warm water being found near the base of the permanent pycnocline (Pak, Beardsley and Smith, 1970; Mooers, Collins and Smith, 1976). The mean north-south (approximately alongshore) velocity field exhibits a baroclinic structure over the continental shelf and upper slope with a southward surface current ($\simeq$ 20 cm sec^{-1}) and a northward undercurrent ($\simeq$ 10 cm sec^{-1}), the region of high velocity shear coinciding with the frontal zone

(i.e., the region influenced by the permanent pycnocline). The mean east-west (approximately onshore-offshore) velocity field exhibits weak onshore flow over the shelf below an offshore surface transport extending down to a depth of about 20 meters (Collins et al., 1968; Collins and Pattullo, 1970; Mooers, Collins and Smith, 1976). Vertical velocities, estimated by Smith, Pattullo and Lane (1966) from displacement of isopycnals, varied from 7×10^{-3} cm sec^{-1} nearshore to 2×10^{-4} cm sec^{-1} further offshore.

On the basis of the above characteristics, Mooers, Collins and Smith (1976) developed a conceptual model of upwelling off Oregon. The model hypothesizes the formation of a local water mass in the nearshore surface layer by solar heating and wave/wind-induced mixing of recently upwelled water. As this water is moved offshore by the action of wind stress and Coriolis force, it encounters warmer, less saline surface waters and begins to sink along the base of the permanent pycnocline. This tongue of sinking water is characterized by the temperature inversion which, as it extends offshore, is gradually broadened and dissipated by diffusion and mixing caused by dynamic instabilities in the frontal zone region. The horizontal density gradient across the inclined permanent pycnocline is related by the thermal-wind relationship to the vertical shear of the alongshore currents, which implies that the alongshore currents are essentially in geostrophic equilibrium. This model is schematically represented in Figure 1. (It is interesting to note that Sverdrup (1938), in an early model of coastal upwelling, argues for a similar onshore-offshore circulation pattern, where the

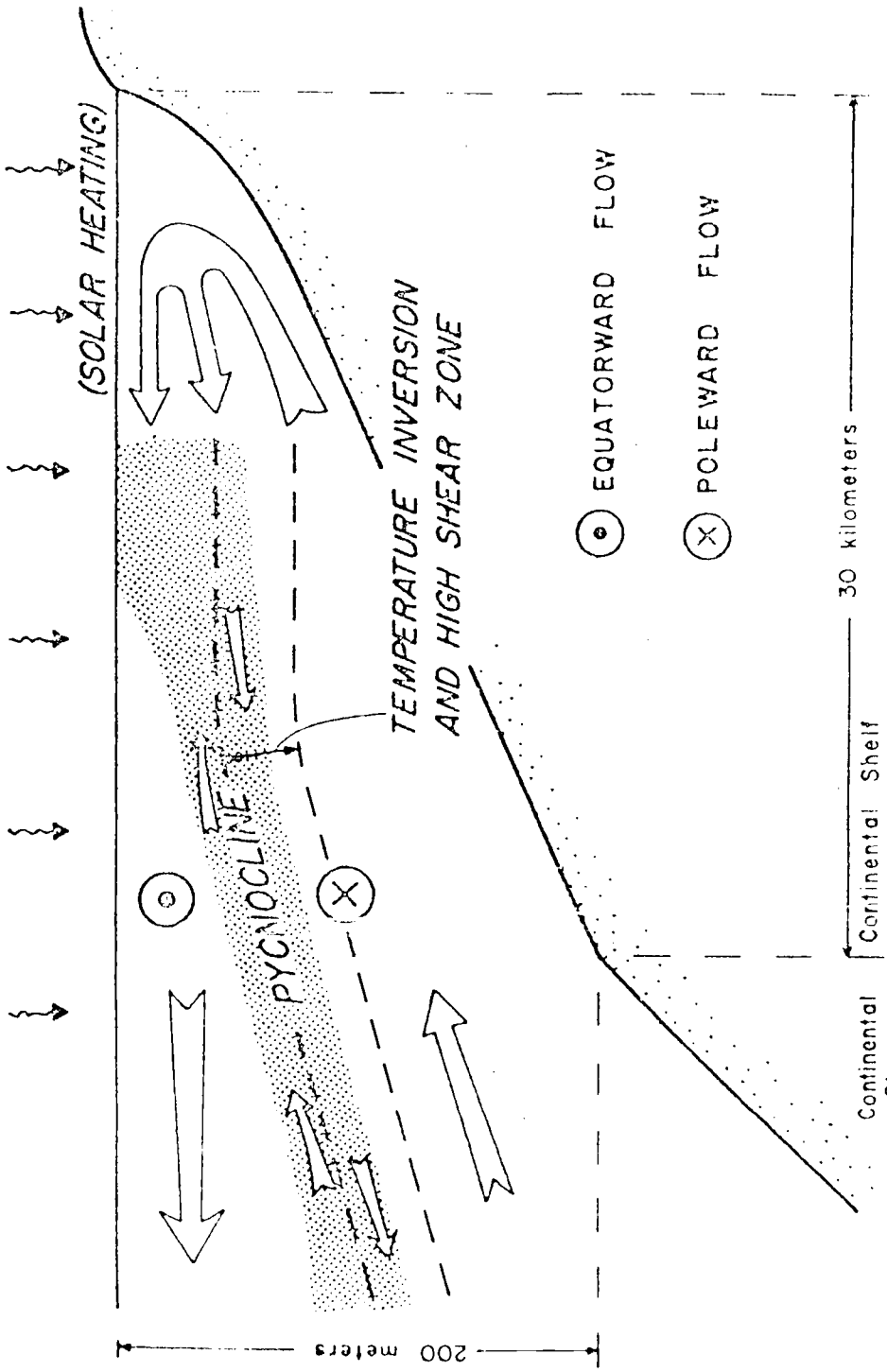

Figure 1. A schematic representation of a conceptual model for the Oregon coastal upwelling region (from Smith, Mooers and Enfield, 1971).

sinking at the base of the permanent pycnocline is due to a convergence at the sea-surface front. The convergence is caused by the high velocity shearing stress near the surface partly balancing the wind stress and thus reducing the Ekman transport offshore in the frontal region.) Although analytical and numerical simulation models, as summarized by O'Brien (1975) and Mooers and Allen (1973), have been only partially successful in representing the main features of the Mooers-Collins-Smith conceptual model, Thompson (1974), by including thermodynamics, has been successful in modelling the hypothesized alongshore and onshore-offshore circulation.

During the 1972 upwelling season, a multi-institutional field study was conducted off the central Oregon coast as an initial phase of the Coastal Upwelling Ecosystems Analysis (CUEA) program sponsored by the National Science Foundation Office for the International Decade of Ocean Exploration (IDOE). Called the Coastal Upwelling Experiment (CUE-I), this study was the largest and most extensive study of an upwelling region to that time. Among the objectives of CUE-I were to obtain a mesoscale description of the region, further refine the conceptual models, and provide a basis for the development of numerical models of coastal upwelling. An overview of the observations from CUE-I and a comparison with conceptual models has been given by Huyer (1974).

From observations made during CUE-I, Smith (1974) and Huyer, Smith and Pillsbury (1974) have studied the low-frequency variations in the currents and their relationship to the winds, sea level and hydrography. Cutchin and Smith (1973) and Huyer et al. (1975) have related alongshore coherence at low frequencies in currents and sea

level to the existence of continental shelf waves. Variations in the density field have been examined by Halpern (1974), and evidence for the existence of a subsurface ribbon of cool water over the continental shelf has been presented by Huyer and Smith (1974). From these and other analyses the following features of the Oregon upwelling region have emerged:

1. The vertical shear observed in the alongshore flow is consistent with the calculated geostrophic shear which should accompany the upward sloping isopycnals in accordance with the thermal-wind relation.

2. The persistence of a relatively constant velocity shear, despite major variations in the alongshore currents, indicates that low-frequency fluctuations in the currents (with a time scale of several days to a week) are largely barotropic.

3. Off Oregon, where reversals in the winds are common during the upwelling season, so-called 'upwelling events' occur when southward winds resume following periods of northward winds; the barotropic impulse imparted to the currents can cause a reversal in the northward undercurrent.

4. Fluctuations in the currents, wind and sea level exhibit high mutual coherence at low-frequencies and suggest the existence of continental shelf waves.

5. Topography, three-dimensional effects due to advection, and instabilities due to the large vertical current shears also appear to affect the currents and hydrography.

6. The greatest variations in the hydrographic regime are in the surface layer, the nearshore region, and along the bottom.

7. A subsurface ribbon of cool water, attributed to a southward advection of subarctic water by the coastal jet associated with upwelling, exists over the continental shelf.

8. Maximum vertical velocities are on the order of 10^{-2} cm sec^{-1}.

The CUE-I field study was repeated off Oregon during the summer of 1973, with certain modifications. Since the alongshore currents in the CUE-I study appeared to be influenced by underwater topographic features (Huyer, Smith and Pillsbury, 1974; Kundu and Allen, 1976), the 1973 Coastal Upwelling Experiment (CUE-II) study was moved north to take advantage of the simpler shelf topography found there. Currents and winds were measured from an array of eight subsurface current meter buoy moorings (four of which had surface meteorological buoys) and three additional surface meteorological buoys. Repeated hydrographic sampling and other physical, chemical, and biological research were conducted from four oceanographic research vessels: Oregon State University's R/V YAQUINA and R/V CAYUSE, the National Oceanic and Atmospheric Administration's OSS OCEANOGRAPHER, and the University of Washington's R/V THOMAS G. THOMPSON. Meteorological and sea-level measurements were made at various shore stations, and meteorological and sea surface temperature observations were measured from aircraft overflights of the upwelling region. A partial listing of the physical oceanographic observations made during CUE-II is given in Table I.

The primary objective of this thesis is to present a mesoscale descriptive overview of the Oregon coastal upwelling region during

Table I. Physical oceanographic observations during CUE-II, 1973.

Type of Observation	Institution	Reference
Summary of Data Listings		Pillsbury and O'Brien, 1973
Hydrography	OSU	Huyer and Gilbert, 1974
	PMEL	Holbrook and Halpern, 1974
	UM	Curtin, Johnson and Mooers, 1975
Surface Hydrographic Fields and Sea-surface Temperatures	UM	Curtin and Mooers, 1974
	FSU/OSU	O'Brien, Woodworth and Wright, 1974
Moored Current Meters and Wind Recorders	OSU	Pillsbury, Bottero, Still and Gilbert, 1974(b)
	PMEL	Halpern, Holbrook and Reynolds, 1974
Profiling Current Meters	UM	Curtin and Mooers, 1975
Cyclesonde Studies	UM	Van Leer, 1974
Drogues	IATTC	
Radiation	PMEL	Reed and Halpern, 1974
Meteorology	FSU	
Theoretical Workshop		Mooers and Allen, 1973

Acronyms for institutions are: OSU - Oregon State University; PMEL - Pacific Marine Environmental Laboratory, National Oceanic and Atmospheric Administration; UM - University of Miami; FSU - Florida State University; IATTC - Inter-American Tropical Tuna Commission.

July and August, 1973. Only observations of the winds, sea level, currents, and hydrography made by the Oregon State University School of Oceanography are considered. Estimates of the wind stress and vertical velocity are made, and hypotheses concerning alongshore geostrophy and onshore-offshore mass transport balance are tested.

II. OBSERVATIONS AND RESULTS

Observations made by Oregon State University as part of the 1973 Coastal Upwelling Experiment (CUE-II) include wind, sea level, and atmospheric pressure measurements at Newport, Oregon, direct current and wind measurements from an array of moored buoys over the continental shelf and upper slope, and a series of hydrographic stations from the R/V YAQUINA. The region of study is shown in Figure 2. (The 1972 CUE-I region, in comparison, extended from about 44°35'N to 45°N.)

Wind speed and direction were measured continuously from the south jetty at Newport and hourly time series were obtained by averaging over a 20-minute interval centered at the hour. Sea level was recorded every six minutes by a tide gauge at Newport and the series decimated to hourly values, i.e., observations between hourly data points were deleted. An hourly series of atmospheric pressure at Newport was also recorded.

Currents were measured from five subsurface moorings extending offshore at about 45°16.5'N latitude and three additional moorings to the north and south; winds were recorded from seven surface meteorological buoys (Figure 2). The mooring system is described by Pillsbury, Smith and Tipper (1969). Each subsurface mooring consisted of Aanderaa recording current meters at fixed depths which measured water temperature, current speed, current direction, and for some meters conductivity and pressure, usually at 10-minute intervals. The surface meteorological buoys measured air and water temperature, wind speed, and wind direction at 10-minute intervals. The depths and record

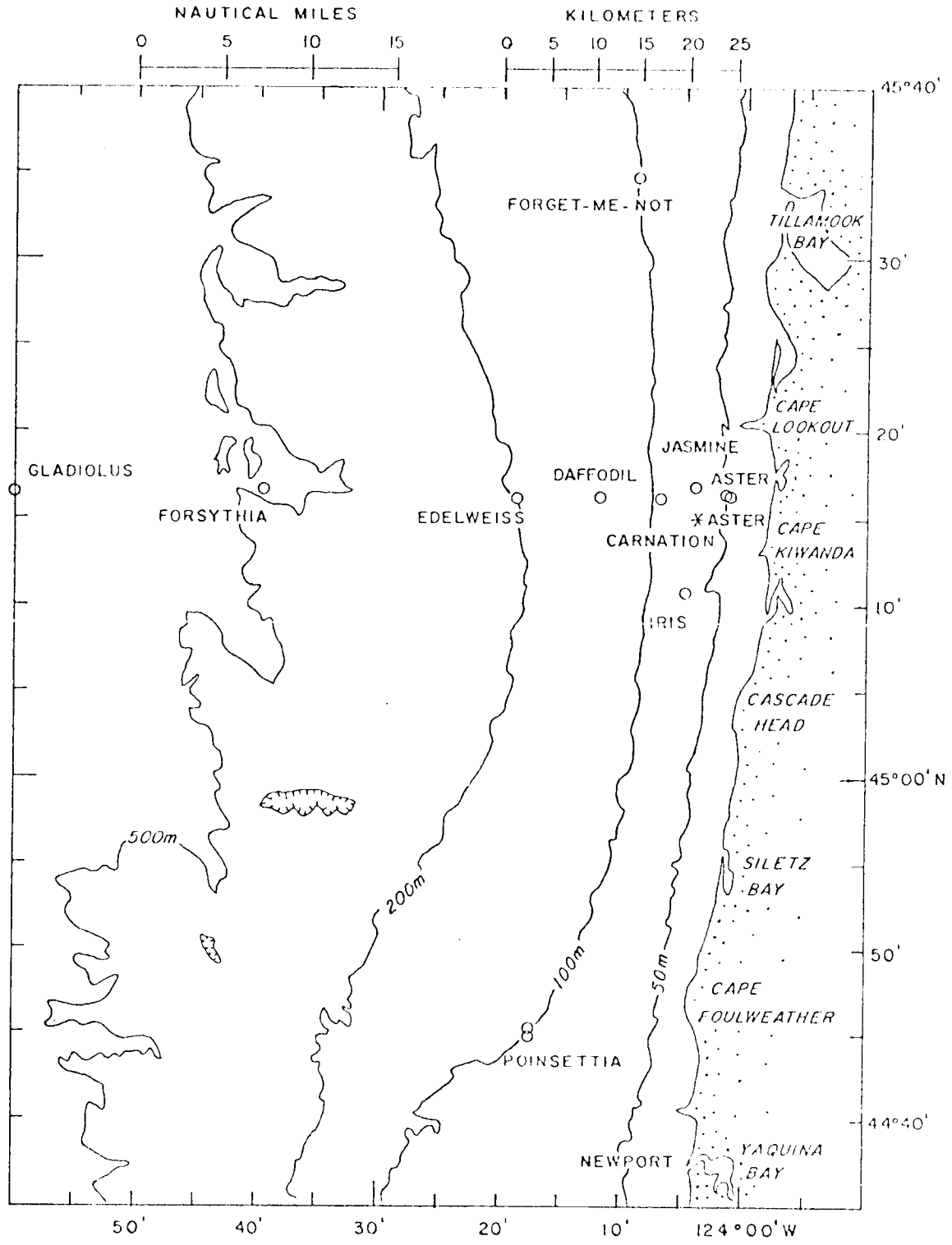

Figure 2. The Oregon upwelling region of study during CUE-II, with bottom contours and the locations of moored instruments shown.

lengths of the current meters and wind recorders are shown in Figure 3. The series thus obtained were filtered to produce hourly series; details of the current meter operations and data processing are given in Pillsbury et al. (1974a). Data from each current meter are described by means of first-order statistics, time series plots of hourly values, progressive vector diagrams, and rotary spectra in Pillsbury et al. (1974b). Table II summarizes the CUE-II O.S.U. current meter array information.

The hourly wind, sea level, atmospheric pressure, and current series were low-pass filtered using a symmetrical filter spanning 121 hours with a half-power point of 40 hours (0.6 cpd) to produce six-hourly records in which the tidal and inertial frequencies are suppressed. The sea level series was adjusted by removing the effect of atmospheric pressure on sea level (i.e., an increase in atmospheric pressure of one millibar decreases sea level by one centimeter). The resulting low-passed series for adjusted sea level and u (north-south) and v (east-west) vector components of the wind and current velocities are shown in Appendix I.

Hydrographic observations of the upwelling region were made during four cruises of the R/V YAQUINA (Table III). Since the objectives of these cruises were different, a uniform survey procedure was not possible; however, on occasions during each of the cruises one or more series of zonal lines of stations between 44°40'N and 45°30'N were sampled. The line occupied most frequently coincided with the current meter buoy line at 45°16.5'N. Although the station separation varied, it generally decreased inshore and was usually no greater than about

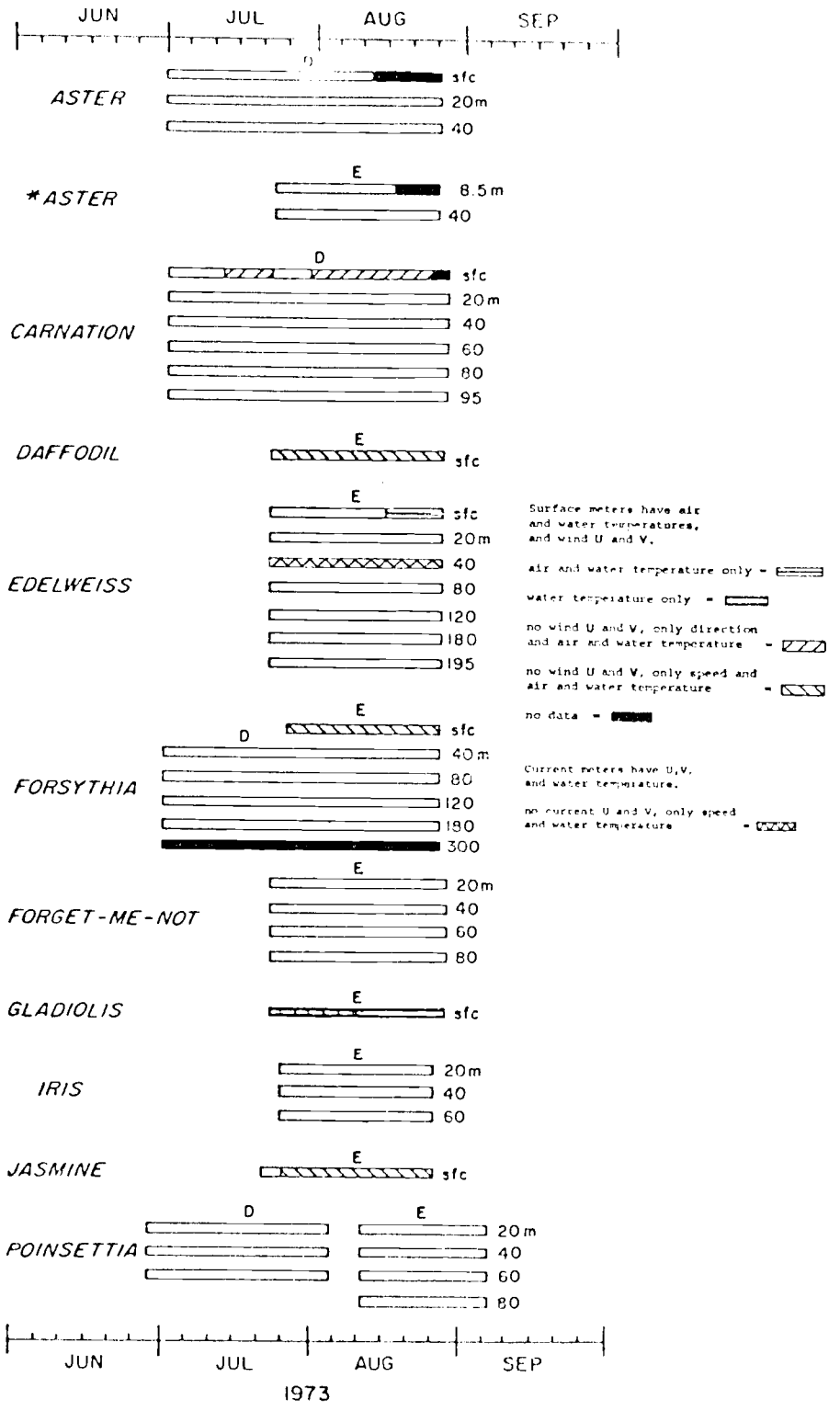

Figure 3. The depths and record lengths of data recovered from moored instruments during CUE-II (from Pillsbury et al., 1974b).

Table II. CUE-II current meter array information (from Pillsbury et al., 1974b).

Array Name	Lat. (°N)	Long. (°W)	Bottom Depth (m)	Current Meter Depths (m)[1]	Data Interval (1973)	Measurements[2]	Sampling Interval (min)
Aster	45°16.4	124°01.5	50	0(0.0)	30 Jun. - 12 Aug.	T, T_a, D, S	10
				20(21.8)	30 Jun. - 26 Aug.	T, D, S	10
				40(43.7)	30 Jun. - 26 Aug.	T, D, S, P	10
*Aster	45°16.4	124°01.4	50	8.5(8.8)	23 Jul. - 17 Aug.	T, D, S, C	5
				40(41.6)	23 Jul. - 26 Aug.	T, D, S, C, P	5
Carnation	45°16.2	124°06.9	100	0(0.0)	30 Jun. - 25 Aug.	T, T_a, D, S[6]	10
				20(20.2)	30 Jun. - 28 Aug.	T, D, S	10
				40(40.4)	30 Jun. - 28 Aug.	T, D, S	10
				60(60.6)	30 Jun. - 28 Aug.	T, D, S	10
				80(80.8)	30 Jun. - 28 Aug.	T, D, S	10
				95(95.9)	30 Jun. - 28 Aug.	T, D, S, P	10
Daffodil	45°16.2	124°11.9	140	0(0)	23 Jul. - 28 Aug.	T, T_a, D, S[3]	10
Edelweiss	45°16.2	124°18.7	200	0(0)	23 Jul. - 28 Aug.	T, T_a, D, S[7]	10
				20(19.3)	23 Jul. - 28 Aug.	T, D, S, C, P	10
				40(46.7)	23 Jul. - 28 Aug.	T, D, S, C, P[8]	10
				80(81.0)	23 Jul. - 28 Aug.	T, D, S	10
				120(121.1)	23 Jul. - 28 Aug.	T, D, S, C, P	10
				160(161.3)	23 Jul. - 28 Aug.	T, D, S	10
				195(196.3)	23 Jul. - 28 Aug.	T, D, S, P	10
Forsythia	45°16.8	124°39.6	500	0(0.0)	25 Jul. - 26 Aug.	T, T_a, D, S[3]	10
				40(44.0)	1 Jul. - 26 Aug.	T, D, S	10
				80(88.0)	1 Jul. - 26 Aug.	T, D, S, P	10
				120(127.0)	1 Jul. - 26 Aug.	T, D, S, P	10
				180(186.0)	1 Jul. - 26 Aug.	T, D, S	10
				300	1 Jul. - 26 Aug.	T, D, S[5]	10

Table II. Cont'd.

Array Name	Lat. (°N)	Long. (°W)	Bottom Depth (m)	Current Meter Depths (m)	Data Interval (1973)	Measurements	Sampling Interval (min)
Forget-Me-Not	45°34.9	124°08.9	100	20(21.0)	22 Jul. - 27 Aug.	T, D, S	10
				40(42.0)	22 Jul. - 27 Aug.	T, D, S	10
				60(63.0)	22 Jul. - 27 Aug.	T, D, S	10
				80(84.0)	22 Jul. - 27 Aug.	T, D, S, P	10
Gladiolus	45°16.6	125°00.0	1200	0(0)	24 Jul. - 26 Aug.	T, T_a, D, S[3,4]	10
Iris	45°10.8	124°04.9	75	20(20.1)	25 Jul. - 26 Aug.	T, D, S	10
				40(40.3)	25 Jul. - 26 Aug.	T, D, S	10
				60(60.4)	25 Jul. - 26 Aug.	T, D, S, P	10
Jasmine	45°16.9	124°04.0	70	0(0)	23 Jul. - 28 Aug.	T, T_a, D, S[3]	10
Poinsettia(D)	44°45.0	124°17.4	100	20(20)	28 Jun. - 4 Aug.	T, D, S	10
				40(40)	28 Jun. - 4 Aug.	T, D, S	10
				60(60)	28 Jun. - 4 Aug.	T, D, S	10
Poinsettia(E)	44°45.5	124°17.5	100	20(20.7)	11 Aug. - 6 Sep.	T, D, S	10
				40(41.4)	11 Aug. - 6 Sep.	T, D, S	10
				60(62.2)	11 Aug. - 6 Sep.	T, D, S	10
				80(82.9)	11 Aug. - 6 Sep.	T, D, S, P	10

Remarks:
1 - Intended depth (actual depth given in parentheses)
2 - Acronyms for measurements are: T - water temperature; T_a - air temperature; D - current/wind direction; S - current/wind speed; C - conductivity; P - pressure
3 - Buoy orientation sensor failed
4 - Air temperature sensor failed
5 - No readable data
6 - Speed not used
7 - Direction sensor failed 15 August; speed sensor failed 23 August
8 - Direction not used

Table III. Hydrographic cruises of the R/V YAQUINA during CUE-II, 1973.

Cruise	Dates	No. of Stations	Other Objectives
Y7306E	27 June - 1 July	47	Current Meter Moorings, Microstructure
Y7307A	9 - 14 July	138	Drogue Studies
Y7308A	16 - 20 August	72	Profiling Current Meter Studies
Y7308B	21 - 24 August	41	Microstructure

7.8 km inshore of 124°42'W. For purposes of comparison, stations at or near 124°00', 124°03', 124°06', 124°09', 124°12', 124°18', 124°24', 124°30', 124°36', 124°42', 124°48', 124°54', and 125°00'W (approximately 3, 6.9, 10.8, 14.7, 18.6, 26.5, 34.3, 42.1, 49.9, 57.7, 65.5, 73.4, and 81.2 km offshore at 45°16.5'N respectively) were used if possible.

At each station occupied the conductivity, temperature, and pressure were measured at depth intervals of about one to three meters using a Geodyne conductivity-temperature-depth (CTD) unit. Real-time values of the salinity and density were computed by an onboard computer interfaced with the CTD system. The sampling, calibration, and data processing procedures, along with depth profiles of temperature, salinity, and density and listings of temperature, salinity, density, specific volume anomaly, dynamic height anomaly, and potential energy at standard depths are given in Huyer and Gilbert (1974). Zonal sections of the vertical distributions of temperature, salinity, and density were contoured and are shown in Appendix II.

Quantities used in the description of the results are referred to a right-handed rectangular coordinate system (x,y,z) where x is positive eastward, y is positive northward, and z is positive upward. Since the coastline and local isobaths in the vicinity of the observations along 45°16.5'N are directed approximately north-south and the major fluctuations in the velocity field appear to be topographically-oriented (Kundu and Allen, 1976), the principal axes (i.e., the axes along which velocity fluctuations are extrema) are not significantly different from the x-y axes defined above (with the exception of the principal axes at

Edelweiss and Poinsettia where the local isobaths are not directed north-south; see Figure 2). Therefore, the velocity vector components (u,v,w) corresponding to the directions (x,y,z) represent approximately alongshore (alongisobath), onshore-offshore (transisobath), and vertical motions, respectively. Hereafter, alongshore and onshore-offshore shall be taken to be synonymous with north-south and east-west, respectively, unless otherwise noted. Table IV, reproduced from Kundu and Allen (1976), gives the mean and standard deviation of the u and v velocity components and the directions of the major principal axes.

With the exception of the current speeds obtained from the Star Aster mooring, results from the Aanderaa recording current meters appear to be reliable in most cases: an intercomparison between the Aanderaa and two other types of current meters in shallow water has yielded good agreement for frequencies less than 0.4 cycles per hour (Halpern, Pillsbury and Smith, 1974). In the case of Star Aster, the uppermost extension of the mooring is at 3 m depth and is therefore more subject to surface wave motion than are the uppermost extensions of other subsurface moorings at 17 m depth. Intercomparison between the 40 m Aanderaa meters at Star Aster and Aster, separated horizontally by only about 200 m, shows that the mean speeds at Star Aster and Aster are 21 and 13 cm sec^{-1}, respectively (Halpern and Pillsbury, 1976). The larger current speeds at Star Aster appear to be due to 'rotor pumping' of the Aanderaa meter by motion of the mooring cable resulting from surface wave action on the upper part of the mooring.

Table IV. Means, standard deviations, and principal axes for CUE-II currents (from Kundu and Allen, 1976).

Station		$\bar{u}$ cm/sec	$\bar{v}$ cm/sec	u_{SD} cm/sec	v_{SD} cm/sec	Major Principal Axis[1]
*Aster	8 m	-2.3	-2.6	5.2	16.5	- 4°
	40 m	0.8	-3.6	2.1	13.9	0°
Aster	20 m	6.0	-11.3	4.0	12.5	1°
	40 m	-0.6	-0.9	1.6	9.4	3°
Carnation	20 m	3.2	-23.9	4.7	10.0	1°
	40 m	4.3	-10.9	3.0	10.5	2°
	60 m	2.7	-2.0	2.9	11.7	1°
	80 m	1.1	2.9	2.0	10.7	4°
	95 m	0.6	2.5	1.7	8.4	6°
Edelweiss	20 m	2.4	-21.7	4.3	6.1	32°
	80 m	2.6	-4.6	2.3	5.5	11°
	120 m	2.0	2.5	1.9	5.4	2°
	180 m	-1.8	7.3	1.7	5.4	12°
	195 m	-1.7	5.5	2.4	4.9	22°
Iris	20 m	-0.3	-18.2	2.9	10.4	-5°
	40 m	1.9	-8.0	2.9	12.2	-8°
	60 m	0.2	-0.3	1.9	11.2	-7°
Forsythia	40 m	1.1	-12.6	2.4	4.0	24°
	80 m	0.2	-8.0	1.5	3.5	9°
	120 m	0.2	-4.3	1.3	3.3	3°
	180 m	0.7	-1.5	1.2	3.1	2°
Forget-me-not	20 m	2.7	-18.3	4.0	5.3	0°
	40 m	2.9	-11.4	3.2	4.5	25°
	60 m	1.5	-3.8	2.8	7.0	2°
	80 m	0.1	0.5	1.7	6.4	0°
Poinsettia	20 m	-8.4	-23.0	5.4	8.3	-26°
	40 m	-3.2	-13.3	4.9	9.2	-20°
	60 m	0.3	-7.3	5.1	8.6	-24°
	80 m	2.3	0.3	3.0	6.2	-14°

[1] measured counterclockwise from north

Wind and Sea Level

Low-passed time series ($f < 0.6$ cpd) of the near surface wind velocities at Newport (solid line), Aster (dotted line), and Edelweiss (dashed line) and the barometrically-adjusted sea level at Newport for the period of July - August 1973 are shown in Figure 4. (The series for the Newport winds and sea level for the longer period of 15 June - 15 September are given in Appendix I.) The high visual correlation in the alongshore (v-component) winds indicates that within the study area the alongshore wind field is fairly coherent over a north-south distance of at least 70 km and an east-west distance of at least 25 km. Little visual correlation exists in the onshore-offshore (u-component) winds except between Aster and Edelweiss; this is perhaps due to the damping effect of the Oregon coastal mountains on the Newport winds and the alongshore separation between Newport and the Aster-Edelweiss buoy locations.

Throughout the period of observation the winds exhibit numerous low-frequency velocity fluctuations. The alongshore winds appear to be predominantly weakly southward; however on several occasions strong southward winds (> 5 m sec^{-1}) lasting from several days to two weeks followed periods of northward winds. The most notable of these 'events' of strong southward wind occurred during 27 June - 2 July, 9 - 16 July, 22 July - 7 August and 14 - 15 August with maximum speeds of approximately 9, 12, 8, and 8 m sec^{-1} respectively. The onshore-offshore winds are predominantly weakly onshore and exhibit smaller fluctuations (< 5 m sec^{-1}) than the alongshore winds with the exception of strong

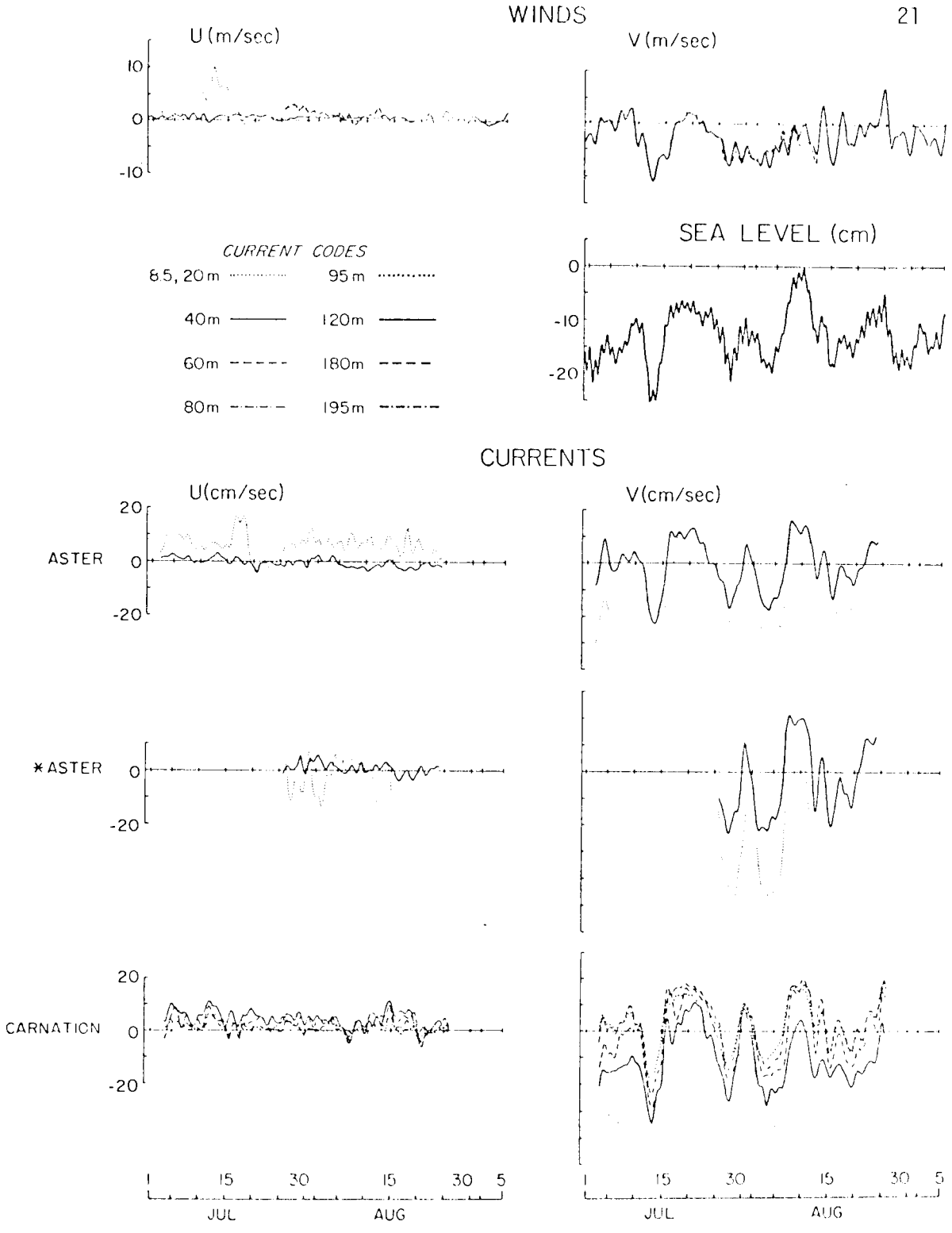

Figure 4. Low-passed (f < 0.6 cpd) time series of the winds, sea level, and currents during July - August, 1973.

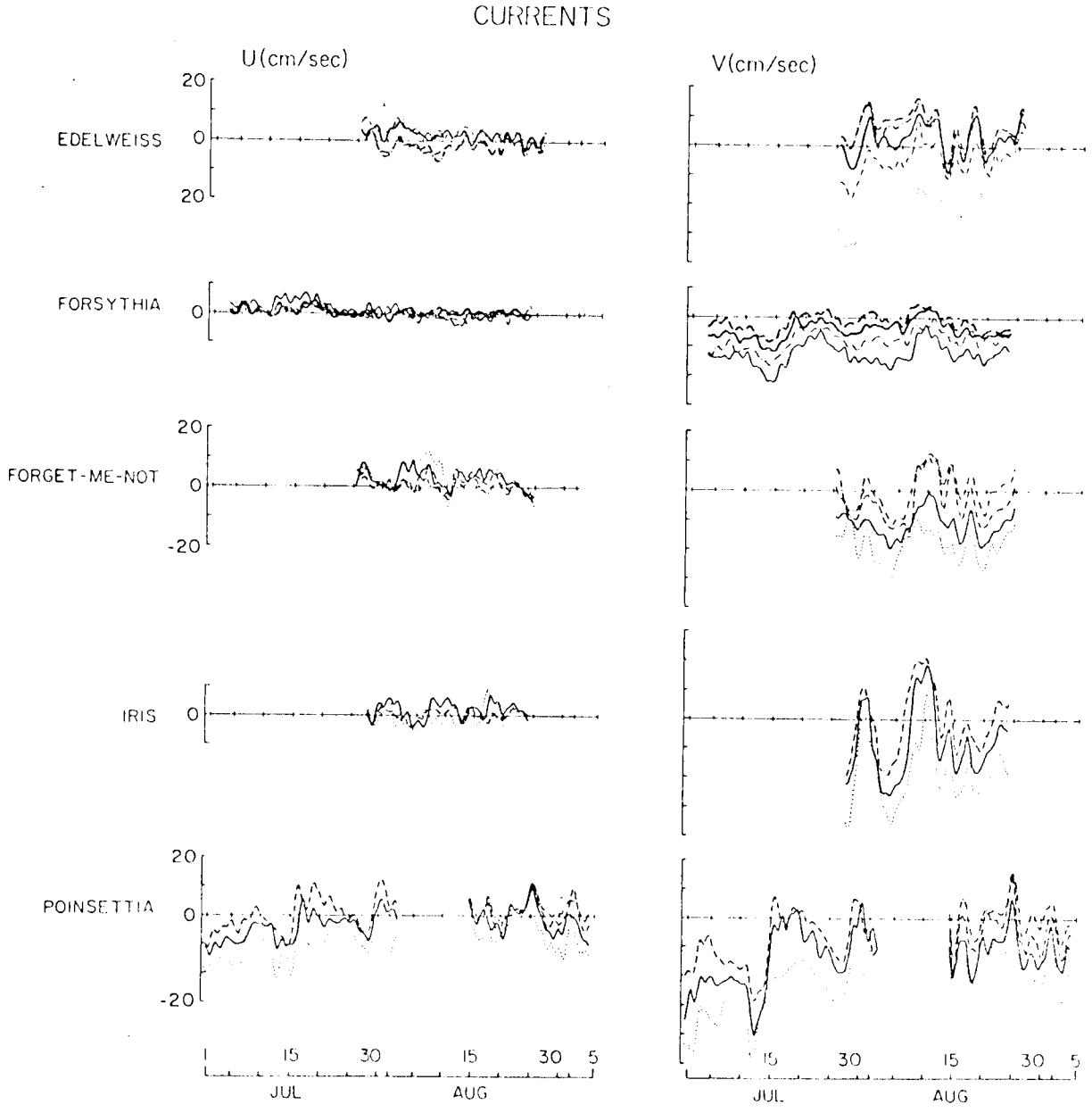

Figure 4. Cont'd.

onshore winds at Aster (maximum speed 10 m sec^{-1}) during the mid-July event and at Aster and Edelweiss (maximum speed 3 - 4 m sec^{-1}) during the late July - early August event. (The wind series for Aster began on 2 July; for Edelweiss on 25 July. The unusually large speeds at Aster during the mid-July event may be the result of instrument failure.) A similar increase in the onshore winds at Newport during the events is not apparent.

Sea level fluctuations appear to correlate with the alongshore wind fluctuations, the sea level lowering with increasing southward winds and rising with decreasing southward winds. There are some exceptions, however, most notably during the late July - early August event when the sea level rises again after lowering despite continued southward winds. During the period of observations (July - August) the sea level is predominantly lower than the yearly mean.

Currents

Low-passed time series ($f < 0.6$ cpd) of the current velocities during the CUE-II observational period are shown in Figure 4. A visual correlation of varying degree exists between the alongshore currents at different mooring locations, and between the alongshore currents and the alongshore winds and sea level. In general the correlation between currents and sea level appears better than between currents and winds. The shallower alongshore currents generally have a larger southward magnitude relative to the deeper currents, with the vertical shear in the alongshore velocity component decreasing with depth. The shear appears to remain relatively constant with time despite low-frequency

velocity fluctuations in the alongshore current; this implies that these low-frequency fluctuations are largely depth-independent or barotropic. The mean alongshore current velocity structure is baroclinic: the shallower currents usually flow southward and the deeper currents northward; however during 'events' the entire water column often moves southward. Regardless of the direction of flow, the alongshore currents at the deepest current meters at Carnation and Edelweiss, which are only about five meters from the bottom, are smaller in magnitude than are the currents observed at higher current meters; this is presumably caused by frictional effects of the bottom (Kundu, 1976).

The onshore-offshore current picture appears to be more complicated. Little visual correlation exists in the velocity fluctuations, which are smaller in magnitude than the velocity fluctuations in the alongshore current. The mean flow at most depths below 20 m is weakly onshore or nearly zero except at Poinsettia (referred to the principal axes system, however, the mean flow at Poinsettia is also onshore in the transisobath sense). The strongest onshore flow is usually at 20 - 40 m depth, with offshore flow sometimes found near the bottom; however, the vertical shear in the onshore-offshore velocity component appears to be significant only at Aster, Poinsettia (where the sense of the shear is reversed, i.e., shallower currents are offshore relative to deeper currents), and occasionally elsewhere, and does not seem to be constant with time. There is offshore flow at 20 m Carnation near the end of the mid-July event on the order of 10 cm sec^{-1}. The mean flow at the 8.5 m current meter at Star Aster is also offshore.

Temporal and spatial features of the currents along 45°16.5'N are shown in time series of the 40 m depth horizontal velocity distributions (Figure 5; values are linearly interpolated between Aster, Carnation, and Forsythia). The velocity field at 40 m depth consists of periods of relatively strong southward flow alternating with periods of northward or weak southward flow and periods of relatively strong onshore flow alternating with periods of offshore or weak onshore flow. Periods of southward flow greater than 20 cm sec^{-1} usually coincide with the wind 'events', and periods of offshore or weak onshore flow often occur near the end of the events.

In time vs. distance plots such as Figure 5, contours parallel to the distance axis imply that the current is independent of distance offshore and contours parallel to the time axis imply that the current is independent of time. From the orientation of the velocity contours in Figure 5, it appears that during events the alongshore flow (v) at 40 m is more time-dependent but independent of distance offshore, whereas between events it is more time-independent but distance-dependent, with the flow becoming relatively more northward in the onshore direction. Although less obviously, it appears that during events the onshore-offshore flow (u) at 40 m is relatively stationary and distance-dependent, whereas between events it is more transient and independent of distance offshore. These results imply that, in general, the stationary or mean features of the 40 m current field are dependent on distance offshore and consist of relatively weak southward or northward alongshore flow and relatively strong onshore flow. Associated with the intensification of the winds during events is a

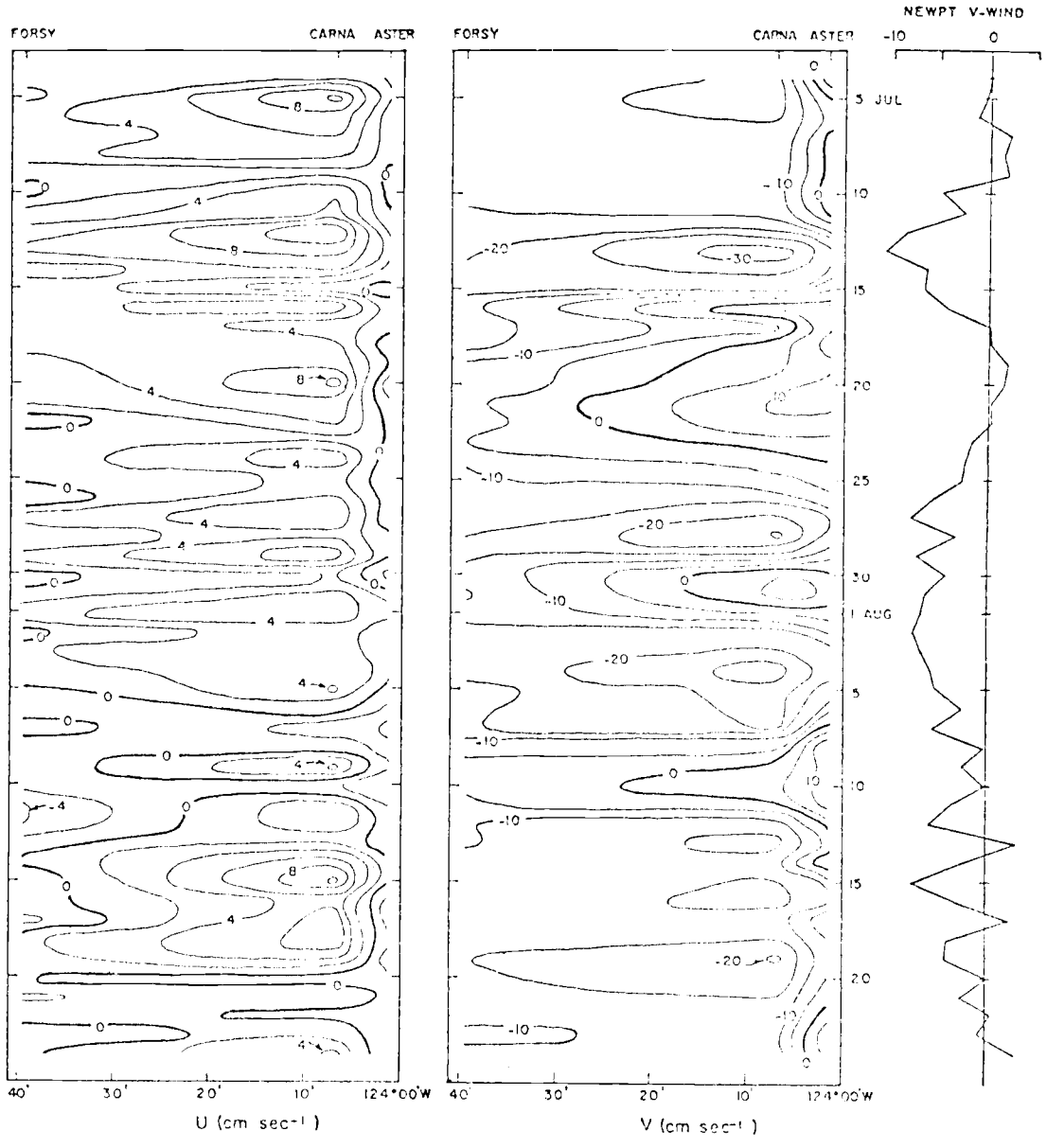

Figure 5. Time series of the zonal distribution of the 40 m depth horizontal velocity components along 45°16.5'N.

broad, transient increase in southward flow; and associated with the relaxation of the winds after events is a broad, transient decrease in onshore flow.

Zonal sections of the current velocity distributions with depth for the mean seasonal flow and during the events of mid-July and late July - early August are shown in Figure 6. Since the shallowest current meters were at 20 m the velocity distribution in the upper 20 m could not be determined. In addition, during the earlier event no values were available at Edelweiss and the contouring is somewhat subjective.

The mean v-velocity distribution shows southward flow in the upper layers (maximum of about 20 cm sec^{-1} at 20 m depth between Carnation and Edelweiss) and a northward 'undercurrent' above the continental shelf and slope (maximum of about 5 cm sec^{-1} above the shelf break at Edelweiss). The depth of no motion extends downward offshore from a depth of about 50 m at Aster to over 200 m at Forsythia. The mean u-velocity is essentially onshore above 200 m except near the bottom where offshore flow exists. An onshore maximum of greater than 4 cm sec^{-1} occurs at about 40 m depth at Carnation and at shallower depths inshore of Carnation.

Near the beginning of the mid-July event, on 10 July, the velocity distribution resembles the mean distribution except that the maximum of the northward undercurrent is at Carnation and the onshore flow is greater at 20 m depth. On 13 July, when southward winds reach a maximum the flow is everywhere southward (maximum of about 50 cm sec^{-1} at 20 m Carnation) and onshore (maximum greater than 8 cm sec^{-1} at 40 m

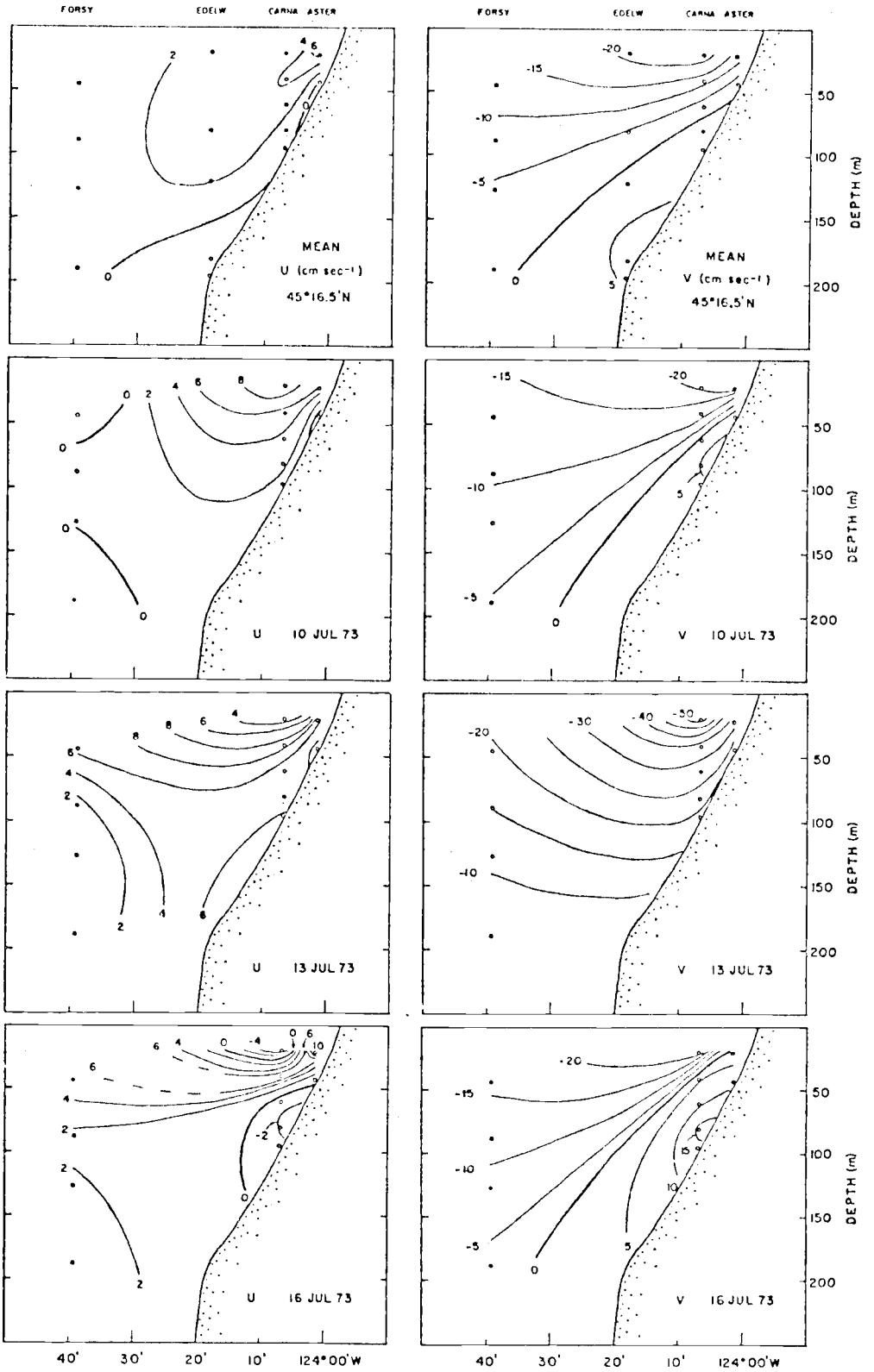

Figure 6. Zonal sections of the vertical distribution of horizontal velocity components near 45°16.5'N.

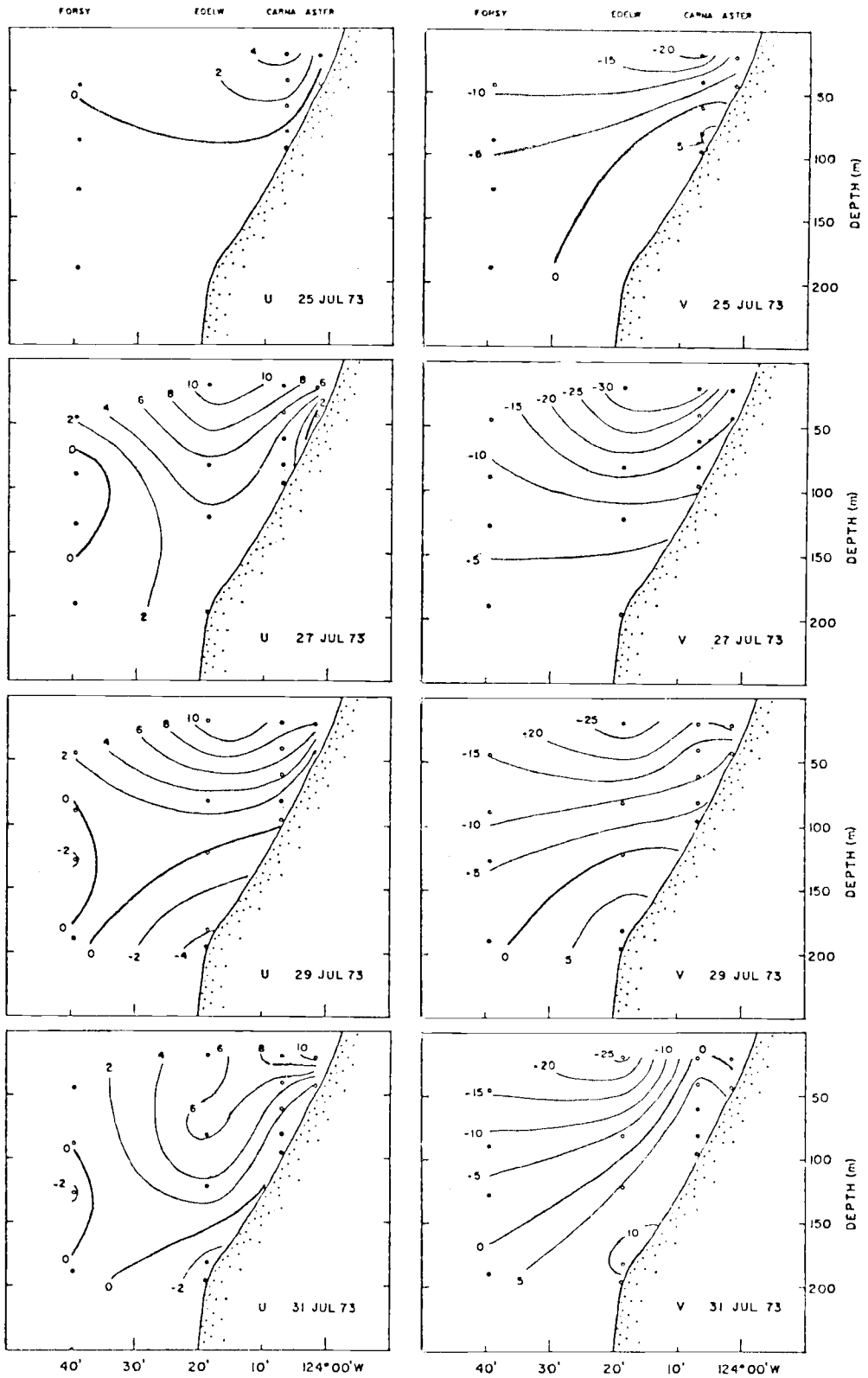

Figure 6. Cont'd.

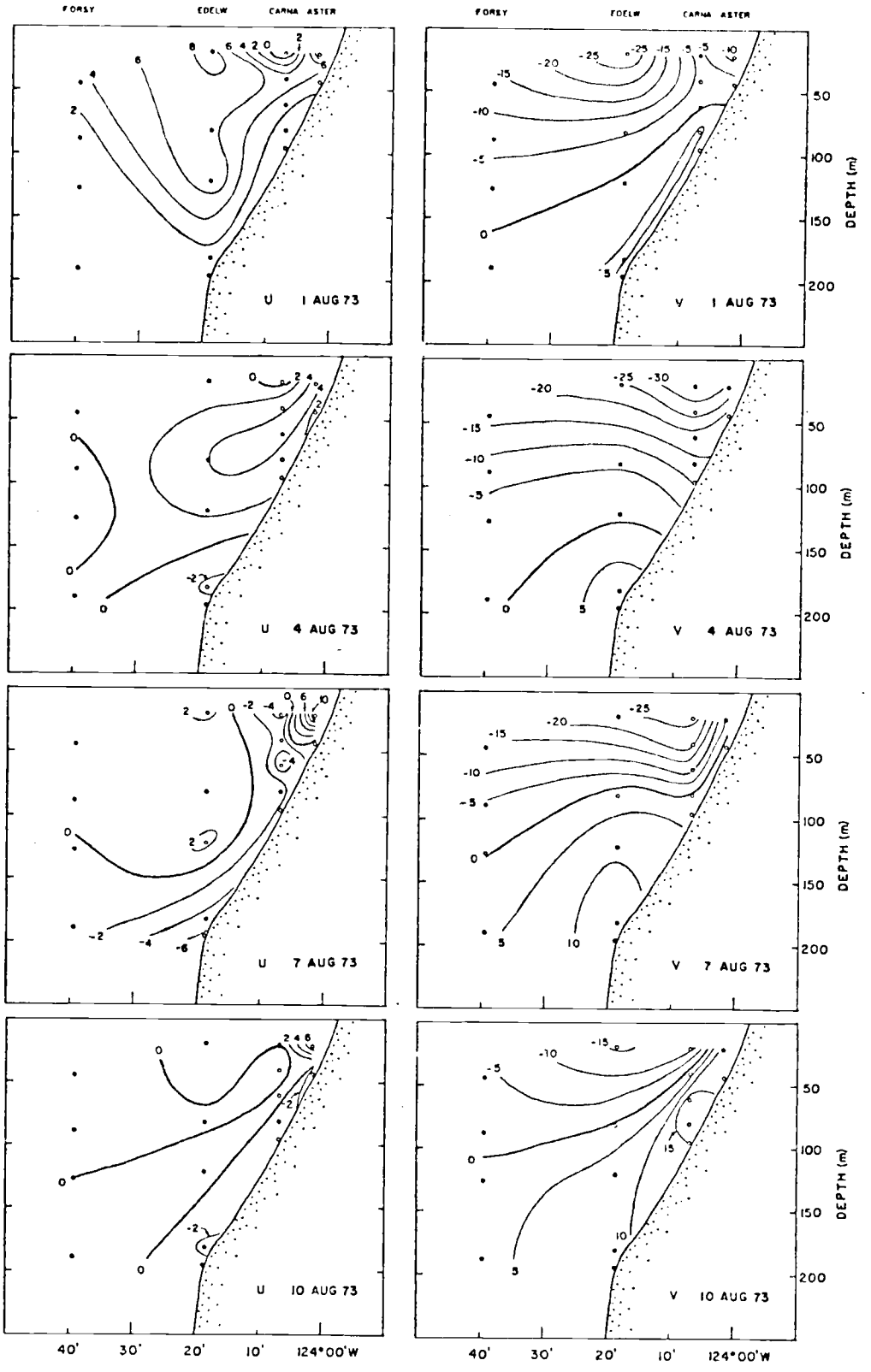

Figure 6. Cont'd.

Carnation) below 20 m depth. On 16 July, as the winds relax near the end of the event, the northward undercurrent reappears over the shelf (maximum greater than 15 cm sec^{-1} at 80 m Carnation), the intensity of the southward flow decreases, and offshore flow resumes near the bottom over the central shelf region and down to 30 m depth in the surface layer near Carnation.

On 25 July, near the beginning of the late July - early August event, the flow resembles the mean distribution. Intensification of southward and onshore flow occurs between 25 and 27 July, and by 27 July the flow is nearly everywhere southward and onshore below 20 m depth. On 29 July, northward and offshore flow have reappeared over the shelf break. On 31 July the location of the strongest southward flow is found farther offshore (at 20 m Edelweiss), and northward flow has resumed over most of the shelf. On 1 August a second intensification of the southward flow occurs nearshore along with a decrease in the northward undercurrent. The flow is again entirely onshore except for offshore flow at 20 m Carnation. On 4 August a maximum in the southward intensity is reached, but northward flow still exists over the shelf break and offshore flow has resumed in lower depths and offshore. Near the end of the event on 7 August the southward flow has again relaxed and northward flow returned over the shelf. Offshore flow has also returned in the lower layer over the shelf and occurs throughout the water column at Carnation. By 10 August, the alongshore flow again resembles the mean but with relatively intense northward flow below the depth of no motion, which extends upward towards the coast from about 100 m depth at Forsythia to 20 m depth offshore of Aster. At

Aster the flow appears to be everywhere northward below 20 m. Offshore flow occurs in the region of the depth of no alongshore motion and near the bottom over the shelf, with onshore flow occurring elsewhere.

Hydrography

Surface distributions of temperature, salinity, and density (sigma-t) were contoured for two cruises: Y7306E (27 June - 1 July, during strong southward winds) and Y7308A (16 - 20 August, during fluctuating winds following strong southward winds). These are presented in Figure 7. The main features are typical of upwelling: colder, more saline, and denser water near the coast. However, several spatial variations exist. During both cruises upwelling appears more intense near the coast south of Cape Lookout (≃ 45°20'N) and Cape Foulweather (≃ 44°47'N). An intrusion of relatively fresh water (< 31.5 o/oo) occurs around 45°15'N and 124°25'W during Y7306E and along 124°10'W north of 45°20'N during Y7308A. This probably represents modified Columbia River plume water advected south by the southward surface current.

On several occasions during the observational period the line of stations at approximately 45°16.5'N was repeated within several days of its initial occupation, and it is possible to note changes which occurred in the hydrographic regime on the order of several days or less. These occupations of the 45°16.5'N line occurred on 28 - 29 June and 30 June; 9 - 10 July, 12 - 13 July, and 13 July; and 18 - 20 August and 22 - 23 August. Zonal sections of the vertical distributions

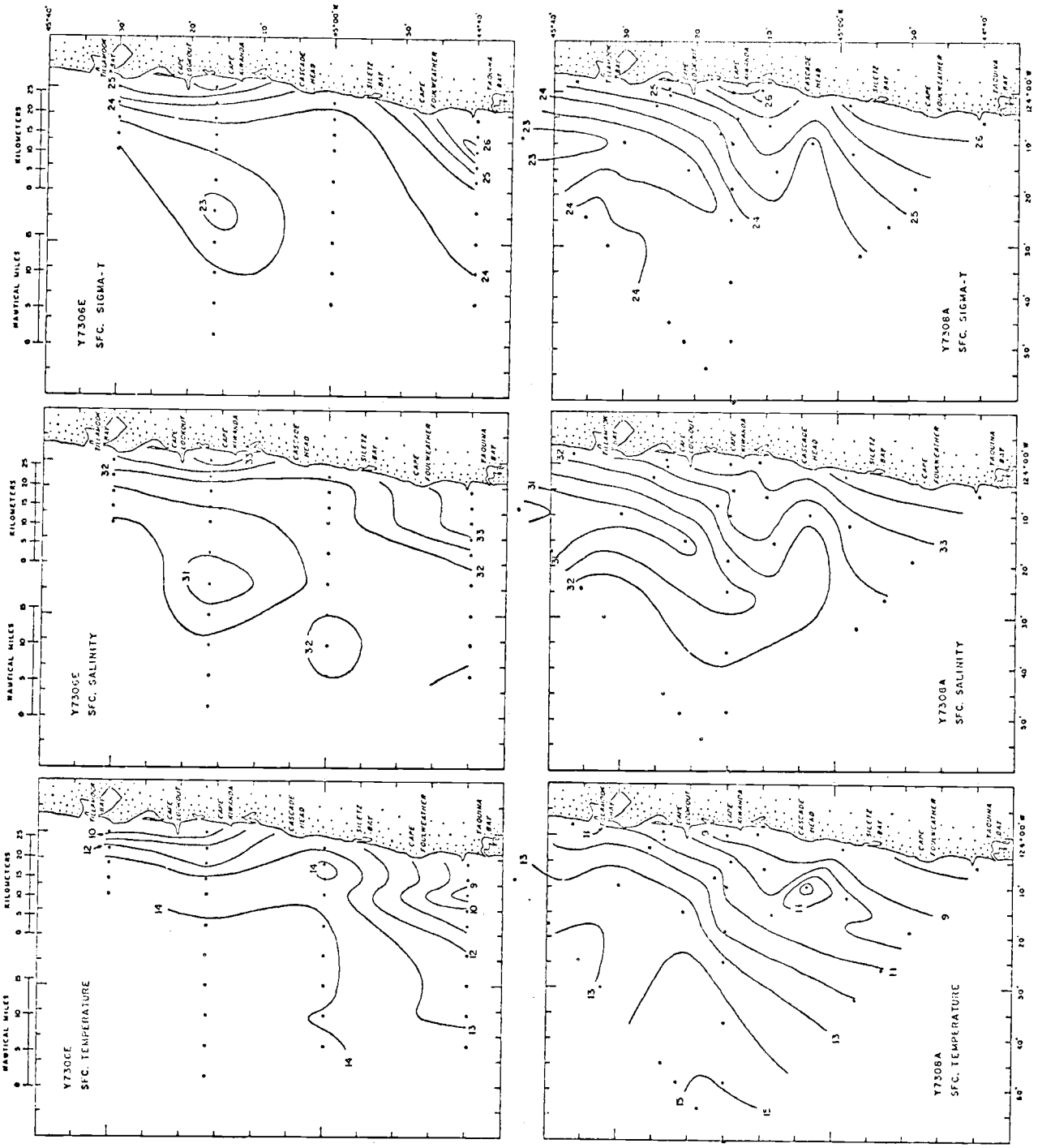

Figure 7. Surface distributions of temperature (°C), salinity (o/oo), and density (σ_t) during late June (Y7306E) and mid-August (Y7308A), 1973.

of temperature, salinity, and density (sigma-t) for these dates are shown in Figure 8. The salinity and density increase monotonically with depth but there are numerous temperature inversions. The choice as to whether an inversion represented anomalously cold water above or warm water below was made through examination of temperature-salinity diagrams and the density sections.

In general, isolines of the various parameters curve upward and converge toward the coast above 300 m depth and within 80 km (i.e., from about 125°W) of the coast. The interiors of the sections exhibit little change; most variation occurs in the nearshore region within 20 km of the coast; the surface layer down to 30 m, or along the bottom. The permanent pycnocline, defined by Collins (1964) as the region between the 25.5 and 26.0 σ_t isopycnals, is normally found at about 100 m depth 80 km from the coast, rising to about 50 m depth 20 km from the coast, and often intersecting the surface (as on 13 July in Figure 8) some 5 - 10 km from the coast.

The occupations of the hydrographic line in June and July in Figure 8 coincided with upwelling 'events', i.e., periods when the wind blew strongly southward. Changes in the hydrographic sections associated with the events include the removal of low salinity (< 31.5 o/oo), low density (< 23.5 σ_t), warm (> 14°C) water from the surface layer and the upward movement of the isolines in the nearshore region. This is especially notable between the sections of 9 - 10 July, where the isolines in the nearshore region are nearly horizontal, and 12 - 13 July, where the isolines intersect the surface. Comparison with Figure 6

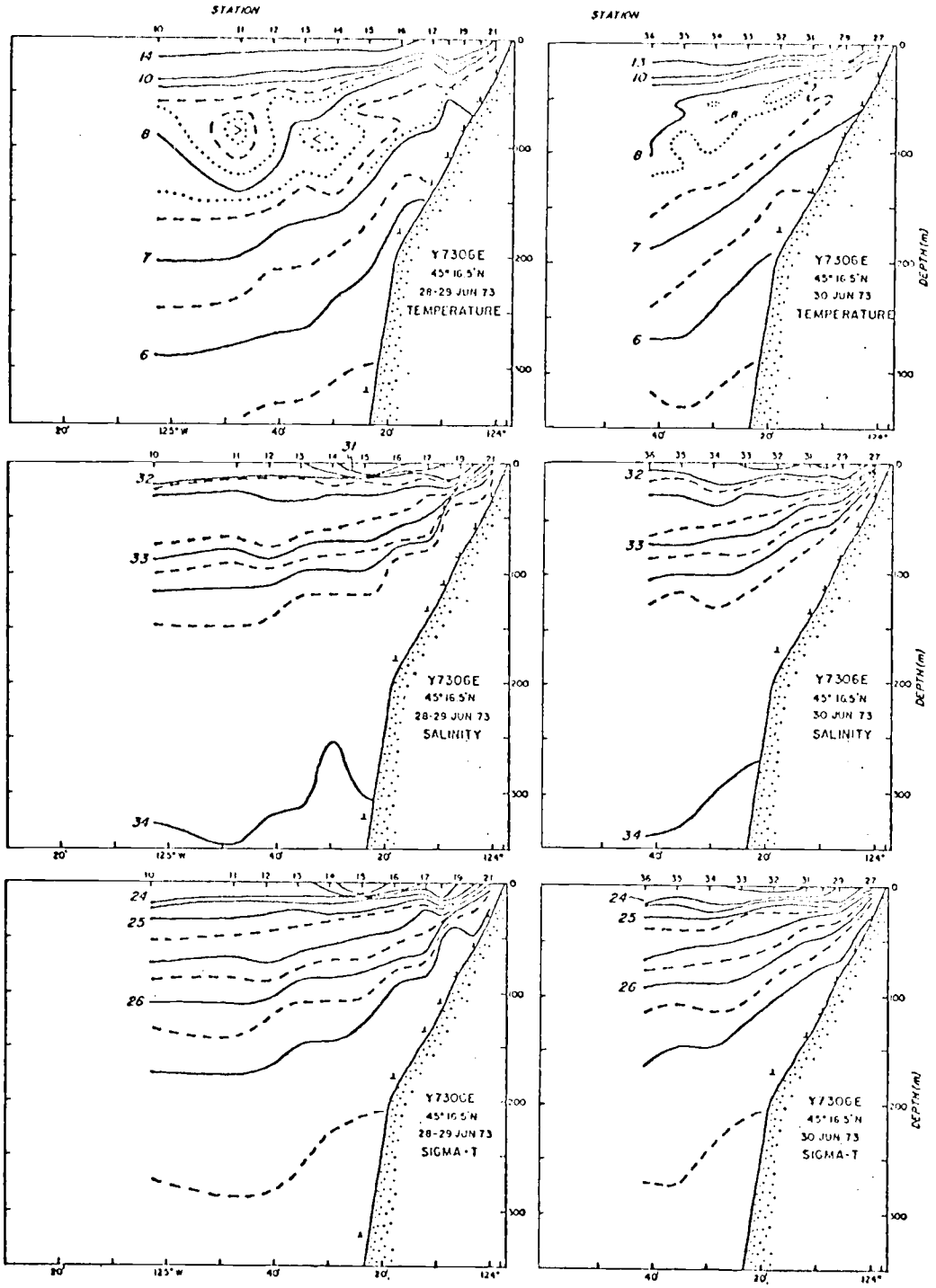

Figure 8. Zonal sections of the vertical distribution of temperature (°C), salinity (o/oo), and density (σ_t) near 45°16.5'N. Contour intervals: 1°C, 0.5 o/oo, 0.5 σ_t (solid line); 0.5°C, 0.25 o/oo, 0.25 σ_t (dashed line); 0.25°C (dotted line).

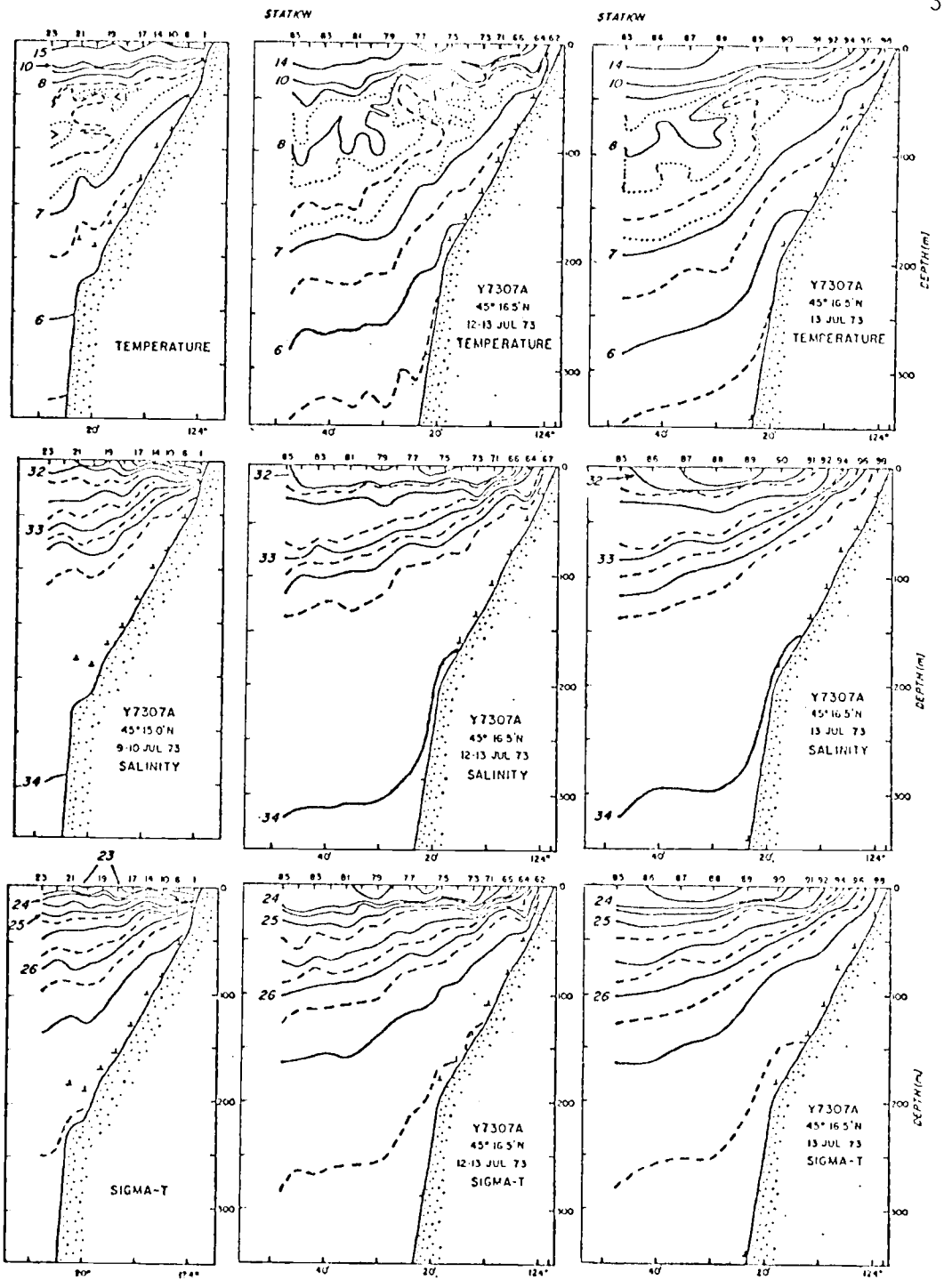

Figure 8. Cont'd.

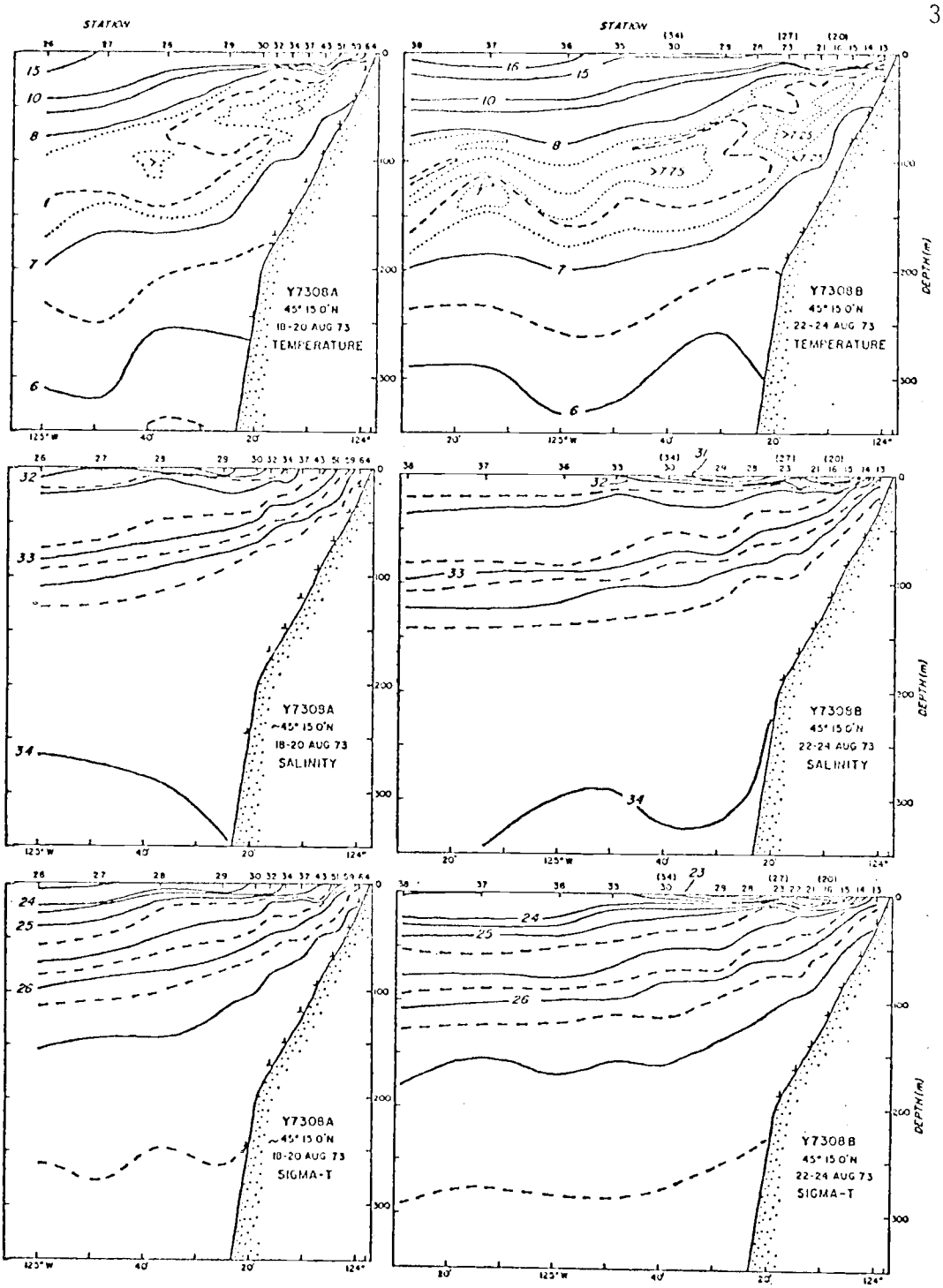

Figure 8. Cont'd.

shows that the 9 - 10 July section coincided with southward and onshore flow in the upper layers, and northward flow in the lower layers, whereas the 12 - 13 July section coincided with southward and onshore flow at all depths. The occupations of the line in August, which coincided with a relaxation of the southward winds and even some northward wind reversals, show the return of low salinity, low density, warm water in the surface layer and some lowering of the nearshore isolines.

In many of the temperature sections (Figure 8 and Appendix II) a region of anomalously cold water at 25 to 75 m depth 10 to 40 km offshore is found above higher density, warmer water which coincides with the bottom of the permanent pycnocline. In particular, during the August observations (Figure 8), a weak temperature inversion occurs between about 40 to 70 m depth 10 to 25 km offshore. The locations of these anomalously cool and warm waters correspond respectively to the locations of the cool water ribbon described by Huyer and Smith (1974) and the offshore sinking of a newly-formed water mass as hypothesized in the conceptual model of Mooers, Collins and Smith (1976). In Figure 9, temperature - salinity diagrams are plotted for various stations along 45°15'N during 18 - 20 August. These stations go from regions of offshore (station 26) to nearshore (station 62) waters. At station 29, water with the properties of the cool water ribbon (< 7.75°C, 32.5 - 33.0 o/oo) is observed at sigma-t values of approximately 25.5 to 25.75. The weak warm water anomaly observed at station 37 occurs between sigma-t values of about 26.0 and 26.25 (corresponding to the bottom of the permanent pycnocline) and has properties (> 7.25°C, $\simeq$ 33.5 o/oo) that could be representative of the hypothesized warm water mass.

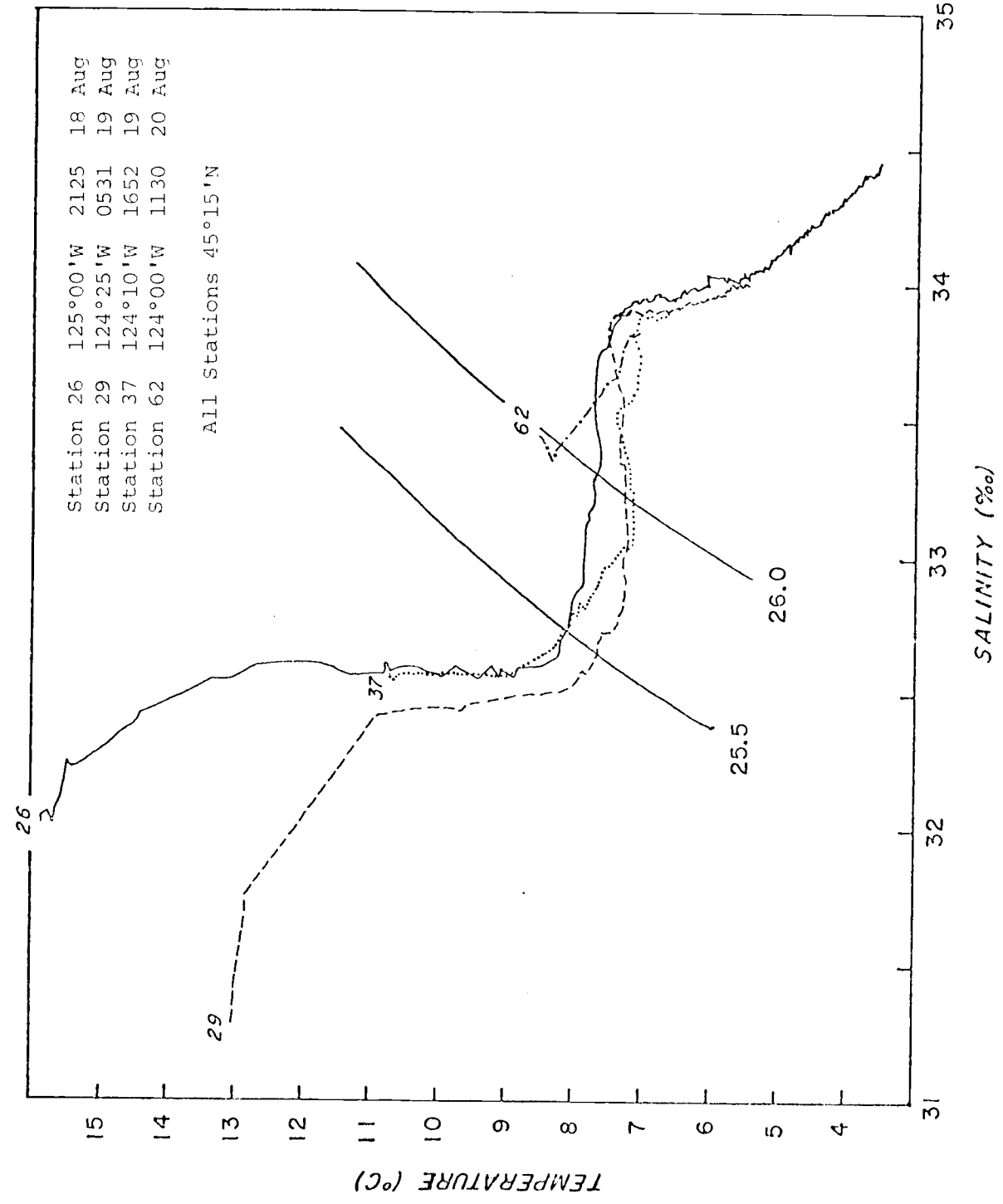

Figure 9. Temperature-salinity relationships for selected stations along 45°15'N during mid-August, 1973.

III. ANALYSIS

Wind Stress

Estimates of the near-surface wind stress, $\vec{\tau} = (\tau_x, \tau_y)$, were computed from hourly time series of the winds at Newport, Aster, and Edelweiss using the empirical relations:

$$\tau_x = C_D \rho_a (u^2 + v^2)^{\frac{1}{2}} u \qquad (1a)$$

$$\tau_y = C_D \rho_a (u^2 + v^2)^{\frac{1}{2}} v \qquad (1b)$$

where u and v are the eastward and northward velocity components of the winds, $\rho_a \simeq 1.25 \times 10^{-3}$ gm cm^{-3} is the density of air, and $C_D \simeq 1.3 \times 10^{-3}$ is the nondimensional drag coefficient (Smith and Banke, 1975). The hourly series for the wind stress were then low-pass filtered to produce six-hourly records in which higher frequencies (> 0.6 cpd) have been suppressed. Plots of the filtered wind stress, decimated to daily values, are shown in Figure 10.

The seasonal wind stress is primarily southward and eastward. At Newport, the 52-day mean southward and eastward wind stress components are 0.33 and 0.06 dynes cm^{-2}, respectively, with maximum southward (2.04 dynes cm^{-2}) and eastward (0.20 dynes cm^{-2}) wind stress occurring during the mid-July event (13 July). At Aster ($\simeq$ 5 km offshore) the maximum southward (0.96 dynes cm^{-2}) and eastward (1.66 dynes cm^{-2}) wind stress also occurred during the mid-July event; these maxima are respectively smaller and larger than the maximum southward ($\simeq$ 3.5 dynes cm^{-2}) and eastward ($\simeq$ 0.3 dynes cm^{-2}) wind stress computed by Halpern (1975b) during the same time at a colatitudal mooring

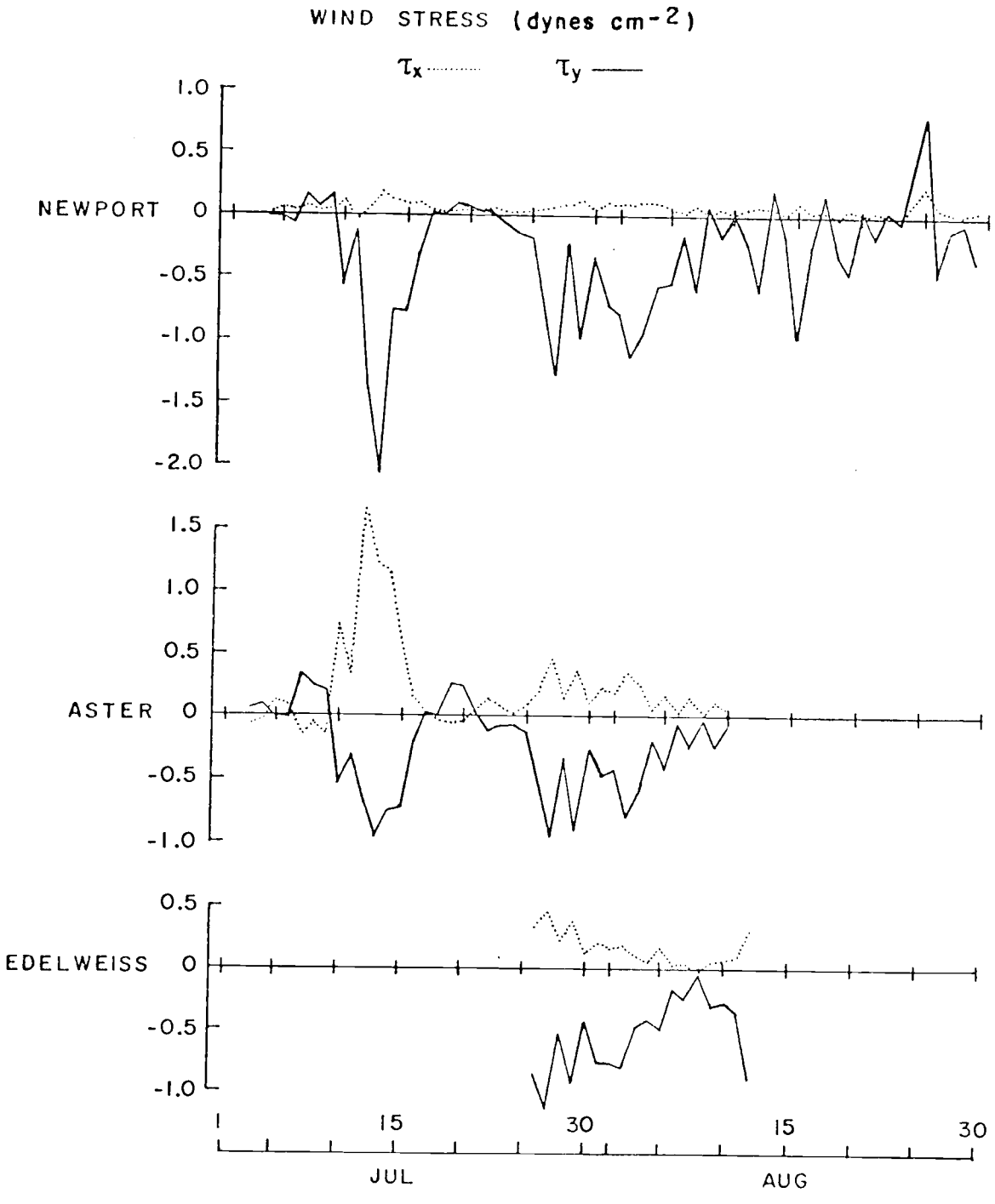

Figure 10. Low-passed (f < 0.6 cpd) time series of the wind stress during July - August, 1973 (decimated to daily values).

approximately 13 km offshore. It is likely that the Aster estimates were affected by errors in the measurement of the wind. Comparable data during mid-July were not available at Edelweiss (≈ 27 km offshore).

With the exception of relatively large values at the coast, the alongshore wind stress appears to increase in the offshore direction, i.e., the curl of the wind stress is positive. For the common record interval of 28 July to 10 August (corresponding to the relaxation of winds during the latter part of the late July - early August event), the mean alongshore wind stress is -0.35 dynes cm^{-2} at Aster (standard deviation = 0.26 dynes cm^{-2}) and -0.48 dynes cm^{-2} at Edelweiss (standard deviation = 0.26 dynes cm^{-2}). During the same interval, the mean alongshore wind stress at Newport is -0.50 dynes cm^{-2}, but the standard deviation (0.36 dynes cm^{-2}) is also larger. The average temporal variation of the alongshore wind stress (as measured by the standard deviation) is not large compared to the mean. The onshore-offshore wind stress is considerably reduced at the coast, the mean and standard deviation for the 28 July to 10 August interval being, respectively, 0.07 and 0.04 dynes cm^{-2} at Newport, 0.15 and 0.11 dynes cm^{-2} at Aster, and 0.13 and 0.10 dynes cm^{-2} at Edelweiss. Low-frequency fluctuations in the wind stress are highly correlated (Table V). The correlation between alongshore components appears better than between the onshore-offshore components.

A scatter plot of daily values of the alongshore and onshore-offshore components of the wind stress at Newport, Aster and Edelweiss during 28 July to 10 August is shown in Figure 11. The linear pattern

Table V. Linear correlations between wind stress observations (28 July - 10 August 1973).

			Correlation Coefficient
Newport	τ_x; Aster	τ_x:	0.80
	τ_y;	τ_y:	0.88
Newport	τ_x; Edelweiss	τ_x:	0.67
	τ_y;	τ_y:	0.81
Aster	τ_x; Edelweiss	τ_x:	0.79
	τ_y;	τ_y:	0.89

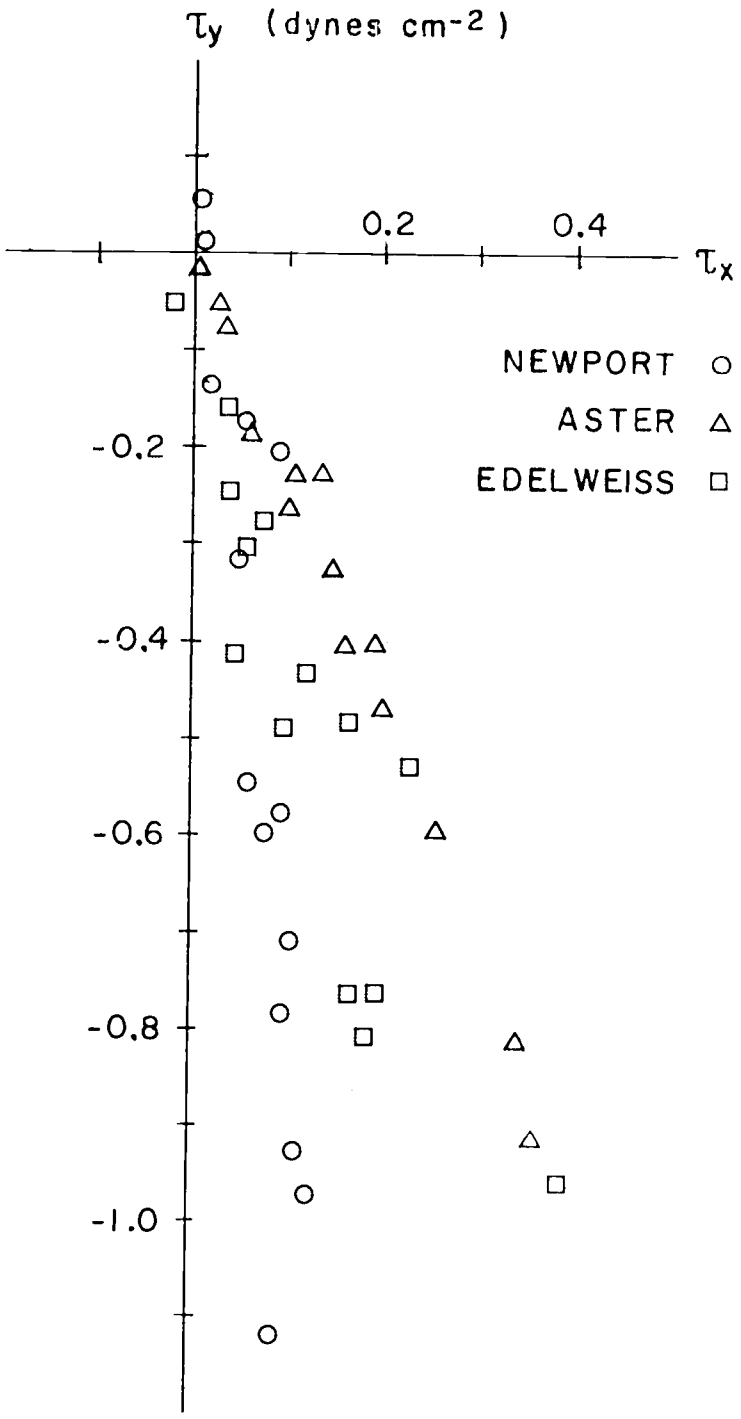

Figure 11. A scatter plot of daily values (0000 UT) of the wind stress during 28 July - 10 August, 1973.

at each location (the coefficients for the linear correlation between the wind stress components at Newport, Aster and Edelweiss are -0.85, -0.99 and -0.89 respectively) suggests that the wind stress is largely unidirectional. The apparent clockwise veering of the wind stress between the offshore moorings and Newport (and the larger southward and smaller eastward components at the coast) may be due to differences in the instrumentation, significant alongshore variations between the locations of the observations, and/or the influence of the nearby coastal mountains.

Vertical Velocity

From successive occupations of the 45°16.5'N hydrographic line an estimation of the vertical velocity, w, as a function of distance offshore was obtained by averaging the vertical velocities computed from the displacements of the 25.5 and 26.0 σ_t isopycnals. In addition, the vertical velocity was computed from theoretical considerations. According to Yoshida (1955), in a two-layer model of coastal upwelling with uniform wind stress, the expression for the vertical velocity, w_{-h}, at the interface between the two layers in coastal regions is

$$w_{-h} = -\frac{k}{\rho}\frac{\tau_y}{f}e^{kx} \qquad (2)$$

where $k = f(gh\Delta\rho/\rho)^{-\frac{1}{2}}$, $f = 2\Omega\sin\phi$ is the Coriolis parameter, g is the gravitational field strength, h is the depth of the upper layer, ρ is the density of the upper layer, $\Delta\rho$ is the density difference between the upper and lower layers, and τ_y is the alongshore wind stress. (A right-handed coordinate system is used with x positive eastward, y

positive northward, z positive upward, and the origin located at the coast.) For successive occupations of the hydrographic line, average values of τ_y, ρ, and $\Delta\rho$ were computed, and vertical velocity as a function of distance offshore was estimated by averaging vertical velocities calculated from Equation (2) using both the 25.5 and 26.0 σ_t isopycnals as the interface between the upper and lower layers. Estimates made by both methods are plotted in Figure 12.

The estimates made from occupations of the line during 9 - 10 July to 12 - 13 July, and 12 - 13 July to 13 July coincided with winds favorable to upwelling, and in general, the vertical velocities during these times are greater than during 19 - 20 August to 22 - 23 August, when the winds were less favorable to upwelling. The agreement in the two estimates is best for the period of 9 - 10 July to 12 - 13 July when the sampling interval between pairs of similar stations remained fairly constant. The large vertical velocities in the offshore region during 12 - 13 July to 13 July are probably the result of a short sampling interval and aliasing caused by the displacement of the isopycnals by internal waves.

Halpern (1974, 1975a) has estimated that during the upwelling season off Oregon, vertical velocities on the order of 10^{-2} cm sec^{-1} occur within 10 to 15 km of the coast. During 9 - 10 July to 12 - 13 July, the estimated vertical velocity at the inshore station ($\sim$ 7 km offshore) is only about 4×10^{-3} cm sec^{-1}. Isopycnal displacements, however, underestimate vertical velocities because mixing is neglected and estimates represent time averages. Underestimation of the wind stress would result in smaller vertical velocities computed from

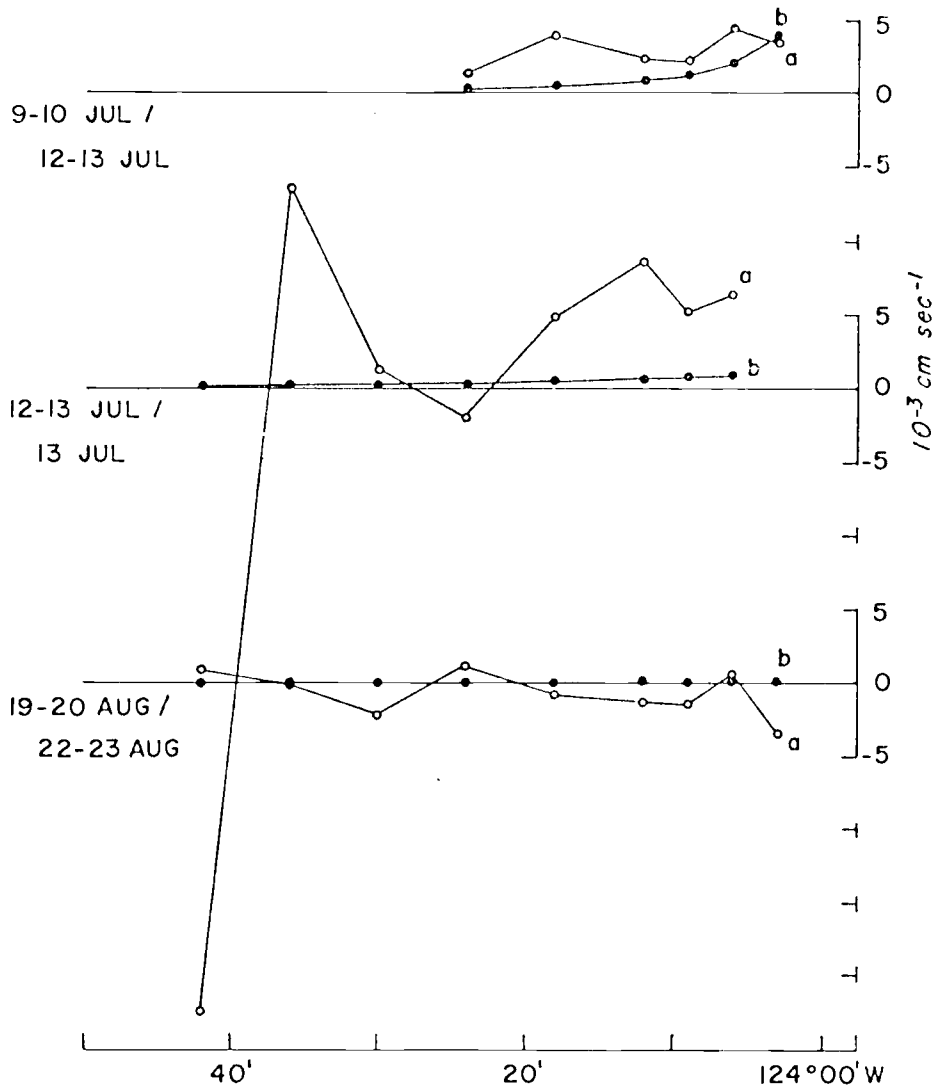

Figure 12. Zonal distributions of vertical velocity along 45°16.5'N as computed from a) isopycnal displacements, and b) theoretical considerations.

Equation (2); however, extrapolation to the coast would yield vertical velocities on the order of 10^{-2} cm sec^{-1}.

If the vertical resolution of the horizontal velocity field provided by current meter measurements is sufficient, estimates of vertical velocities through integration of the continuity equation can be made. Assuming two-dimensional flow orthogonal to the coast (i.e., $\partial v/\partial y = 0$), the continuity equation is

$$\frac{\partial u}{\partial x} + \frac{\partial w}{\partial z} = 0 \ . \tag{3}$$

Vertically integrating (3) between depths z_1 and z_2 gives

$$- \int_{z_2}^{z_1} \frac{\partial u}{\partial x} \, dz = w_{z_1} - w_{z_2} \ . \tag{4}$$

Equation (4) was applied to the Oregon coastal region to estimate the relative vertical velocity between 15 and 50 m depth using measurements of the 20 and 40 m onshore-offshore velocity at Aster and Carnation. The limits of integration, z_1 and z_2, were taken to be the depth of no onshore-offshore motion and the bottom depth at Aster, respectively. The vertical distribution of onshore-offshore velocity was assumed to increase linearly over depths from 15 (where $u = 0$) to 20 m (where $u = u_{20}$), and to be uniform over depths from 20 to 30 m (where $u = u_{20}$), and 30 to 50 m (where $u = u_{40}$). A time series plot of the relative vertical velocity is shown in Figure 13. (Johnson [1976], has shown that, during weak winds at a location in 100 m of water about 30 km south of Carnation, the depth of no vertical motion is 55 to 60 m; also at Aster the vertical velocity at the bottom must

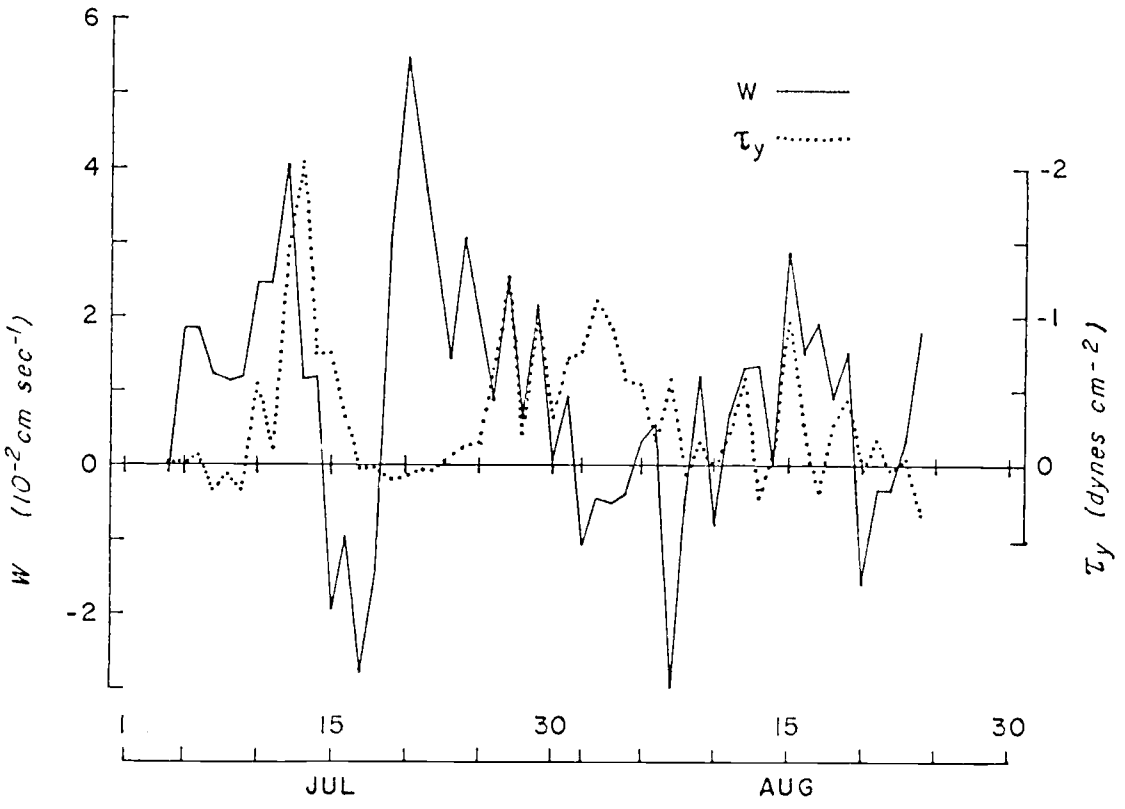

Figure 13. Time series of the relative vertical velocity (between 15 and 50 m depth) between Aster and Carnation, and the alongshore wind stress at Newport.

vanish. Therefore, if a boundary condition is imposed in Equation (4) such that $w = 0$ at $z_2 = 50$ m, then Figure 13 represents the absolute vertical velocity at 15 m depth between Aster and Carnation, i.e., between about 5 and 12 km offshore.) Maxima in the (relative) vertical velocity on the order of 4 to 5.5 x 10^{-2} cm sec^{-1} coincide with southward and northward wind stress during and following the mid-July event, respectively. Minima occur during relaxation of southward wind stress following events. The 52-day mean (relative) vertical velocity is 0.92 x 10^{-2} cm sec^{-1} (standard deviation = 1.66 x 10^{-2} cm sec^{-1}).

Onshore-Offshore Mass Transport Balance

The estimations of vertical velocity from Equations (2) and (4) assume two-dimensional flow. The hypothesis of a zonal mass transport balance resulting from the compensatory replacement by subsurface water of surface water advected offshore is examined by comparing estimates of the offshore 'Ekman' transport in the surface layer (assumed to be the upper 15 m) with estimates of the onshore transport below the surface layer. Time series for the offshore Ekman transport,

$$M_x = -\frac{\tau_y}{f} , \tag{5}$$

were computed from daily estimates of the wind stress at Newport, Aster and Edelweiss. Time series for the onshore transport,

$$M_x = \int_{z_2}^{z_1} \rho u dz , \tag{6}$$

between 15 m and the bottom were computed from daily records of the observed onshore-offshore currents at Aster ($z_2 = 50$ m), Carnation

(z_2 = 100 m), Edelweiss (z_2 = 200 m) and Forget-Me-Not (z_2 = 100 m) assuming uniform velocity distributions with depth below 20 m (as determined by the current observations within specified depth intervals) and a linear velocity distribution above 20 m (such that u = 0 at z_1 = 15 m depth). These are plotted in Figure 14. Means, standard deviations and linear correlation coefficients for the common data interval of 28 July to 10 August are presented in Table VI.

In Figure 14 there is some correlation between onshore and offshore transports; e.g., there is a tendency for corresponding increases in the transports during periods of strong southward wind stress. A high (negative) correlation would, in fact, be expected between the onshore and offshore transports if the net zonal mass transport is to be zero. The highest correlations for the interval of 28 July to 10 August (-0.68 between the onshore transport at Aster and the offshore transport at Newport, and between the onshore and offshore transports at Edelweiss) are only marginally significant at the 1% significance level, however. (The critical value for the correlation coefficient, r, to be significant at the 1% level for a sample size of 14 is -0.61, i.e., for an uncorrelated population, the probability that $r \geq 0.61$ is ≤ 0.01.) The low correlations between the transport at Forget-Me-Not and the transports elsewhere are probably due to significant alongshore variations in the onshore-offshore circulation.

On a 'seasonal time scale', an imbalance between onshore and offshore transports exists. The ratios of onshore to offshore transports (averaged over 28 July to 10 August) for the transports with the highest correlations are 1.58 (for the onshore transport at Aster and the

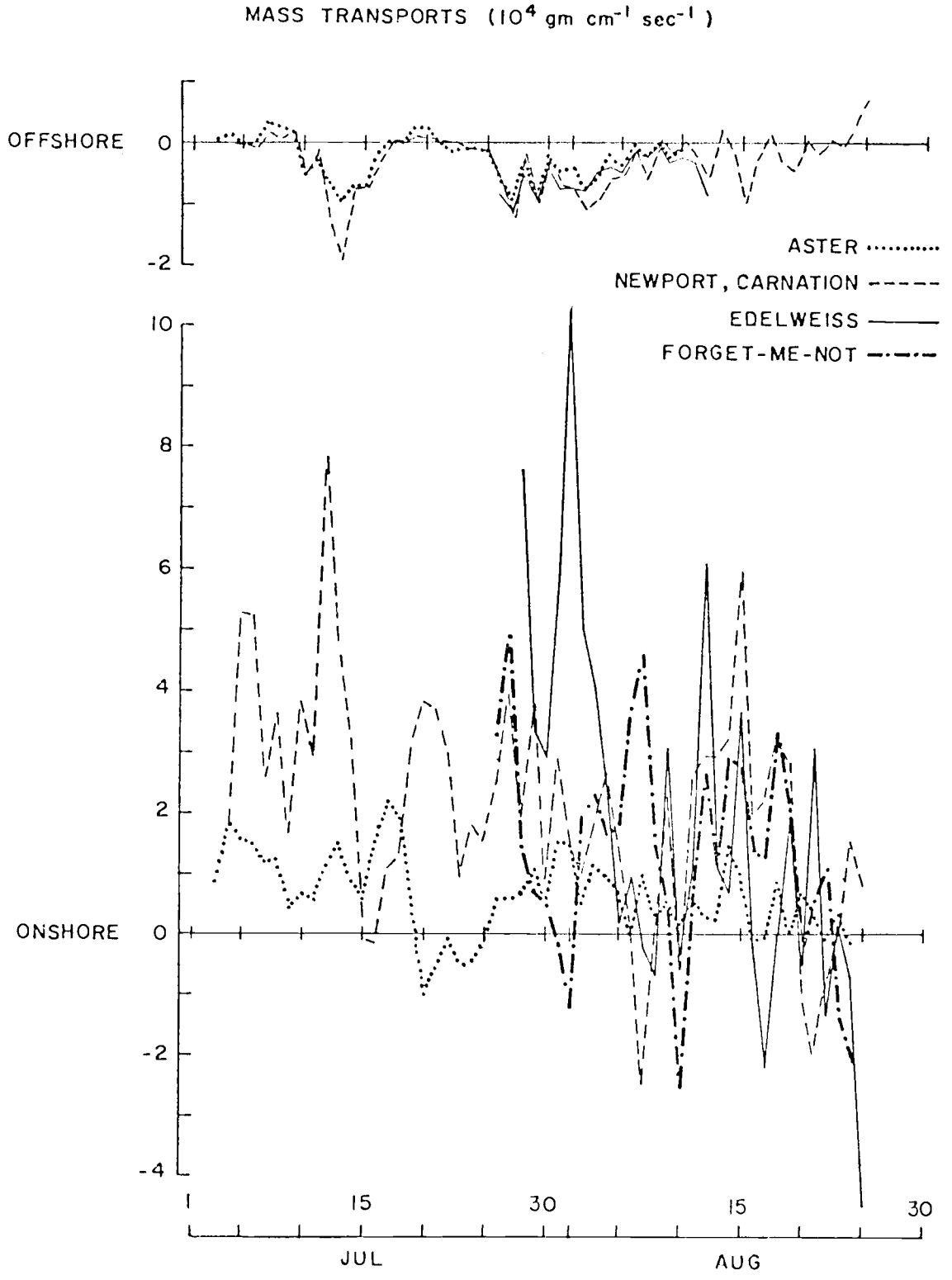

Figure 14. Time series of offshore (Ekman) and onshore (below 15 m) mass transports during July - August, 1973.

TABLE VI. Means, standard deviations and linear correlation coefficients for mass transports (28 July - 10 August 1973).

				Offshore (Ekman) Transports (10^4 gm cm^{-1} sec^{-1})		
				NEWPORT	ASTER	EDELWEISS
		mean →		-0.48	-0.34	-0.46
		↓	s.d.→	0.35	0.25	0.25
			↓			
Onshore Transports (10^4 gm cm^{-1} sec^{-1})	ASTER	0.76	0.46	-0.68**	-0.51*	-0.66**
	CARNATION	1.25	1.55	-0.37	-0.53*	-0.64**
	EDELWEISS	3.18	3.11	-0.45	-0.45	-0.68**
	FORGET-ME-NOT	1.19	1.75	-0.14	0.01	0.29

Correlation Coefficients between Onshore Transports

ASTER	--	CARNATION:	0.43
ASTER	--	EDELWEISS:	0.61**
ASTER	--	FORGET-ME-NOT:	-0.14
CARNATION	--	EDELWEISS:	0.51*
CARNATION	--	FORGET-ME-NOT:	-0.33
EDELWEISS	--	FORGET-ME-NOT:	-0.32

* significant correlation at 5% level
** significant correlation at 1% level

offshore transport at Newport) and 6.91 (for the onshore and offshore transports at Edelweiss; at Edelweiss, the principal axes differ from the x-y axes and the larger onshore transports may be due in part to a component of the north-south velocity). On a seasonal time scale, Halpern (1975a) also observed a zonal transport imbalance using direct current measurements in the upper layer to estimate the offshore transport; the balance improved on the 'event time scale' of a few days. The reason for the apparent imbalance is uncertain, but may be due to inadequate resolution of the vertical distribution of velocity in estimating the onshore transport, inequality of the Ekman transport and the total offshore transport, underestimation of the Ekman transport (from underestimation of the wind stress), and/or alongshore advection.

Alongshore Modal Structure and Geostrophy

From current observations, the alongshore mean flow appears to be largely baroclinic and the low-frequency fluctuations barotropic. That the velocity fluctuations are barotropic is suggested by the high visual correlation between the alongshore currents at different depths and the persistence of the vertical shear in the alongshore velocity component despite the fluctuations, i.e., the fluctuations are depth-independent (Smith, 1974; Huyer, Smith and Pillsbury, 1974). The baroclinic mode results from the mass redistribution associated with upwelling (Halpern, 1974), and is largely in geostrophic equilibrium as suggested by the apparent validity of the 'thermal-wind' relation,

$$\frac{\partial v}{\partial z} = - \frac{g}{\rho f} \frac{\partial \rho}{\partial x} . \qquad (7)$$

The alongshore current shear was estimated by taking velocity differences between 20 and 40 m at Carnation, 20 and 120 m at Edelweiss, and 40 and 180 m at Forsythia. These are plotted in Figure 15. The means and standard deviations of the shear are, respectively, 13.00 and 5.39 cm sec^{-1} for Carnation, 24.14 and 5.07 cm sec^{-1} for Edelweiss, and 11.04 and 2.86 cm sec^{-1} for Forsythia. The shear at Carnation resembles the first baroclinic dynamic mode calculated by Kundu, Allen and Smith (1975), although the mean of the shear is smaller since it was computed from currents in the upper portion of the water column only. Since the standard deviations of the velocity shear are much smaller than the means and the shear is relatively constant, the low-frequency velocity fluctuations are largely depth-independent or barotropic. The larger ratio of shear variability to mean shear between 20 and 40 m depth at Carnation suggests some baroclinic variations in the upper layer currents associated with changes in steric anomalies that are largely confined to the upper layer (Smith, 1974).

The validity of the thermal-wind relation (7) was tested by computing geostrophic estimates of the alongshore velocity shear from the density distribution and comparing these with the observed alongshore velocity shear. Relative geostrophic velocities were computed from the dynamic height anomalies at hydrographic stations along the 45°16.5'N line adjacent to the locations of the Carnation, Edelweiss, and Forsythia current meter moorings. Estimated errors for the geostrophic shears are computed using an uncertainty in the dynamic height anomaly of $\pm$ 0.2 dynamic cm between 20 and 40 m at Carnation, $\pm$ 0.5 dynamic cm between 20 and 120 m at Edelweiss, and $\pm$ 0.7 dynamic cm between 40 and

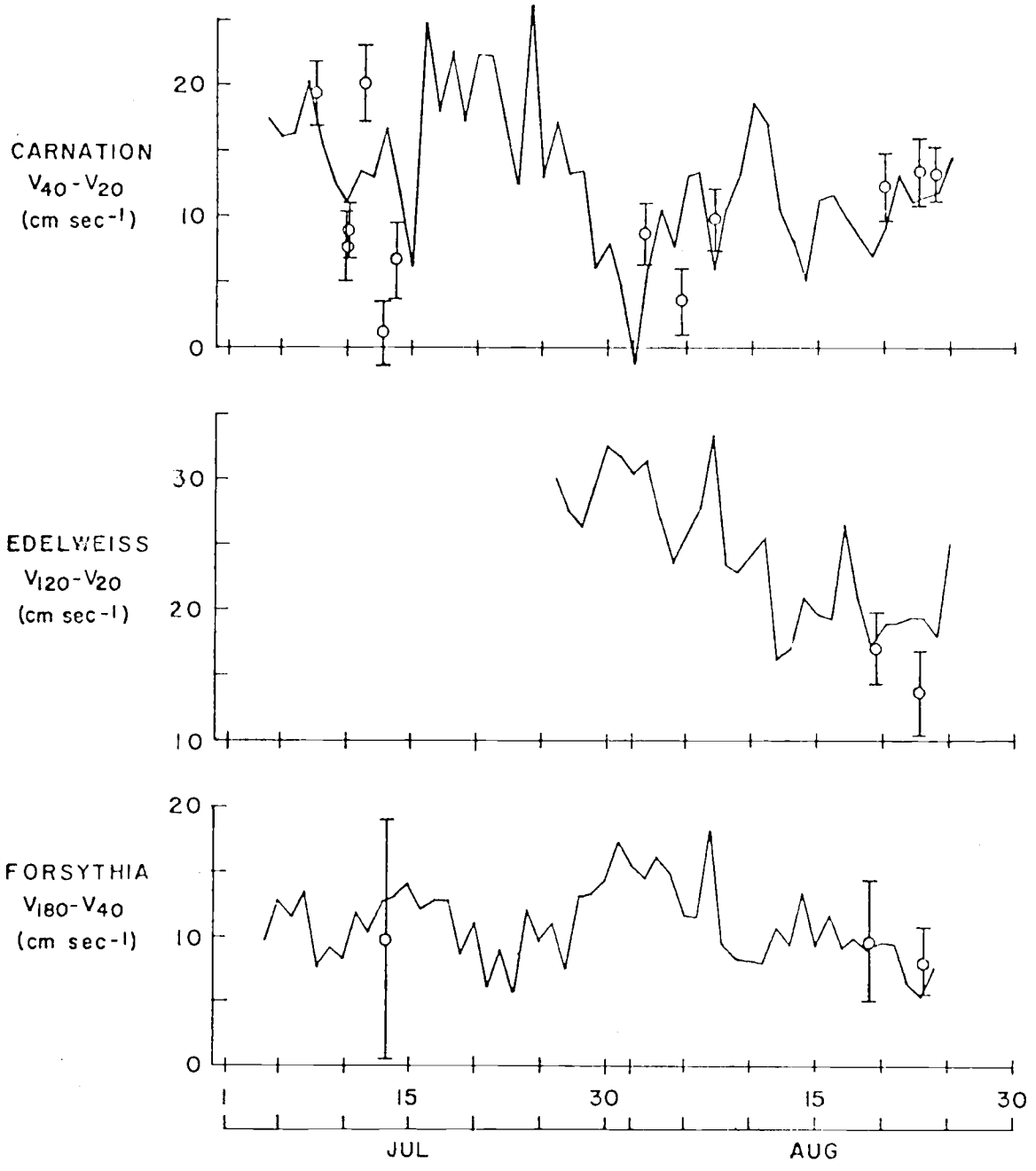

Figure 15. Time series of observed (solid line) and geostrophic (circles with error bars) alongshore velocity differences (shears).

180 m at Forsythia (as determined from repeated CTD casts), and an uncertainty in station separation of 0.5 km. The geostrophic and observed shears are compared in Figure 15. Considering the effect of time and space averaging in the geostrophic estimates and the variability in the observed currents, the agreement appears to be reasonably good. The larger disparity at Carnation may be due in part to the larger variability in the shear observed there. The conclusion that geostrophy usually holds for alongshore currents is consistent with the findings of Smith (1974), Huyer, Smith and Pillsbury (1974), and Halpern (1974).

IV. CONCLUSION

The results from the observations of the Oregon coastal upwelling region during July and August, 1973, are in qualitative and (in most cases) quantitative agreement with results from earlier observations. In the mesoscale description, two time scales seem to be important: a 'seasonal' time scale of several months and an 'event' time scale of several days. The main mesoscale features are summarized as follows:

1. Winds and wind stress. The distribution of winds and wind stress appears to be affected by the proximity of the Oregon coastal mountains. On the seasonal time scale, primarily equatorward (i.e., southward) wind stress of about 0.5 dynes cm^{-2} occurs. The curl of the wind stress is usually positive. On the event time scale, unidirectional fluctuations of the wind stress with maxima of about 2 dynes cm^{-2} occur. These fluctuations generate so called 'upwelling events' in the hydrographic regime. Major events occurred during late June, mid-July, late July - early August, and mid-August in 1973.

2. Sea level. On the seasonal time scale the sea level is about 10 cm lower than the yearly mean. Isostatic adjustment accounts for nearly all of the seasonal departure from the mean (Reid and Mantyla, 1976). On the event time scale fluctuations of the sea level of up to 20 cm occur and are highly correlated with the winds and currents. The steric contribution to the fluctuations is small.

3. Currents. In general, the currents over the continental shelf and upper slope appear to be topographically oriented and governed by three-dimensional dynamics. Alongshore currents are largely geostrophic.

On the seasonal time scale they are baroclinic, with an equatorward surface current of about 20 cm sec^{-1} and a poleward undercurrent of about 5 cm sec^{-1}. On the event time scale highly correlated barotropic fluctuations occur which suggest the existence of continental shelf waves (Cutchin and Smith, 1973; Huyer et al., 1975). During events the barotropic impulse due to the winds often causes a reversal of the undercurrent; during relaxation of events the undercurrent intensifies and sometimes extends upward and shoreward to form a surface countercurrent in the nearshore region (as on 10 August). Onshore-offshore currents may have a cellular circulation pattern. On the seasonal time scale, they are onshore in the interior region and offshore in the upper 15 to 20 m (Halpern, 1975a; Stevenson, Garvine and Wyatt, 1974) and along the bottom. On the event time scale the flow pattern is complicated by shorter time/length scale processes. During events the flow below the surface layer is onshore; during relaxation of events offshore flow sometimes occurs in the frontal zone. Upwelling is largely confined to the inshore 10 to 15 km. On the seasonal time scale vertical velocities are on the order of 10^{-3} to 10^{-2} cm sec^{-1}; on the time scale they are on the order of 10^{-2} to 10^{-1} cm sec^{-1}.

4. Hydrography. The hydrographic regime off Oregon is greatly influenced by the upwelling of cold, high salinity subsurface water and the presence of the relatively fresh Columbia River plume in the surface layer. A homogeneous mixed layer about 0 to 20 m deep normally exists above stratified waters marked by the presence of a seasonal and permanent pycnocline. On the seasonal time scale surfaces

of constant temperature, salinity, and density slope upward toward the coast, and an anomalous ribbon of cool water exists over the shelf. On the event time scale, the greatest changes occur in the surface layer down to about 20 m depth, the nearshore region within about 20 km of the coast, and along the bottom. During events plume water is advected offshore, nearshore isopycnals rise to intersect the surface, and the static stability is decreased; during relaxation of events temperature inversions often occur at the base of the permanent pycnocline, coinciding with offshore flow (as on 20 August).

It is apparent from the description that physical processes of the coastal upwelling region off Oregon consist of highly complex and time-dependent interactions between the winds, currents and hydrography. Results from major field experiments such as CUE-I and CUE-II have helped elucidate many of these interactive processes; however, the need for additional study is also apparent. For example:

1. The details of the wind distribution remain unresolved. Present wind records are too few, too short, or unreliable. An adequate representation of the wind field is necessary since a great deal of the dynamics of upwelling systems depend upon the nature of the forcing.

2. The nature of the onshore-offshore circulation is not completely understood and suggests the need for greater spatial resolution of onshore-offshore currents.

3. The question of two- versus three-dimensional mass balance remains unanswered. An adequate three-dimensional sampling array that includes the surface 'Ekman' layer appears to be necessary to satisfactorily resolve this question.

4. The role of shorter time/length scale processes (such as higher frequency velocity fluctuations, mixing and diffusion) in the dynamics of upwelling systems is still largely unknown.

BIBLIOGRAPHY

Collins, C. A. 1964. Structure and kinematics of the permanent oceanic front off the Oregon coast. M.S. Thesis, Oregon State University, Corvallis. 53 pp.

Collins, C. A., C. N. K. Mooers, M. R. Stevenson, R. L. Smith, and J. G. Pattullo. 1968. Direct current measurements in the frontal zone of a coastal upwelling region. J. Oceanogr. Soc. Japan., 24, 295-306.

Collins, C. A. and J. G. Pattullo. 1970. Ocean currents above the continental shelf off Oregon as measured with a single array of current meters. J. Mar. Res., 28, 51-68.

Curtin, T. B., W. R. Johnson, and C. N. K. Mooers. 1975. Coastal Upwelling Experiment - II, hydrographic data report. Scientific Report, UM-RSMAS-75003. Rosenstiel School of Marine and Atmospheric Science, University of Miami, Miami. 100 pp.

Curtin, T. B. and C. N. K. Mooers. 1974. Coastal Upwelling Experiment - I and II, surface hydrographic fields data report. Scientific Report, UM-RSMAS-74026. Rosenstiel School of Marine and Atmospheric Science, University of Miami, Miami. 94 pp.

_____ 1975. Coastal Upwelling Experiment - II, profiling current meter data report. Scientific Report, UM-RSMAS-75022. Rosenstiel School of Marine and Atmospheric Science, University of Miami, Miami. 179 pp.

Cutchin, D. L. and R. L. Smith. 1973. Continental shelf waves: low-frequency variations in sea level and currents over the Oregon continental shelf. J. Phys. Oceanogr., 3, 73-82.

Halpern, D. 1974. Variations in the density field during coastal upwelling. Tethys, 6, 363-374.

_____ 1975a. Structure of a coastal upwelling event observed off Oregon during July, 1973. Submitted to Deep-Sea Res.

_____ 1975b. Mesoscale variations of near-surface wind-stress over an upwelling region near the Oregon coast. Unpublished ms.

Halpern, D., J. R. Holbrook, and R. M. Reynolds. 1974. A compilation of wind, current, and temperature measurements: Oregon, July and August 1973. CUEA Technical Report 6, Ref. M74-73. Pacific Marine Environmental Laboratory/NOAA, University of Washington, Seattle. 190 pp.

Halpern, D. and R. D. Pillsbury. 1976. Influence of surface waves upon subsurface current measurements in shallow water. Submitted to Limnol. Oceanogr.

Halpern, D., R. D. Pillsbury, and R. L. Smith. 1974. An intercomparison of three current meters operated in shallow water. Deep-Sea Res., 21, 489-497.

Holbrook, J. R. and D. Halpern. 1974. STD measurements off the Oregon coast, July/August 1973. CUEA Data Report 12, Ref. M74-17. Pacific Marine Environmental Laboratory/NOAA, University of Washington, Seattle. 397 pp.

Huyer, A. 1974. Observations of the coastal upwelling region off Oregon during 1972. Ph.D. Thesis, Oregon State University, Corvallis. 149 pp.

Huyer, A. and W. E. Gilbert. 1974. Coastal Upwelling Experiment hydrographic data report, June - August 1973. Data Report 59, Ref. 74-8. School of Oceanography, Oregon State University, Corvallis. 102 pp.

Huyer, A., B. M. Hickey, J. D. Smith, R. L. Smith, and R. D. Pillsbury. 1975. Alongshore coherence at low frequencies in currents observed over the continental shelf off Oregon and Washington. J. Geophys. Res., 80, 3495-3505.

Huyer, A. and R. L. Smith. 1974. A subsurface ribbon of cool water over the continental shelf off Oregon. J. Phys. Oceanogr., 4, 381-391.

Huyer, A., R. L. Smith, and R. D. Pillsbury. 1974. Observations in a coastal upwelling region during a period of variable winds (Oregon coast, July 1972). Tethys, 6, 391-404.

Johnson, D. R. 1976. Determining vertical velocities during upwelling off the Oregon coast. Submitted to Deep-Sea Res.

Kundu, P. K. 1976. Ekman veering observed near the ocean bottom. J. Phys. Oceanogr., 6, 238-242.

Kundu, P. K. and J. S. Allen. 1976. Some three-dimensional characteristics of low-frequency current fluctuations near the Oregon coast. J. Phys. Oceanogr., 6, 181-191.

Kundu, P. K., J. S. Allen, and R. L. Smith. 1975. Modal decomposition of the velocity field near the Oregon coast. J. Phys. Oceanogr., 5, 683-704.

Mooers, C. N. K. and J. S. Allen. 1973. Final report of the Coastal Upwelling Ecosystems Analysis Summer 1973 Theoretical Workshop. School of Oceanography, Oregon State University, Corvallis. 210 pp.

Mooers, C. N. K., C. A. Collins, and R. L. Smith. 1976. The dynamic structure of the frontal zone in the coastal upwelling region off Oregon. J. Phys. Oceanogr., 6, 3-21.

O'Brien, J. J. 1975. Models of coastal upwelling. Numerical Models of Ocean Circulation, ISBN 0-309-02225-8, National Academy of Sciences, 204-215.

O'Brien, J. J., B. M. Woodworth, and D. J. Wright. 1974. The Coho Project, living resources prediction feasibility study. Vol. II - Environmental Report. School of Oceanography, Oregon State University, Corvallis. 126 pp.

Pak, H., G. F. Beardsley, Jr., and R. L. Smith. 1970. An optical and hydrographic study of a temperature inversion off Oregon during upwelling. J. Geophys. Res., 75, 629-636.

Park, K., J. G. Pattullo, and B. Wyatt. 1962. Chemical properties as indicators of upwelling along the Oregon coast. Limnol. Oceanogr., 7, 435-437.

Pillsbury, R. D. 1972. A description of hydrography, winds, and currents during the upwelling season near Newport, Oregon. Ph.D. Thesis, Oregon State University, Corvallis. 163 pp.

Pillsbury, R. D., J. S. Bottero, R. E. Still, and W. E. Gilbert. 1974a. A compilation of observations from moored current meters. Vol. VI. Oregon continental shelf, April - October 1972. Data Report 57, Ref. 74-2. School of Oceanography, Oregon State University, Corvallis. 230 pp.

_____ 1974b. A compilation of observations from moored current meters. Vol. VII. Oregon continental shelf, July - August 1973. Data Report 58, Ref. 74-7. School of Oceanography, Oregon State University, Corvallis. 87 pp.

Pillsbury, R. D. and J. J. O'Brien. 1973. A summary listing of data collected during Coastal Upwelling Experiment - Phase II (CUE-II). School of Oceanography, Oregon State University, Corvallis. 120 pp.

Pillsbury, R. D., R. L. Smith, and R. C. Tipper. 1969. A reliable low cost mooring system for oceanographic instrumentation. Limnol. Oceanogr., 14, 307-311.

Reed, R. K. and D. Halpern. 1974. Radiation measurements off the Oregon coast, July/August 1973. CUEA Data Report 13, Ref. M74-18.

Pacific Marine Environmental Laboratory/NOAA, University of Washington, Seattle. 51 pp.

Reid, J. L. and A. W. Mantyla. 1976. The effect of the geostrophic flow upon coastal sea elevations in the Northern North Pacific Ocean. Submitted to J. Geophys. Res.

Smith, R. L. 1968. Upwelling. Oceanogr. Mar. Biol. Ann. Rev., 6, 11-46.

_____ 1974. A description of current, wind, and sea level variations during coastal upwelling off the Oregon coast, July - August 1972. J. Geophys. Res., 79, 435-443.

Smith, R. L., C. N. K. Mooers, and D. B. Enfield. 1971. Mesoscale studies of the physical oceanography in two coastal upwelling regions: Oregon and Peru. In: Fertility of the Sea, Vol. 2, Edited by J. D. Costlow, Jr., Gordon and Breach Science Publishers, New York. pp. 513-535.

Smith, R. L., J. G. Pattullo, and R. K. Lane. 1966. An investigation of the early stage of upwelling along the Oregon coast. J. Geophys. Res., 71, 1135-1140.

Smith, S. D. and E. G. Banke. 1975. Variation of the sea surface drag coefficient with wind speed. Quart. J. R. Met. Soc., 101, 665-673.

Stevenson, M. R., R. W. Garvine, and B. Wyatt. 1974. Lagrangian measurements in a coastal upwelling zone off Oregon. J. Phys. Oceanogr., 4, 321-336.

Sverdrup, H. U. 1938. On the process of upwelling. J. Mar. Res., 1, 155-164.

Thompson, J. D. 1974. The coastal upwelling cycle on a beta-plane: hydrodynamics and thermodynamics. Technical Report. Dept. of Meteorology, Florida State University, Tallahassee. 141 pp.

Van Leer, J. 1974. Progress report on cyclesonde development and use. Technical Report, UM-RSMAS-74029. Rosenstiel School of Marine and Atmospheric Science, University of Miami, Miami. 77 pp.

Yoshida, K. 1955. Coastal upwelling off the California coast. Rec. Oceanogr. Works Jap., 2, 8-20.

APPENDICES

APPENDIX I.

Low-passed Time Series of Sea Level,
Winds, and Currents.

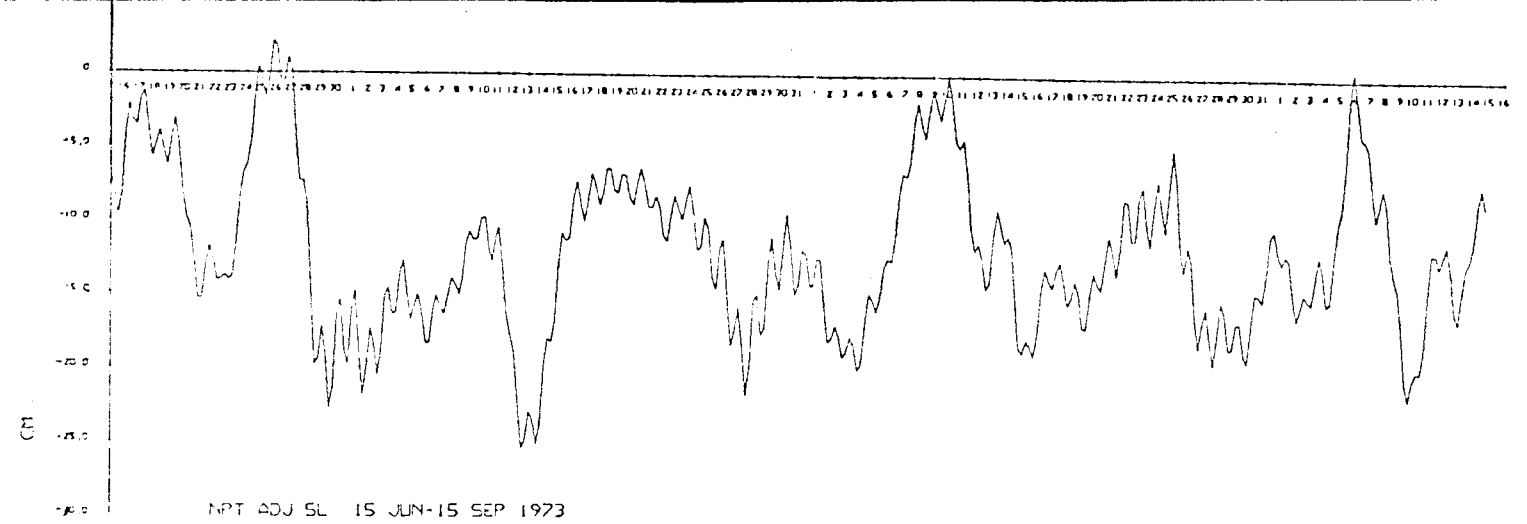
CM
NPT ADJ SL 15 JUN-15 SEP 1973

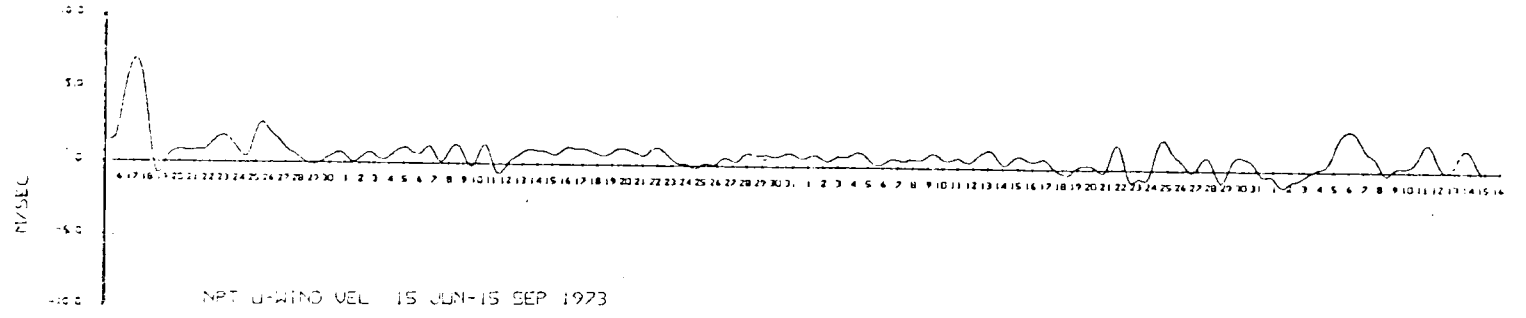
M/SEC
NPT U-WIND VEL 15 JUN-15 SEP 1973

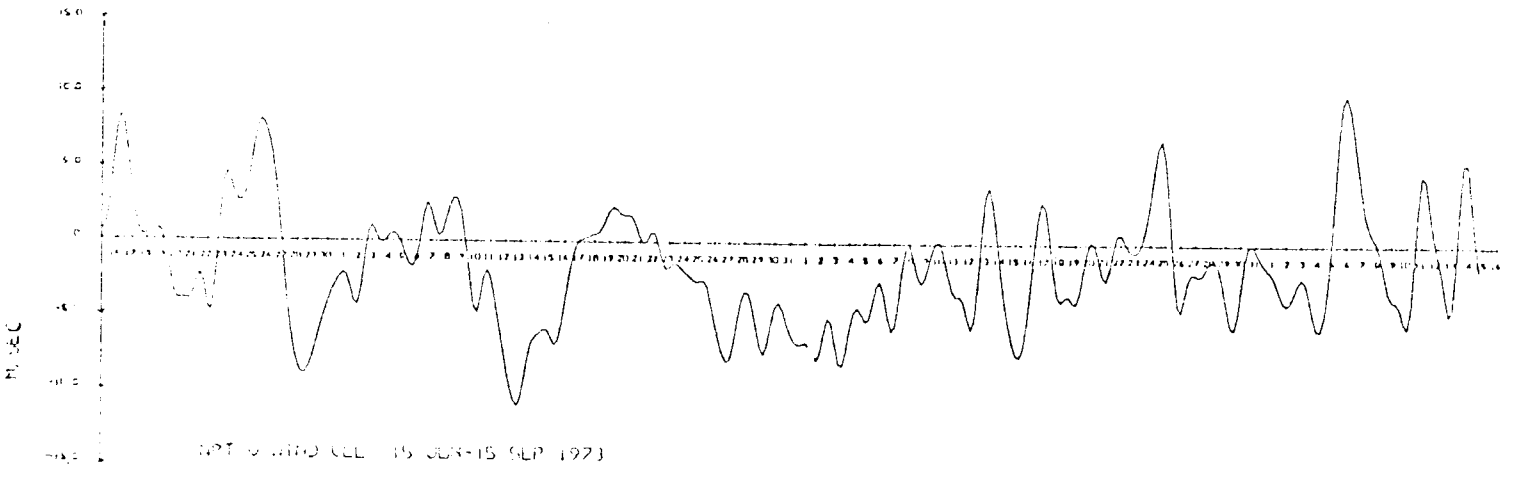
M/SEC
NPT V-WIND VEL 15 JUN-15 SEP 1973

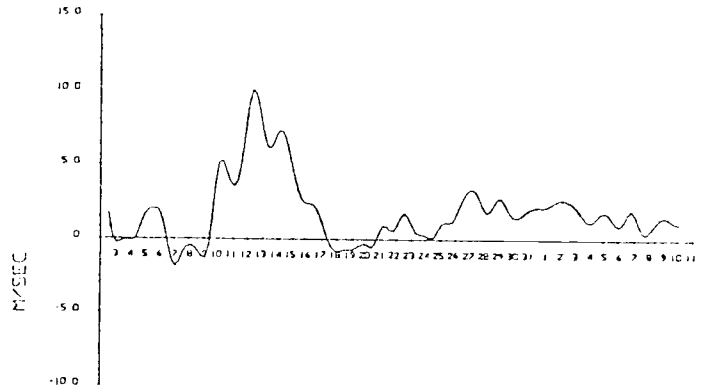

SFC ASTER LLU-WIND VEL 2 JUL - 10 AUG 73

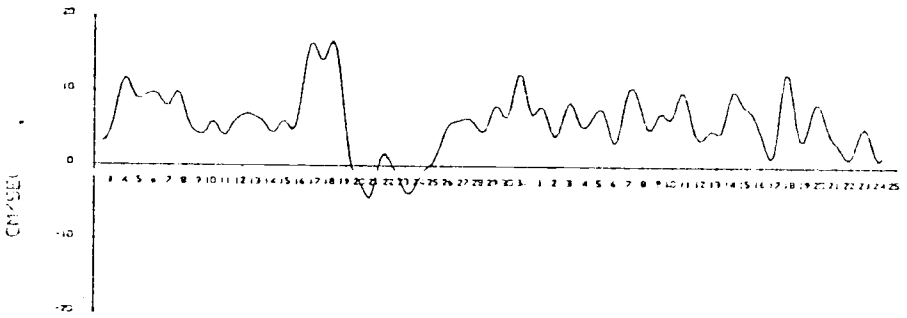

20M ASTER LLU-CURRENT VEL 2 JUL - 24 AUG 73

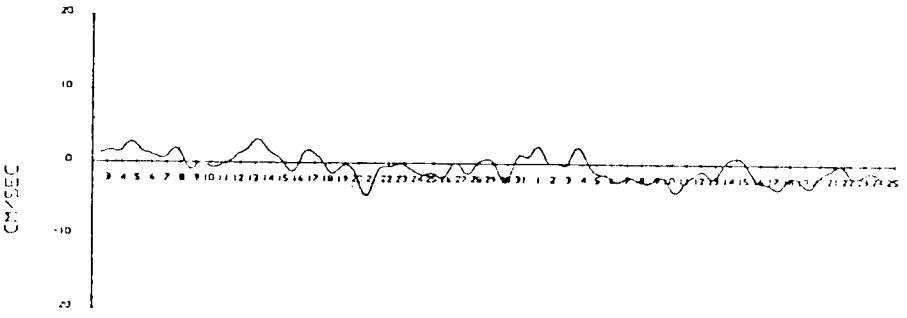

40M ASTER LLU-CURRENT VEL 2 JUL-24 AUG 73

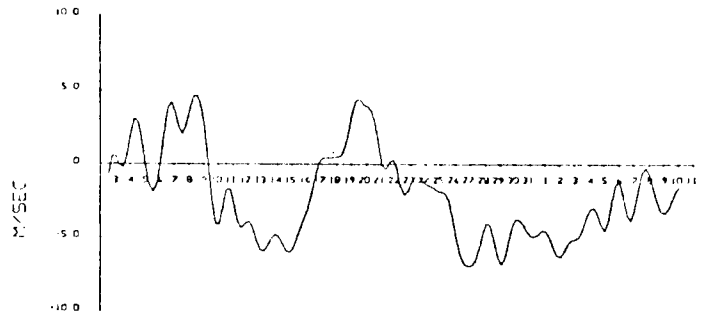

SFC ASTER LLV-WIND VEL 2 JUL- 10 AUG 73

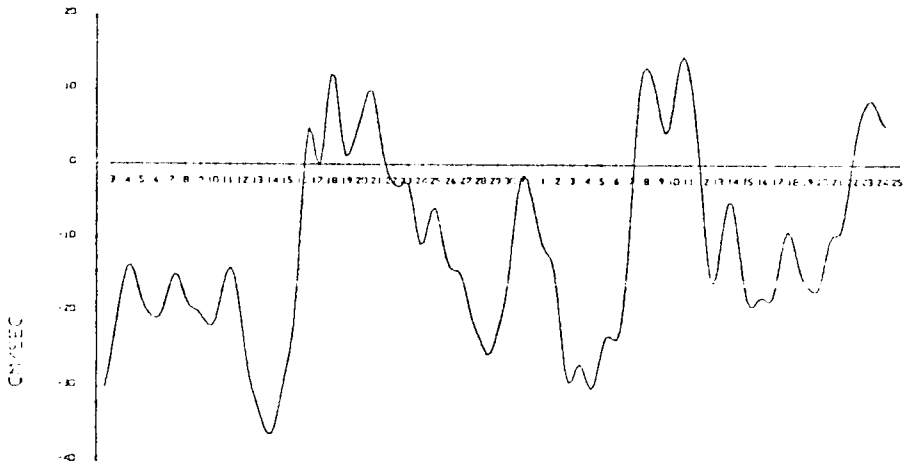

20M ASTER LLV-CURRENT VEL 2 JUL- 24 AUG 73

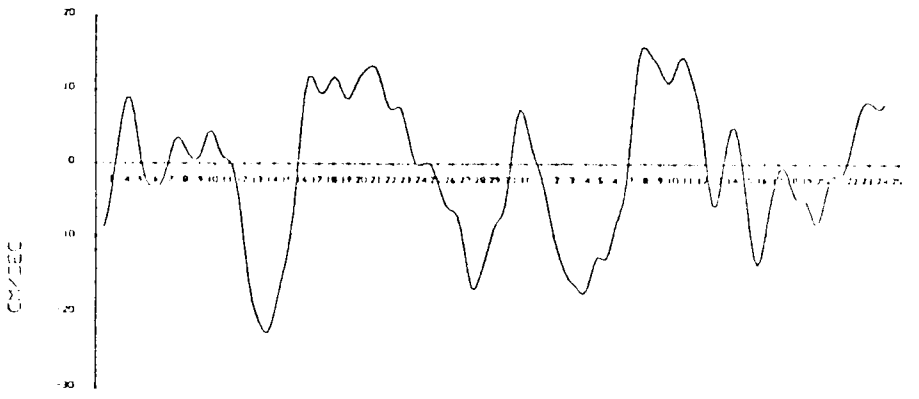

40M ASTER LLV-CURRENT VEL 2 JUL-24 AUG 73

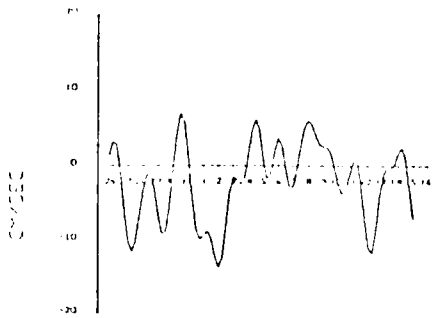

8.5M *ASTR LLU-CURRENT VEL 25 JUL-14 AUG 73

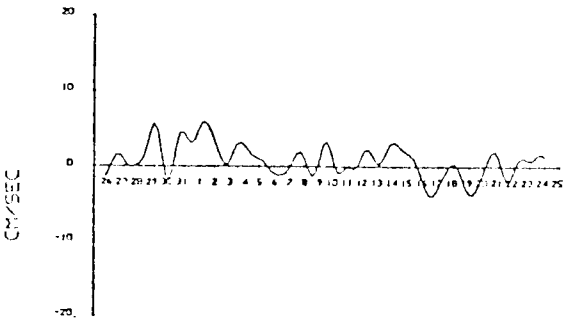

40M *ASTR LLU-CURRENT VEL 25 JUL- 23 AUG 73

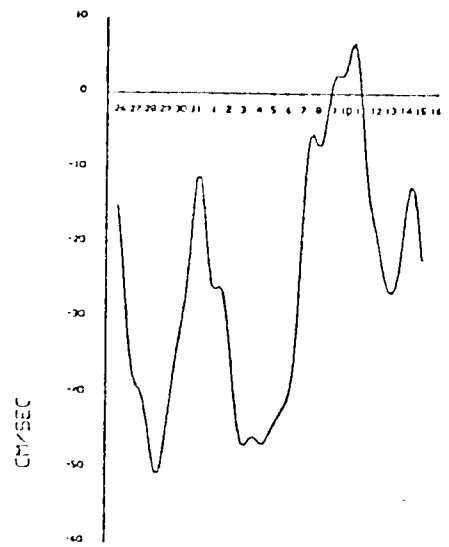

8.5M *ASTR LLU-CURRENT VEL 25 JUL- 14 AUG 73

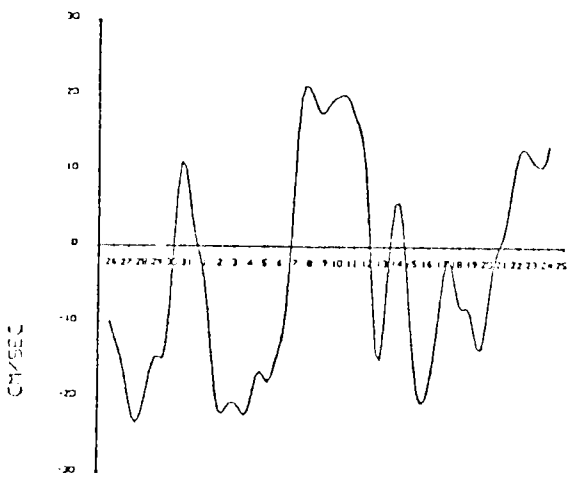

40M *ASTR LLU-CURRENT VEL 25 JUL- 23 AUG 73

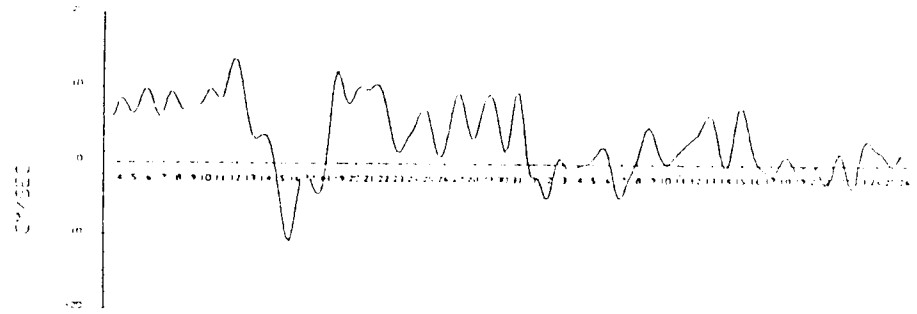

20M CARNA LLU-CURRENT VEL 3 JUL- 25 AUG 73

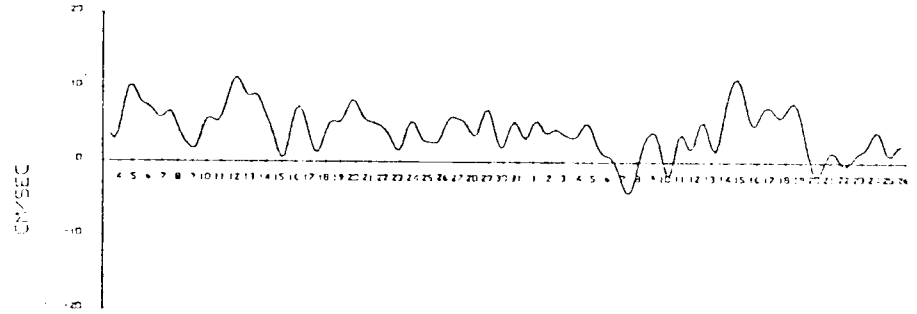

40M CARNA LLU-CURRENT VEL 3 JUL- 25 AUG 73

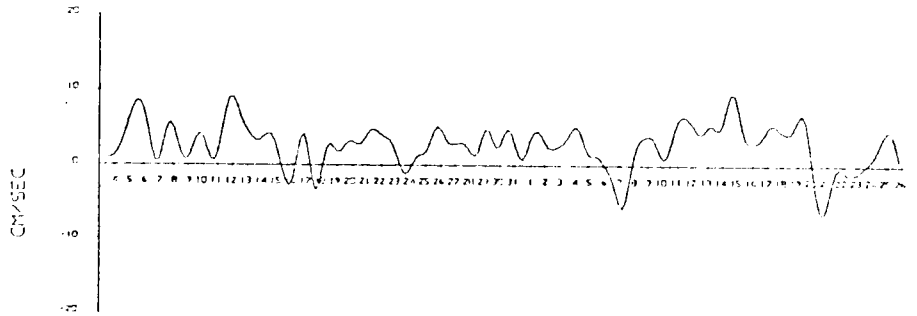

60M CARNA LLU-CURRENT VEL 3 JUL- 25 AUG 73

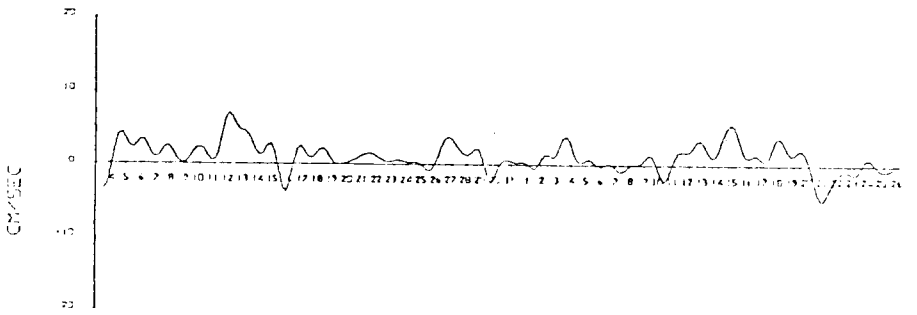

80M CARNA LLU-CURRENT VEL 3 JUL- 25 AUG 73

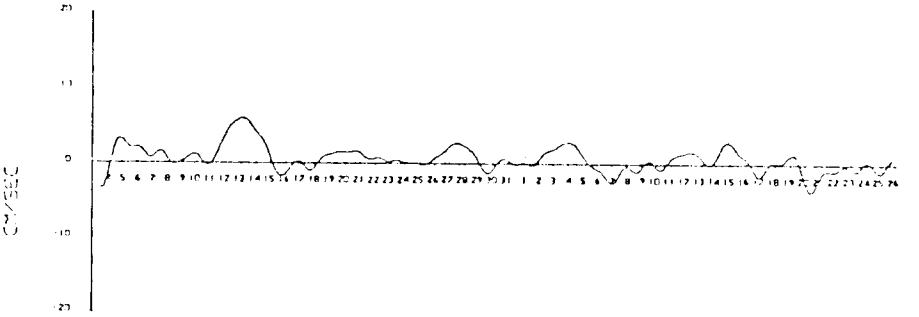

95M CARNA LLU-CURRENT VEL 3 JUL- 25 AUG 73

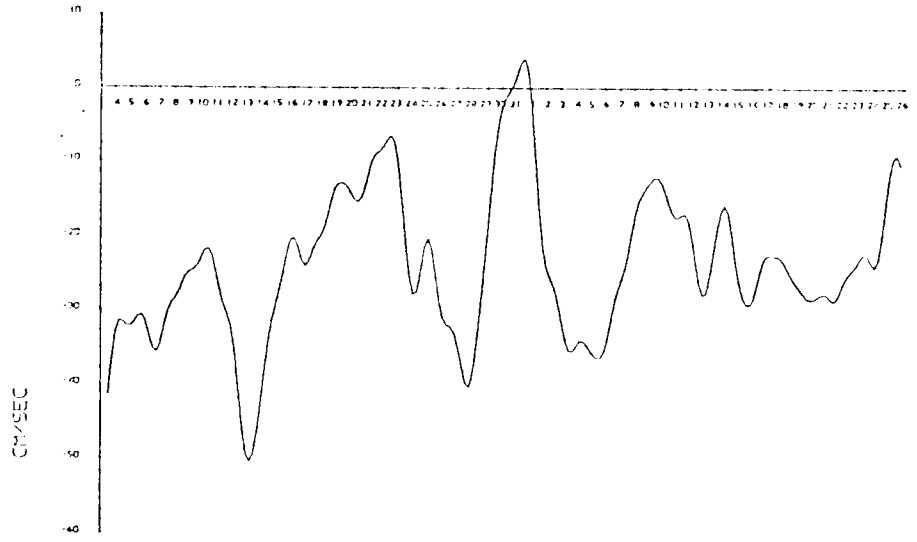

20M CARNA LLV-CURRENT VEL 3 JUL- 25 AUG 73

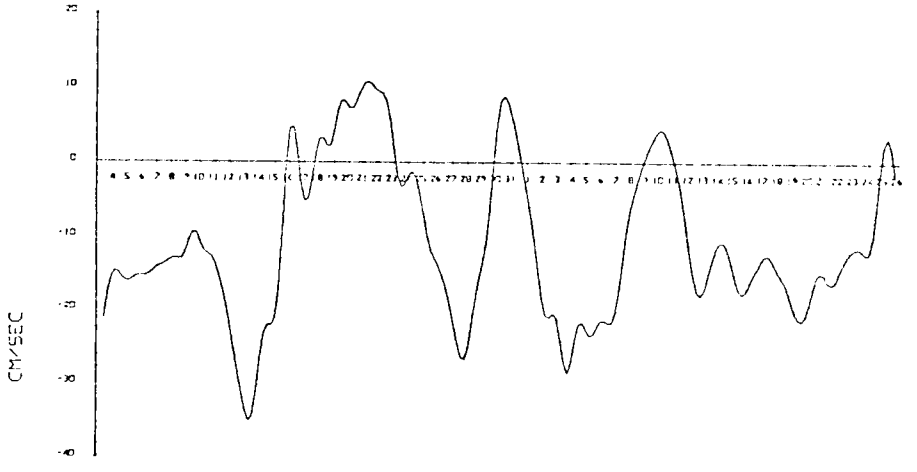

40M CARNA LLV-CURRENT VEL 3 JUL- 25 AUG 73

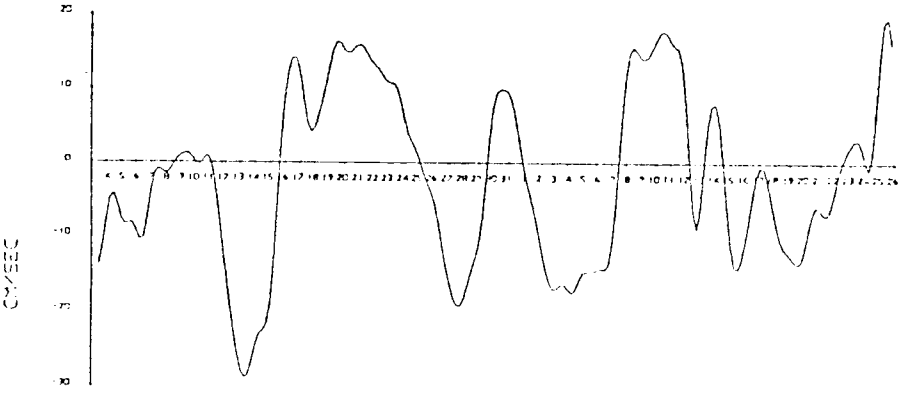

60M CARNA LLV-CURRENT VEL 3 JUL- 25 AUG 73

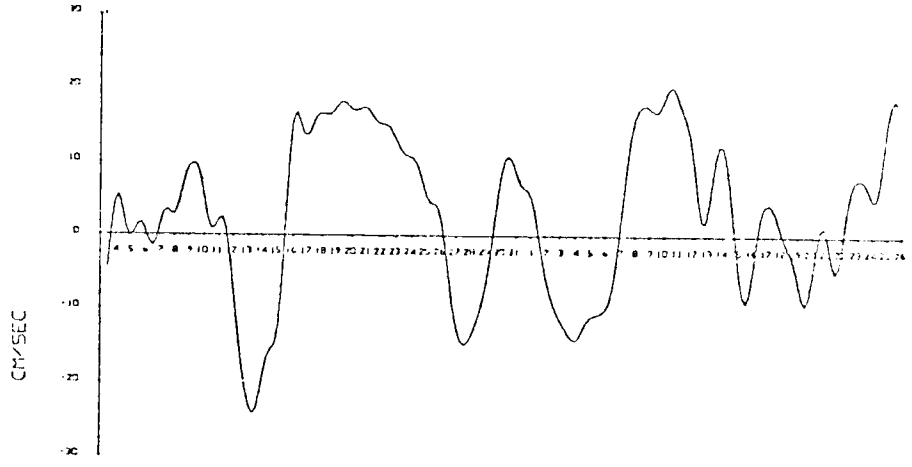

BOM CARNA LLV-CURRENT VEL 3 JUL- 25 AUG 73

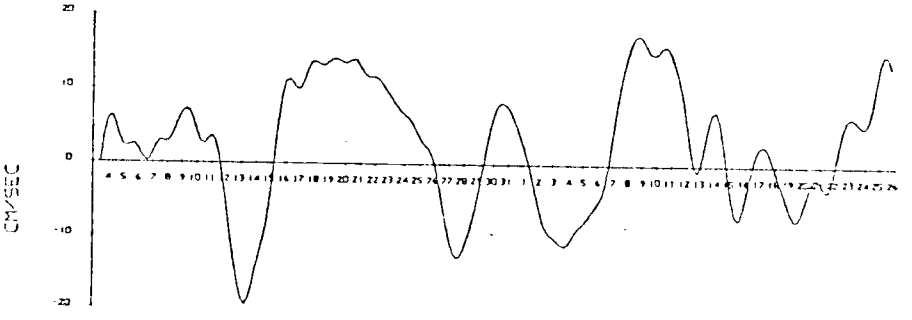

95M CARNA LLV-CURRENT VEL 3 JUL- 25 AUG 73

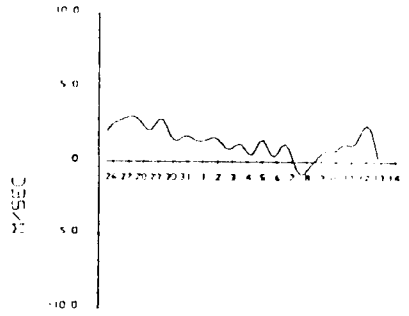

SFC EDELW LLU-WIND VEL 25 JUL- 12 AUG 73

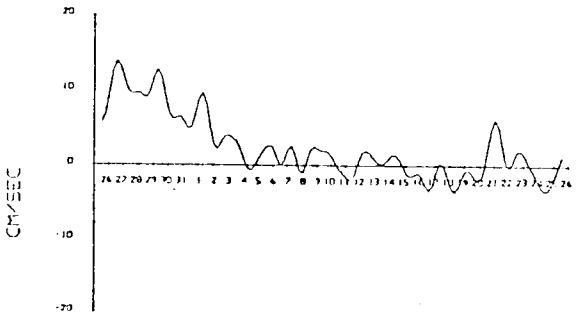

20M EDELW LLU-CURRENT VEL 25 JUL- 25 AUG 73

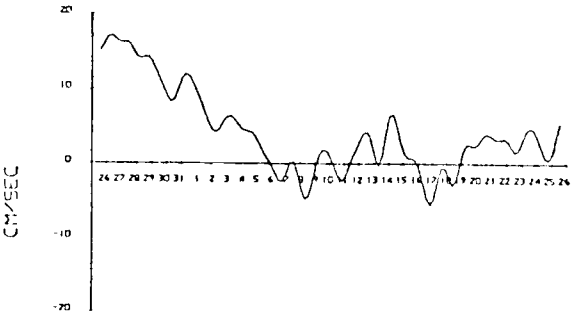

40M EDELW LLU-CURRENT VEL 25 JUL- 25 AUG 73

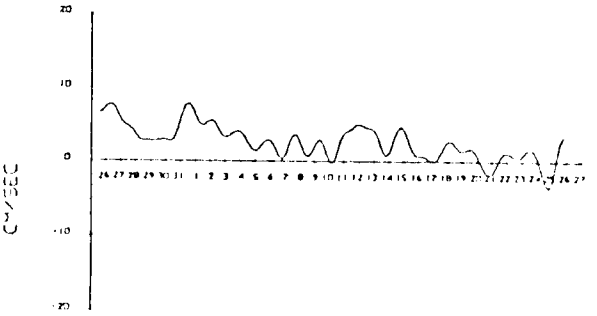

80M EDELW LLU-CURRENT VEL 25 JUL- 25 AUG 73

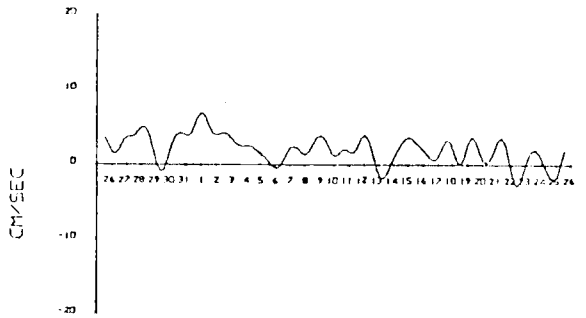

120M EDELW LLU-CURRENT VEL 25 JUL- 25 AUG 73

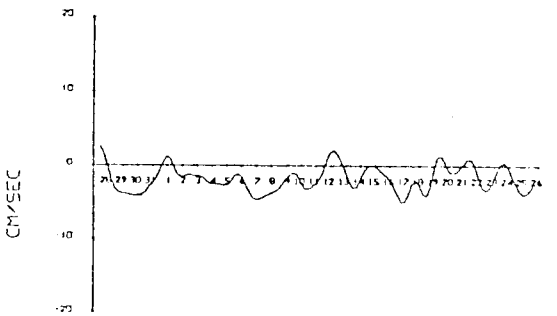

180M EDELW LLU-CURRENT VEL 27 JUL- 25 AUG 73

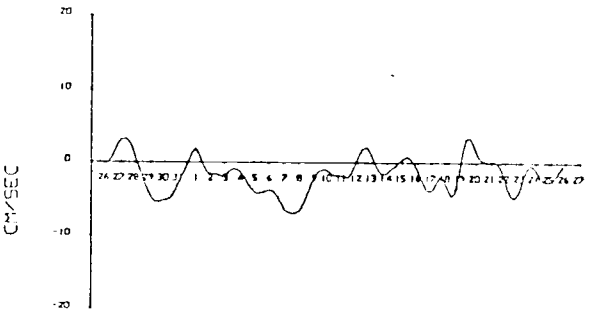

195M EDELW LLU-CURRENT VEL 25 JUL- 25 AUG 73

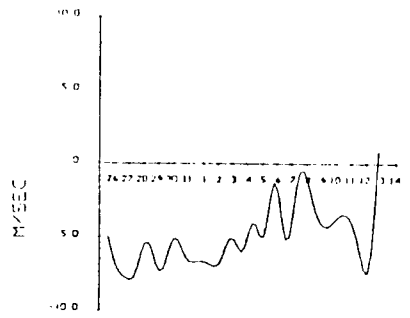

SFC EDELW LLV-WIND VEL 25 JUL- 12 AUG 23

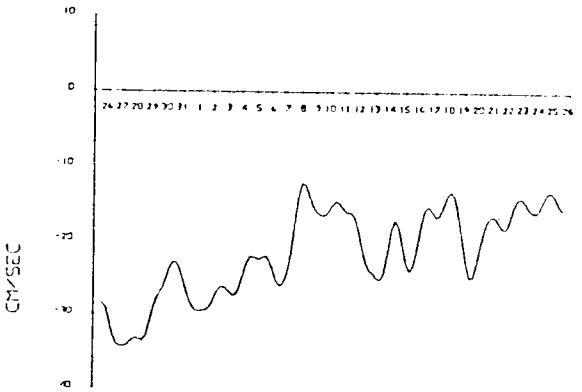

20M EDELW LLV-CURRENT VEL 25 JUL- 25 AUG 23

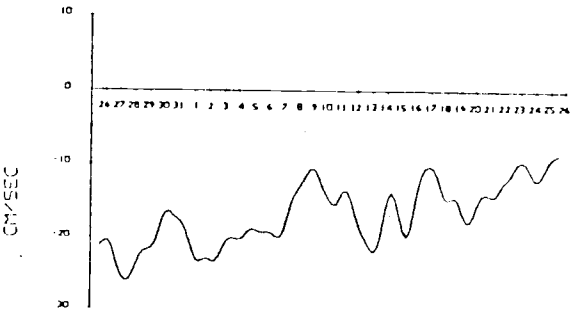

40M EDELW LLV-CURRENT VEL 25 JUL- 25 AUG 23

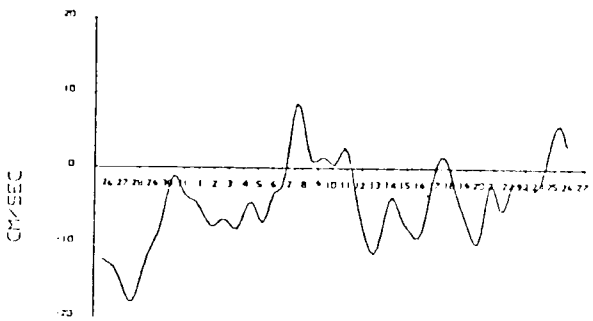

80M EDELW LLV-CURRENT VEL 25 JUL- 25 AUG 23

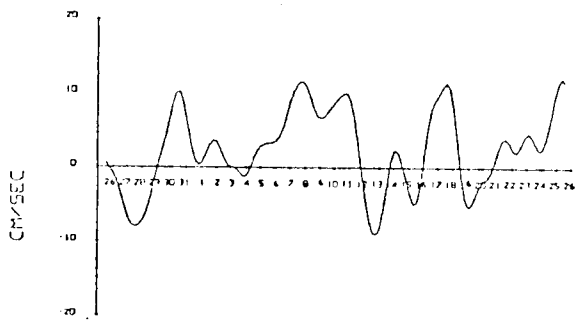

120M EDELW LLV-CURRENT VEL 25 JUL- 25 AUG 73

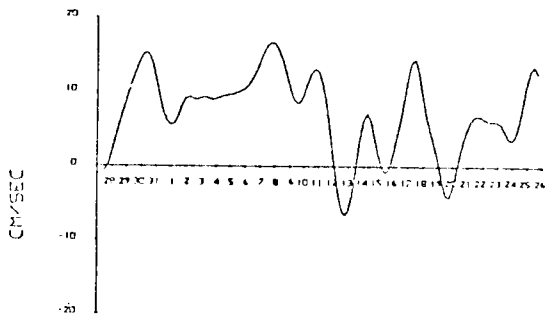

180M EDELW LLV-CURRENT VEL 27 JUL- 25 AUG 73

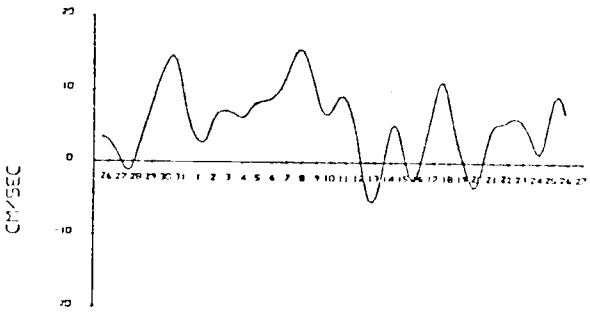

195M EDELW LLV-CURRENT VEL 25 JUL- 25 AUG 73

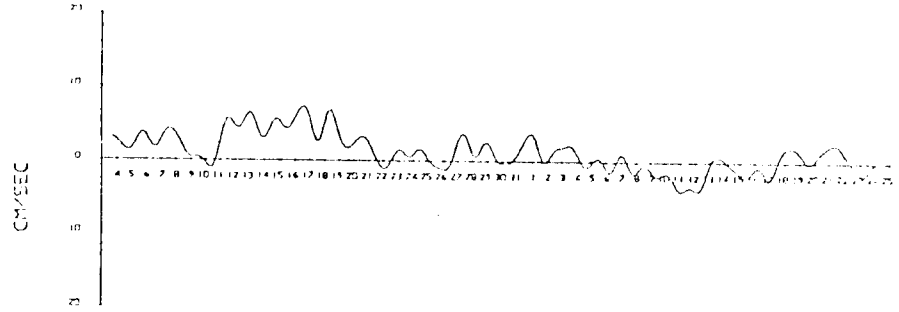

40M FGRSY LLU-CURRENT VEL 3 JUL- 23 AUG 73

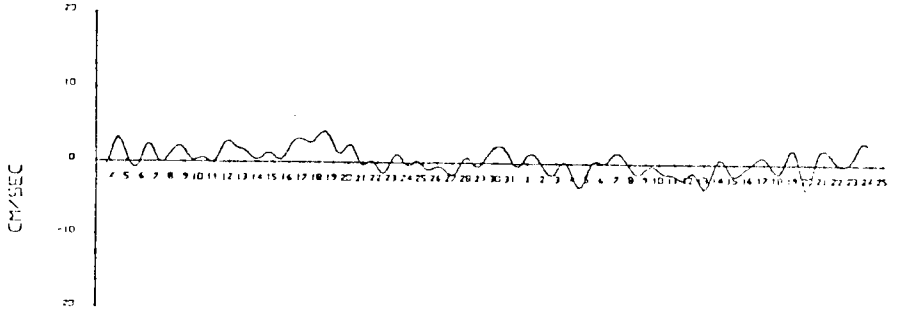

80M FGRSY LLU-CURRENT VEL 3 JUL- 23 AUG 73

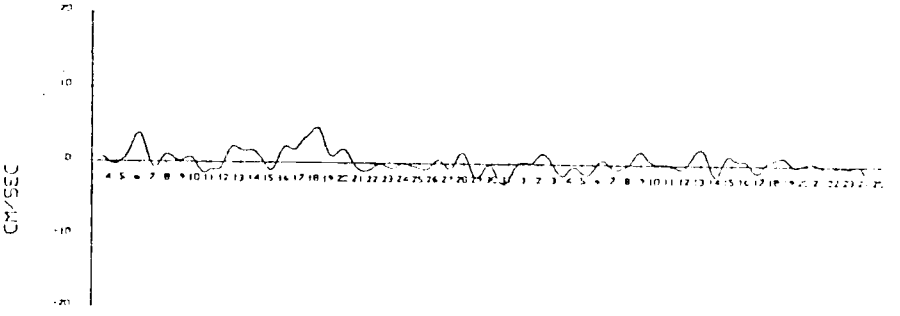

120M FGRSY LLU-CURRENT VEL 3 JUL-23 AUG 73

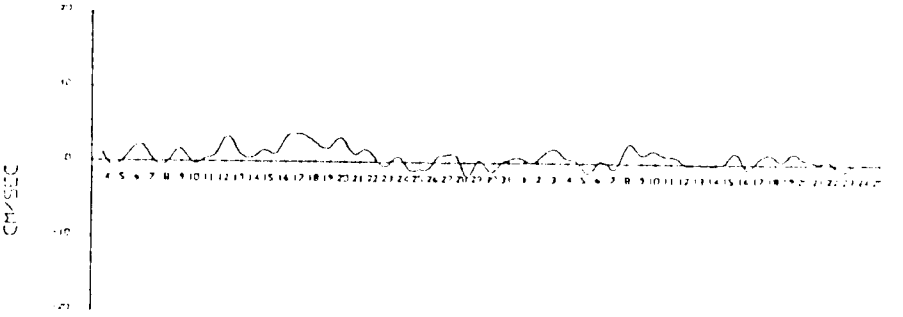

180M FGRSY LLU-CURRENT VEL 3 JUL- 23 AUG 73

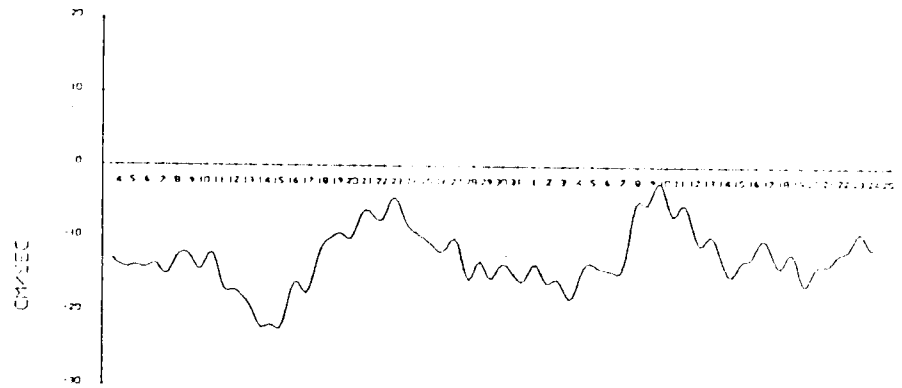

401 FGRSY LLU-CURRENT VEL 3 JUL- 23 AUG 73

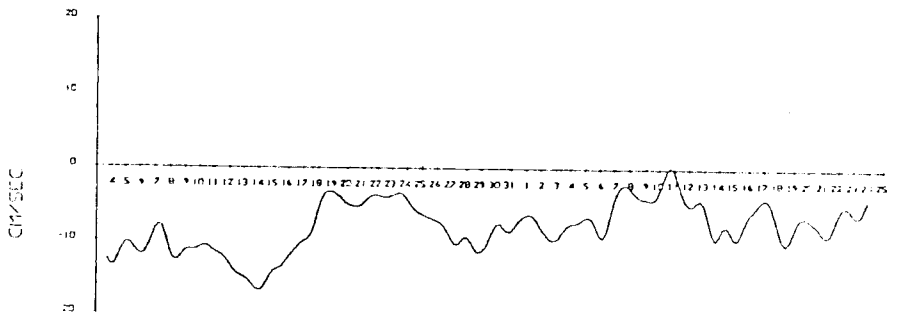

801 FGRSY LLU-CURRENT VEL 3 JUL- 23 AUG 73

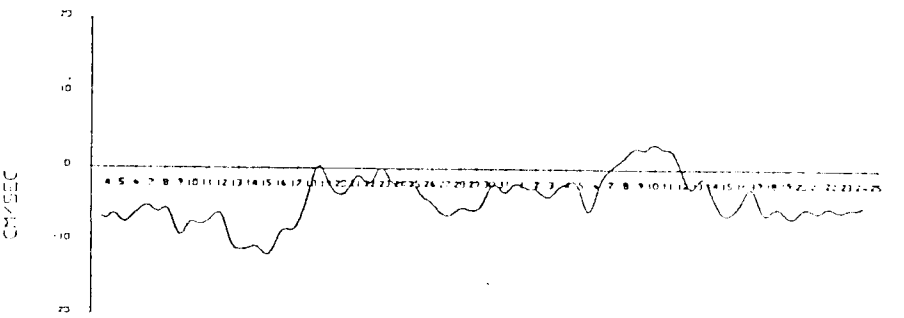

1201 FGRSY LLU-CURRENT VEL 3 JUL- 23 AUG 73

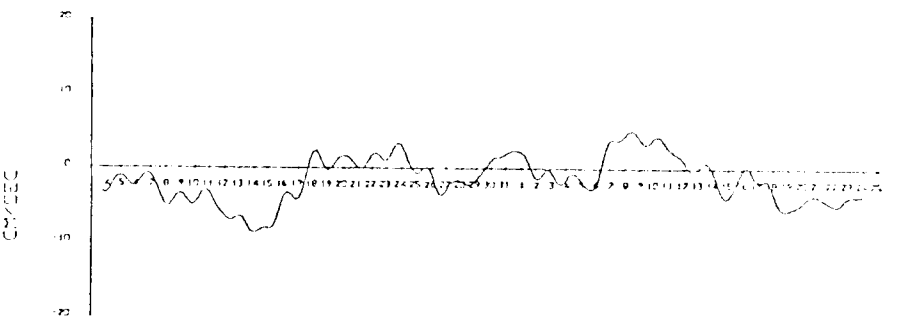

1801 ENRGY LLU-CURRENT VEL 3 JUL- 23 AUG 73

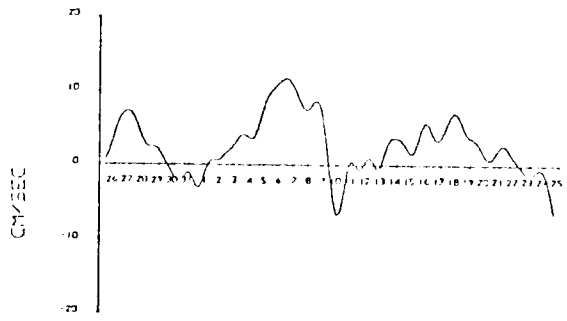

20M F-M-N LLU-CURRENT VEL 25 JUL-24 AUG 73

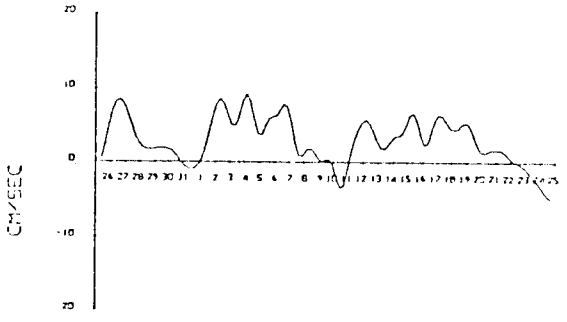

40M F-M-N LLU-CURRENT VEL 25 JUL-24 AUG 73

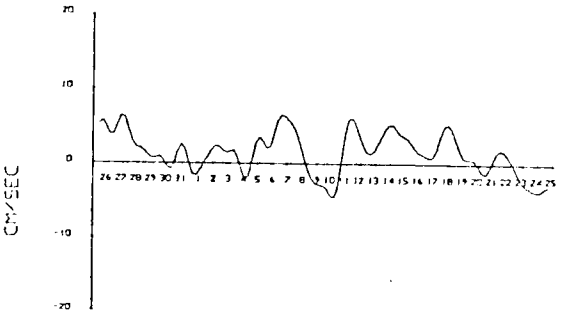

60M F-M-N LLU-CURRENT VEL 25 JUL-24 AUG 73

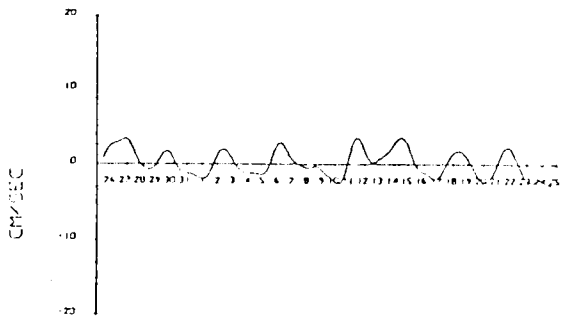

80M F-M-N LLU-CURRENT VEL 25 JUL-24 AUG 73

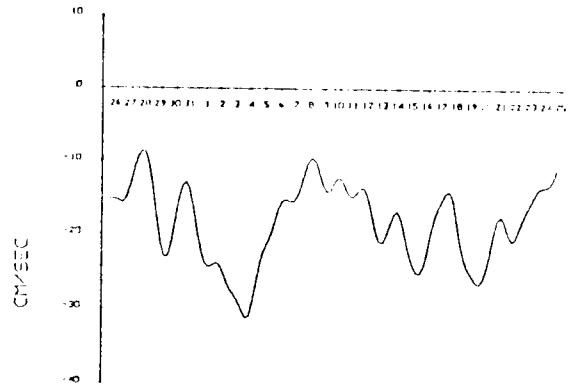

20M F-M-N LLV-CURRENT VEL 25 JUL-24 AUG 73

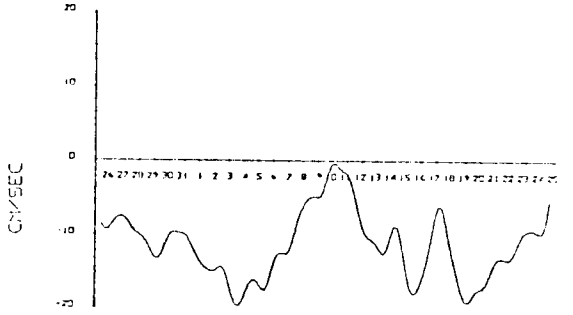

40M F-M-N LLV-CURRENT VEL 25 JUL-24 AUG 73

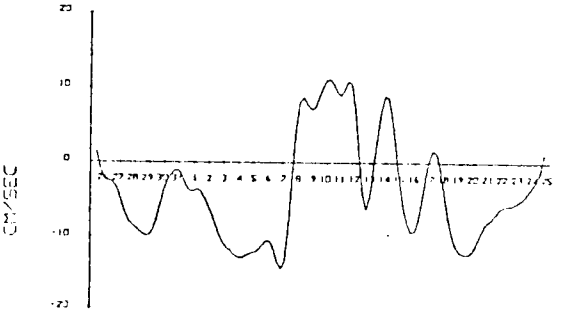

60M F-M-N LLV-CURRENT VEL 25 JUL-24 AUG 73

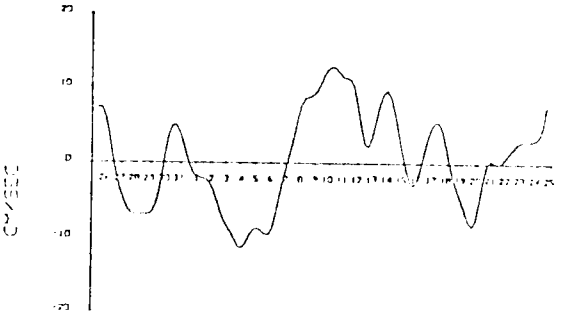

80M F-M-N LLV-CURRENT VEL 25 JUL-24 AUG 73

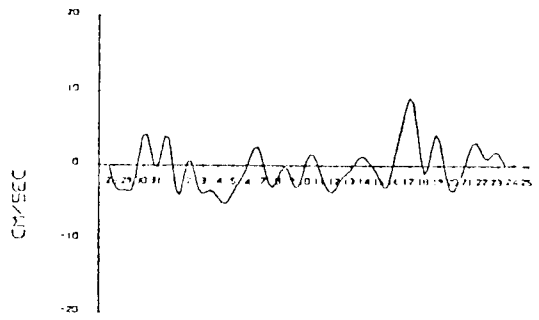

20M IRIS LLU-CURRENT VEL 27 JUL-24 AUG 73

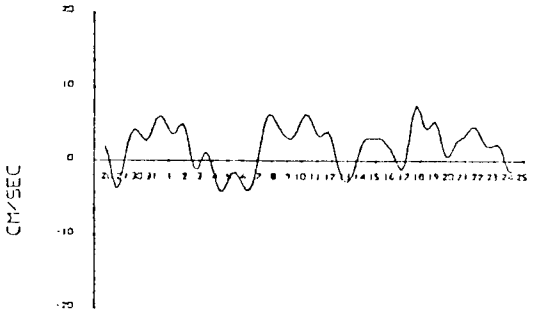

40M IRIS LLU-CURRENT VEL 27 JUL-24 AUG 73

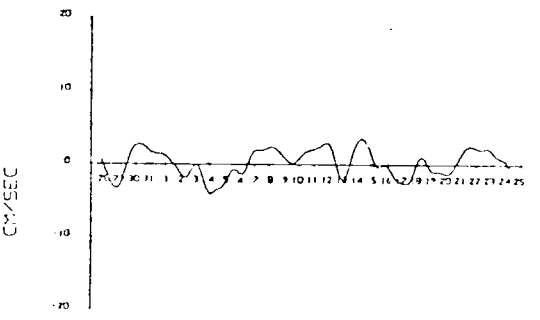

60M IRIS LLU-CURRENT VEL 27 JUL-24 AUG 73

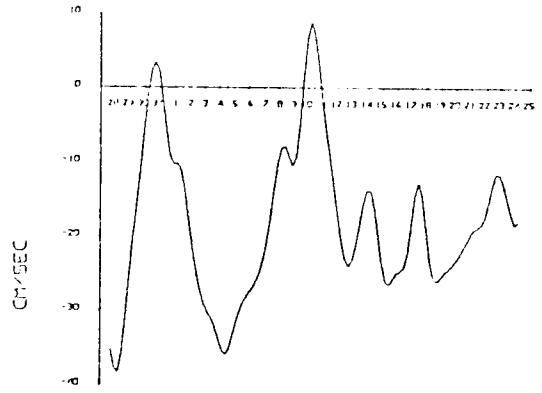

20M IRIS LLV-CURRENT VEL 27 JUL-24 AUG 73

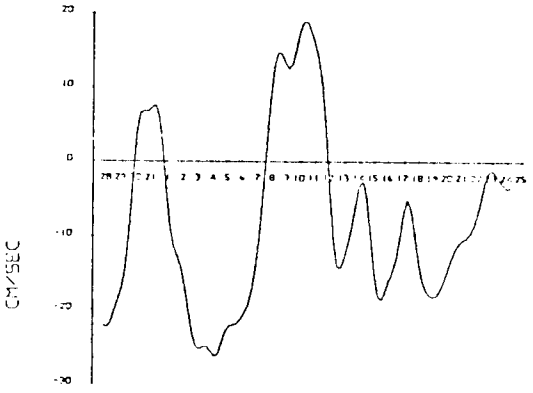

40M IRIS LLV-CURRENT VEL 27 JUL-24 AUG 73

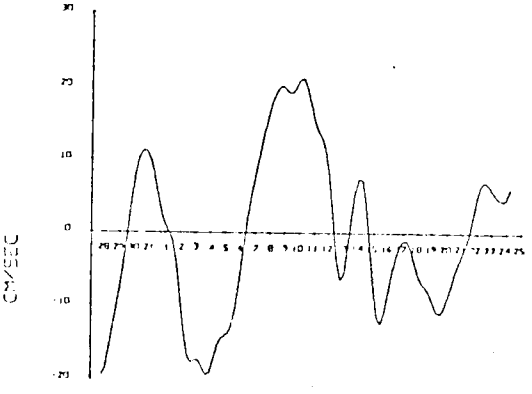

60M IRIS LLV-CURRENT VEL 27 JUL-24 AUG 73

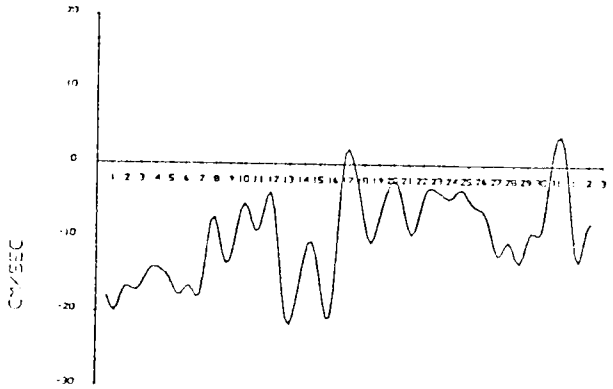

20M PS(D) LLU-CURRENT VEL 30 JUN- 2 AUG 73

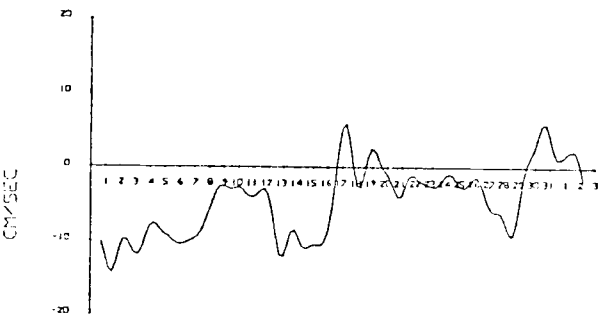

40M PS(D) LLU-CURRENT VEL 30 JUN- 2 AUG 73

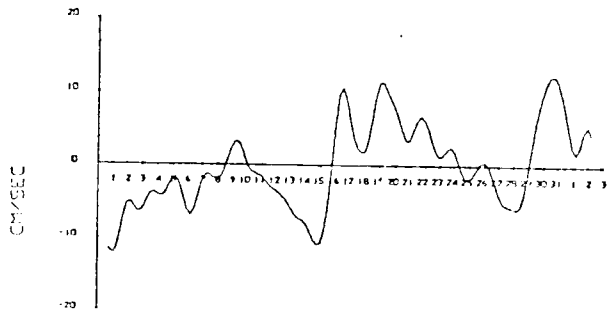

60M PS(D) LLU-CURRENT VEL 30 JUN- 2 AUG 73

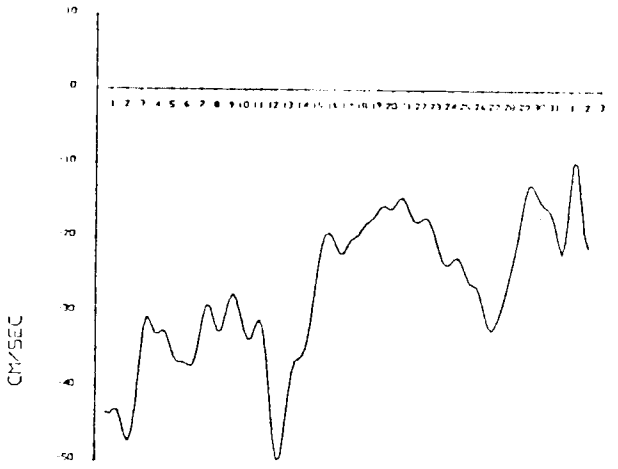

20M PS(D) LLV-CURRENT VEL 30 JUN- 2 AUG 73

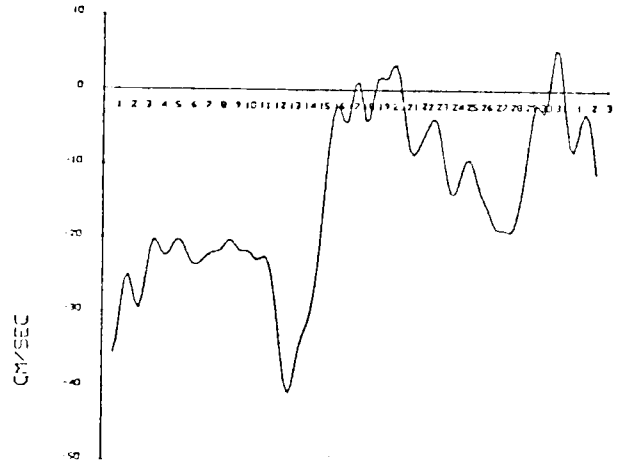

40M PS(D) LLV-CURRENT VEL 30 JUN- 2 AUG 73

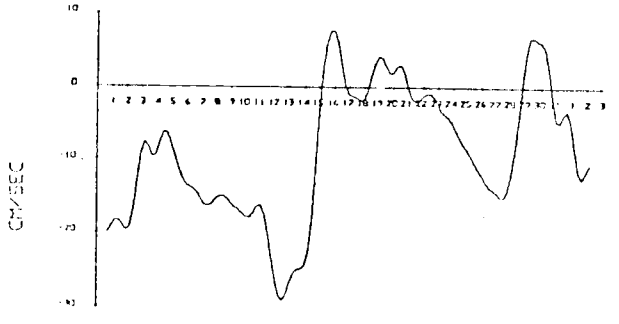

60M PS(D) LLV-CURRENT VEL 30 JUN- 2 AUG 73

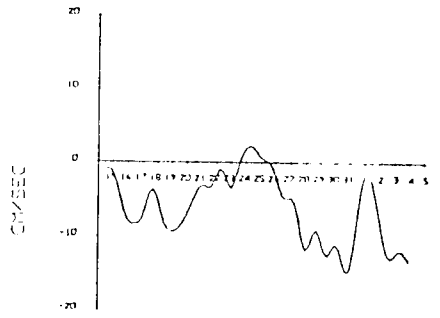

20M PS(E) LLU-CURRENT VEL 14 AUG- 3 SEP 73

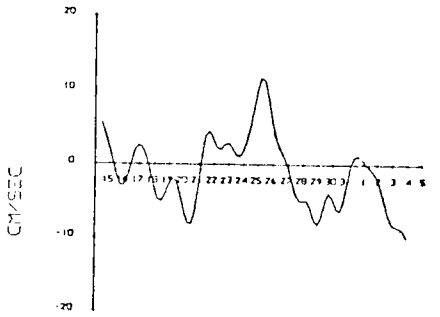

40M PS(E) LLU-CURRENT VEL 14 AUG- 3 SEP 73

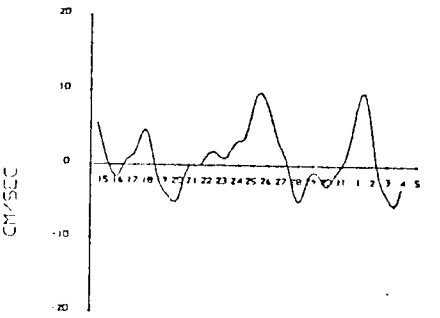

60M PS(E) LLU-CURRENT VEL 14 AUG- 3 SEP 73

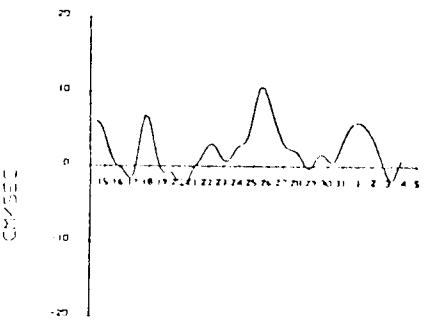

80M PS(E) LLU-CURRENT VEL 14 AUG- 3 SEP 73

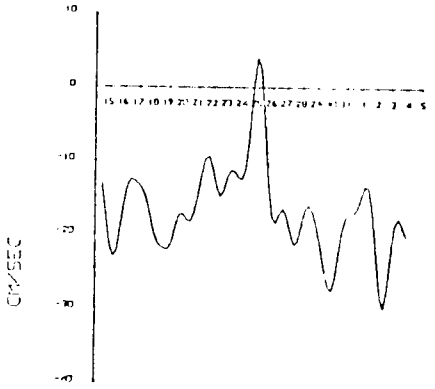

20M PS(E) LLV-CURRENT VEL 14 AUG- 3 SEP 73

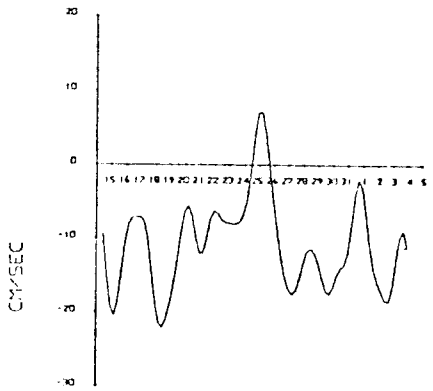

40M PS(E) LLV-CURRENT VEL 14 AUG- 3 SEP 73

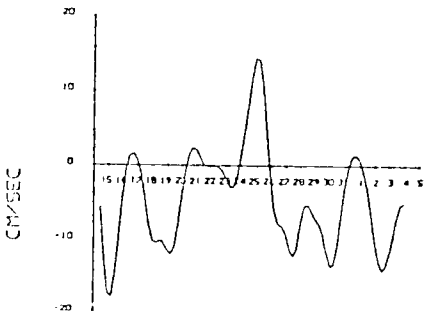

60M PS(E) LLV-CURRENT VEL 14 AUG- 3 SEP 73

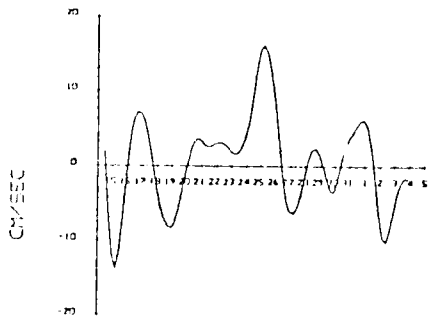

80M PS(E) LLV-CURRENT VEL 14 AUG- 3 SEP 73

APPENDIX II.

Zonal Sections of the Vertical Distribution of Temperature, Salinity and Density (σ_t).

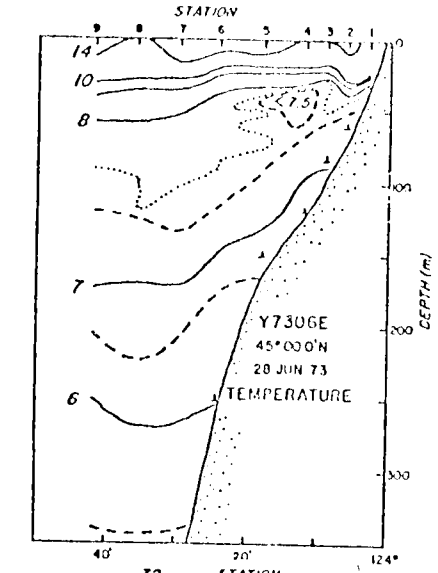
STATION
9 8 7 6 5 4 3 2 1
14
10
8
7
6
Y7306E
45°00.0'N
28 JUN 73
TEMPERATURE
DEPTH (m)
0
100
200
300
40'
20'
124°

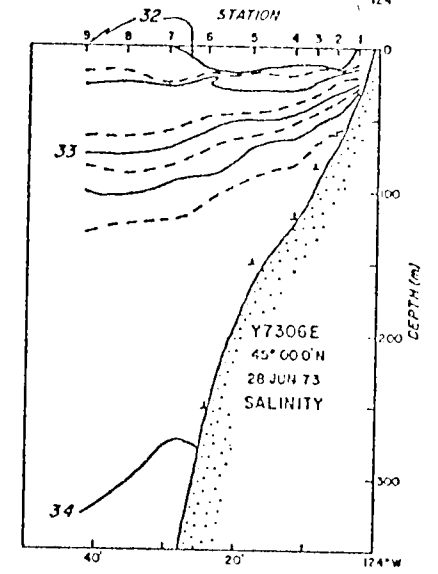
32
STATION
9 8 7 6 5 4 3 2 1
33
34
Y7306E
45°00.0'N
28 JUN 73
SALINITY
DEPTH (m)
0
100
200
300
40'
20'
124°W

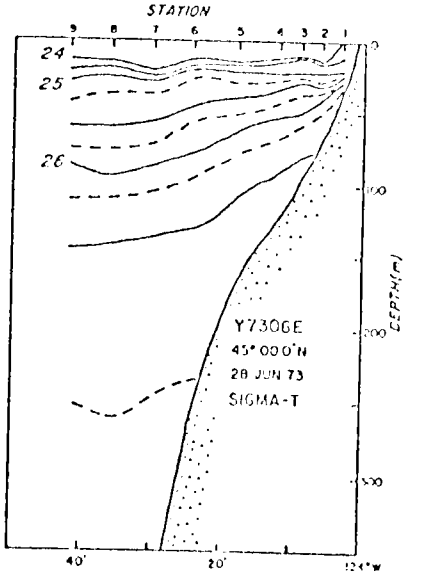
STATION
9 8 7 6 5 4 3 2 1
24
25
26
Y7306E
45°00.0'N
28 JUN 73
SIGMA-T
DEPTH (m)
0
100
200
300
40'
20'
124°W

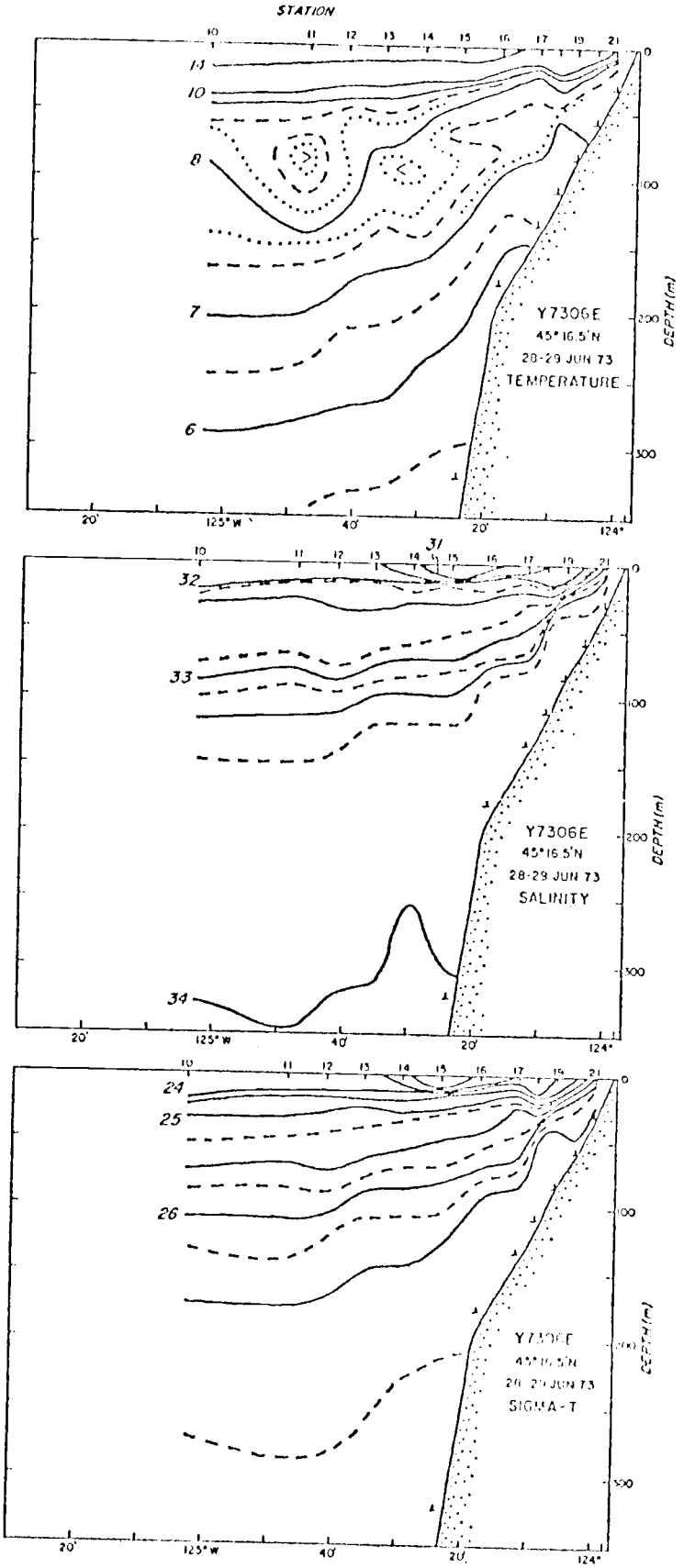
STATION
10 11 12 13 14 15 16 17 19 21
13
10
8
7
6
Y7306E
45°16.5'N
28-29 JUN 73
TEMPERATURE
DEPTH(m)
0
100
200
500
20'
125°W
40'
20'
124°
31
32
33
34
Y7306E
45°16.5'N
28-29 JUN 73
SALINITY
24
25
26
Y7306E
45°16.5'N
28-29 JUN 73
SIGMA-T

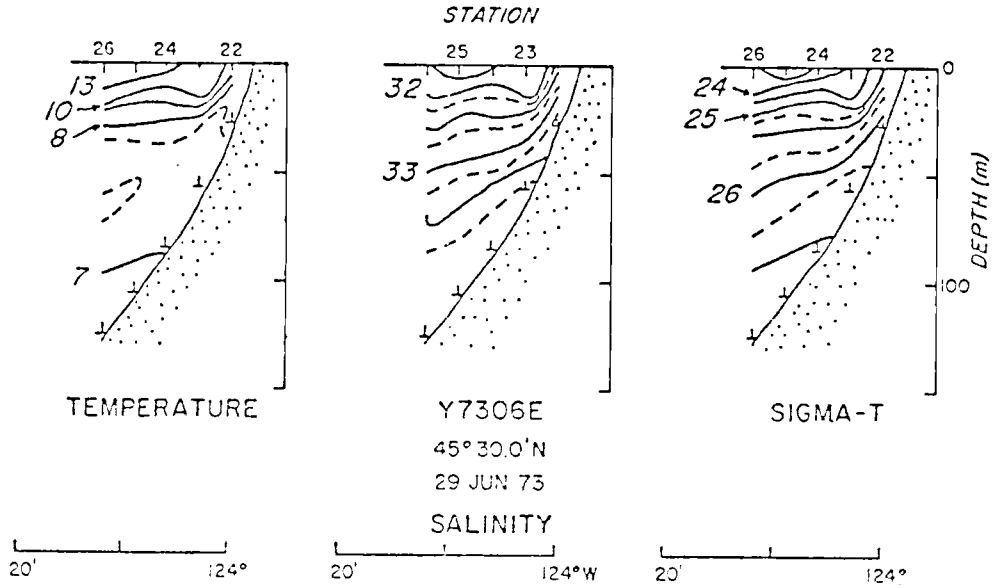
STATION
26
24
22
13
10
8
7
TEMPERATURE
25
23
32
33
Y7306E
45°30.0'N
29 JUN 73
SALINITY
26
24
22
24
25
26
0
100
DEPTH (m)
SIGMA-T
20'
124°
20'
124°W
20'
124°

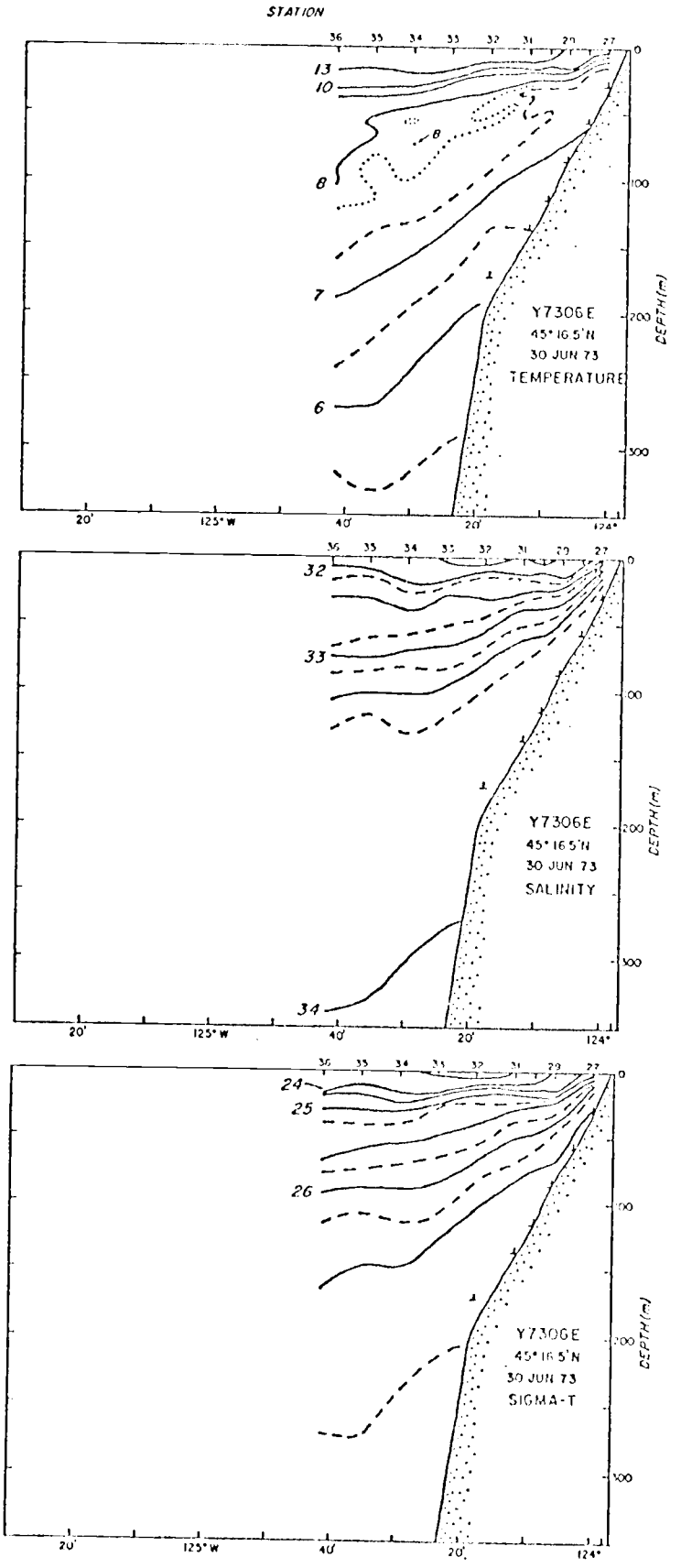
STATION
13
10
8
7
6
Y7306E
45°16.5'N
30 JUN 73
TEMPERATURE
DEPTH (m)
125°W
32
33
34
SALINITY
24
25
26
SIGMA-T

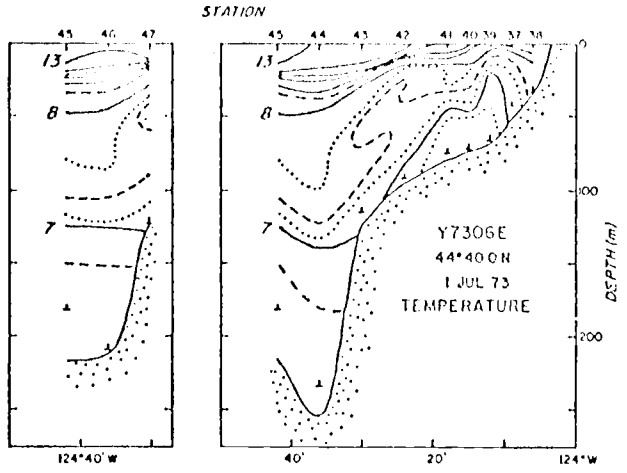
STATION
45 46 47
45 44 43 42 41 40 39 38 37 36
13
8
7
Y7306E
44°40.0N
1 JUL 73
TEMPERATURE
DEPTH (m)
0
100
200
124°40'W
40'
20'
124°W

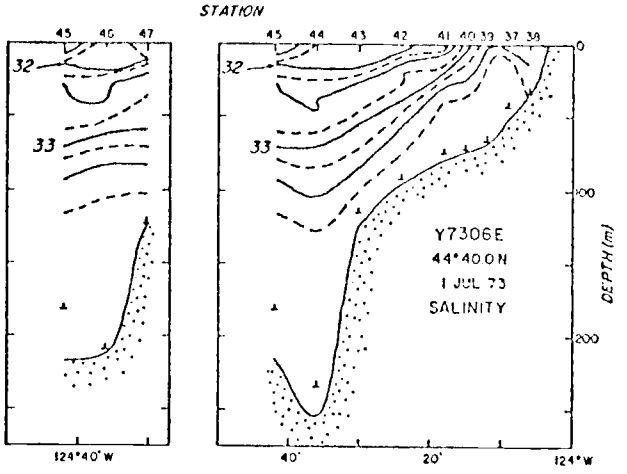
STATION
45 46 47
45 44 43 42 41 40 39 38 37 36
32
33
Y7306E
44°40.0N
1 JUL 73
SALINITY
DEPTH (m)
0
100
200
124°40'W
40'
20'
124°W

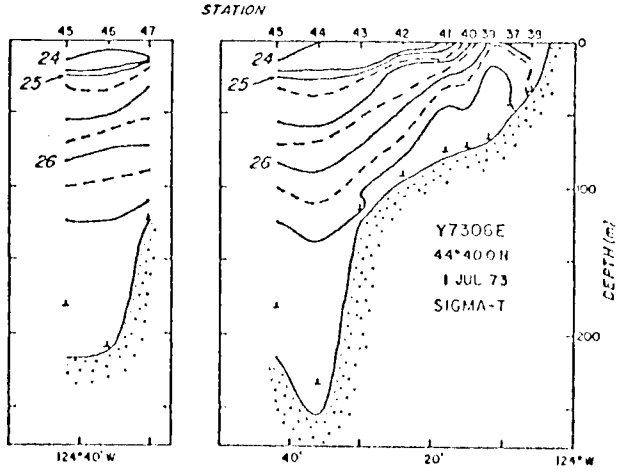
STATION
45 46 47
45 44 43 42 41 40 39 38 37 36
24
25
26
Y7306E
44°40.0N
1 JUL 73
SIGMA-T
DEPTH (m)
0
100
200
124°40'W
40'
20'
124°W

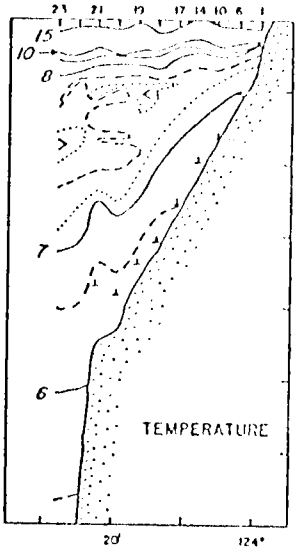
23 21 19 17 14 10 6 1
15
10
8
7
6
TEMPERATURE
20°
124°

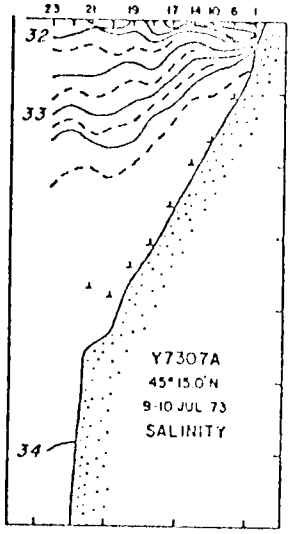
23 21 19 17 14 10 6 1
32
33
Y7307A
45°15.0'N
9-10 JUL 73
SALINITY
34

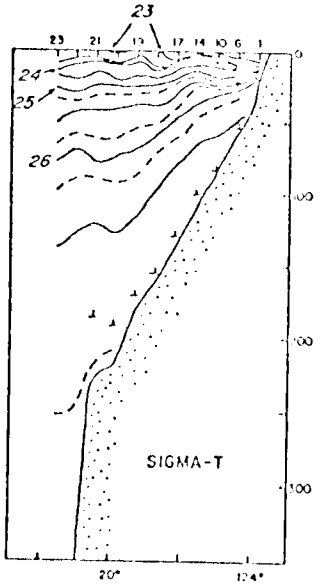
23
23 21 19 17 14 10 6 1
24
25
26
SIGMA-T
20°
124°

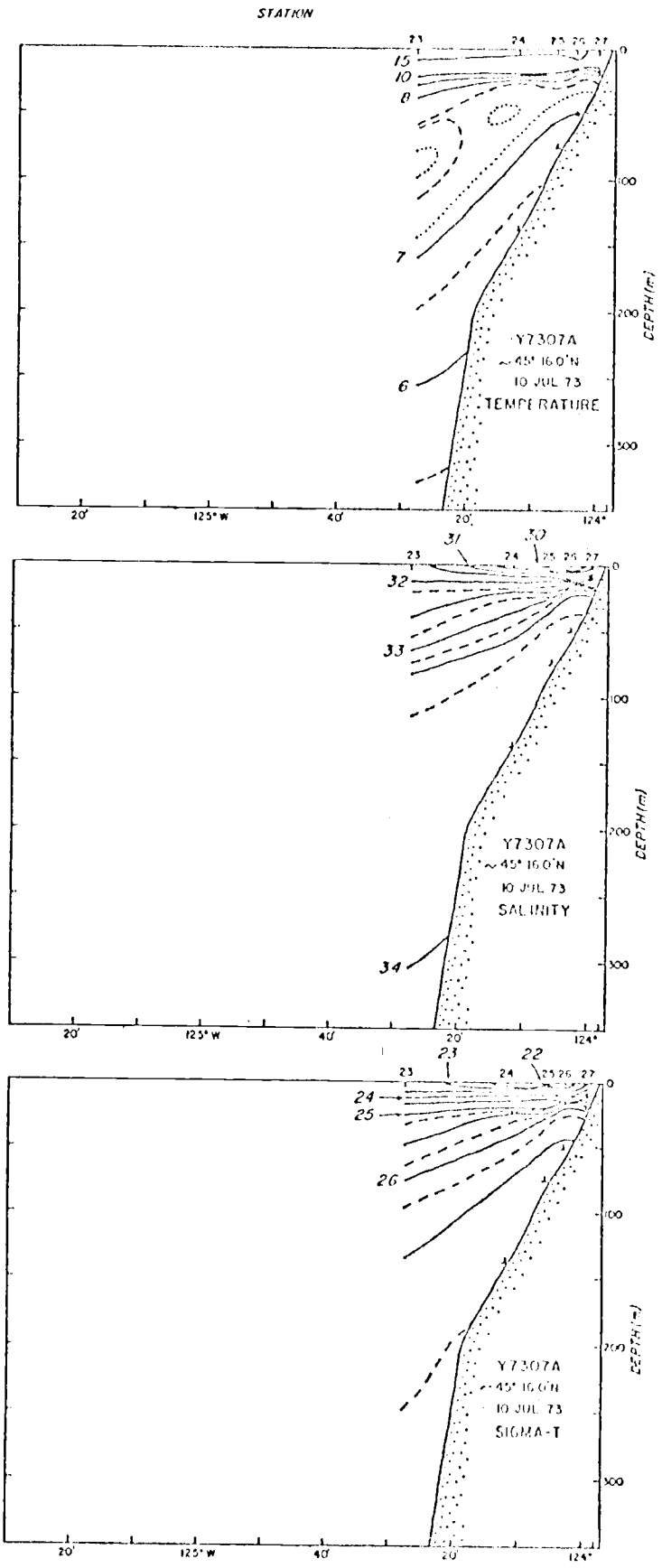
STATION
15
10
8
7
6
Y7307A
~45° 16.0'N
10 JUL 73
TEMPERATURE
DEPTH (m)
0
100
200
300
20'
125° W
40'
20'
124°
31
30
32
33
34
SALINITY
23
22
24
25
26
SIGMA-T

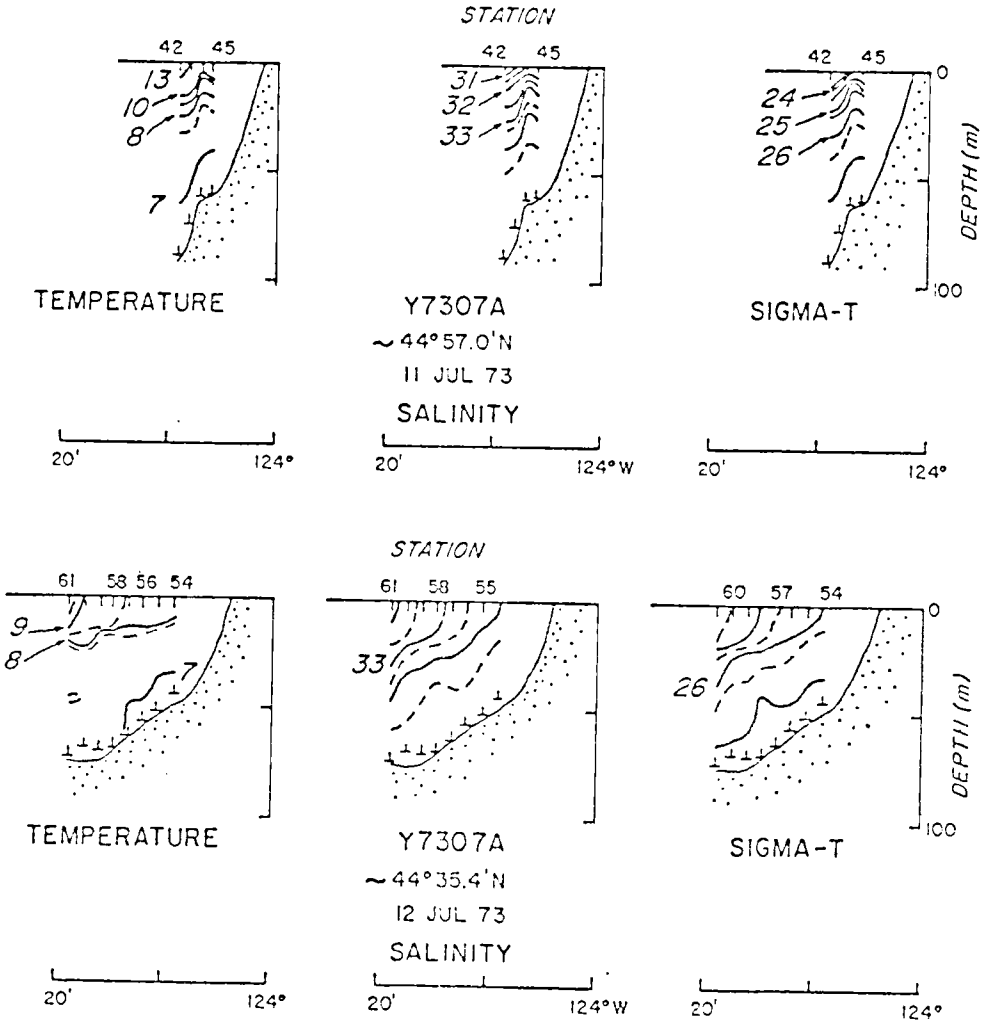
STATION
42 45
13
10
8
7
TEMPERATURE
20'
124°
42 45
31
32
33
Y7307A
~44°57.0'N
11 JUL 73
SALINITY
20'
124°W
42 45
0
24
25
26
DEPTH (m)
100
SIGMA-T
20'
124°
STATION
61 58 56 54
9
8
7
TEMPERATURE
20'
124°
61 58 55
33
Y7307A
~44°35.4'N
12 JUL 73
SALINITY
20'
124°W
60 57 54
0
26
DEPTH (m)
100
SIGMA-T
20'
124°

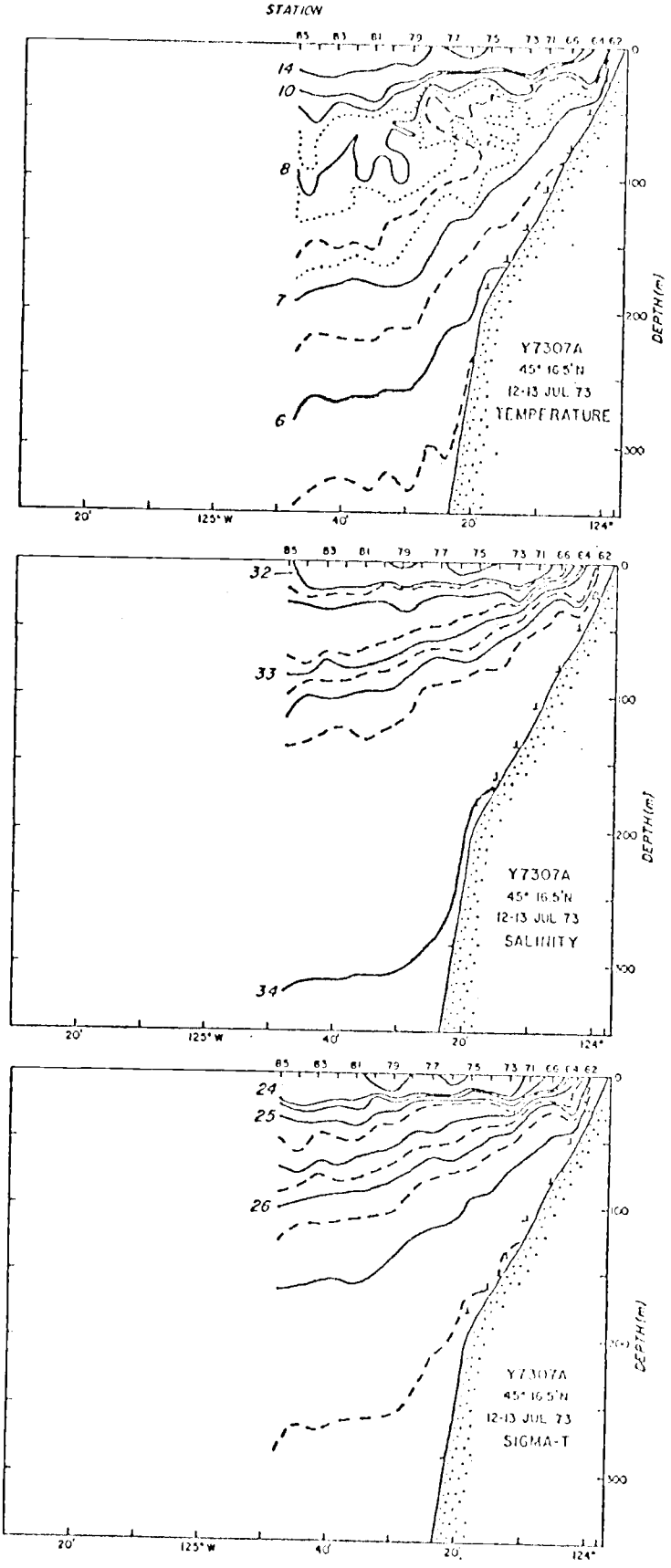
STATION
85 83 81 79 77 75 73 71 66 64 62
14
10
8
7
6
Y7307A
45° 16.5'N
12-13 JUL 73
TEMPERATURE
DEPTH(m)
0
100
200
500
20'
125° W
40'
20'
124°
32
33
34
SALINITY
24
25
26
SIGMA-T

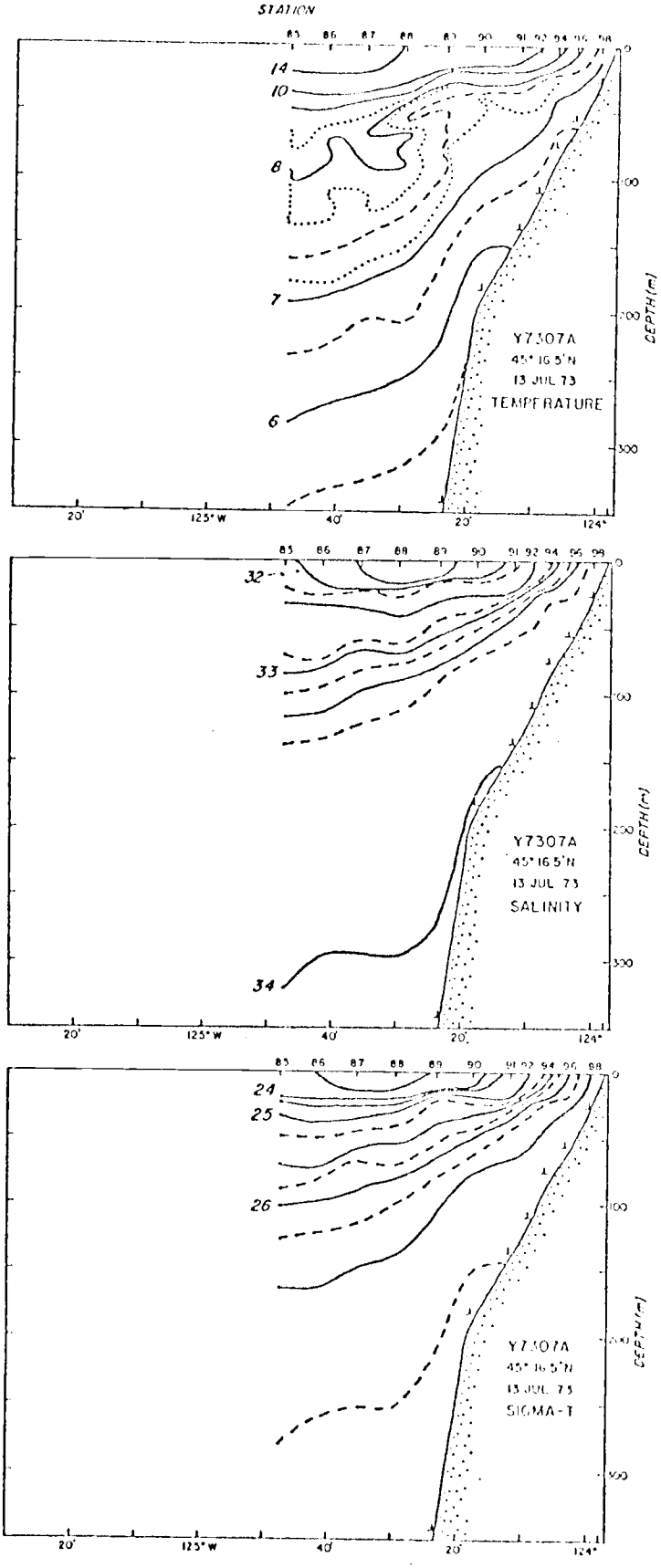
STATION
83 86 87 88 89 90 91 92 94 96 98
14
10
8
7
6
Y7307A
45° 16.5'N
13 JUL 73
TEMPERATURE
DEPTH (m)
0
100
200
300
20'
125° W
40'
20'
124°
83 86 87 88 89 90 91 92 94 96 98
32
33
34
Y7307A
45° 16.5'N
13 JUL 73
SALINITY
DEPTH (m)
0
100
200
300
20'
125° W
40'
20'
124°
83 86 87 88 89 90 91 92 94 96 98
24
25
26
Y7307A
45° 16.5'N
13 JUL 73
SIGMA-T
DEPTH (m)
0
100
200
300
20'
125° W
40'
20'
124°

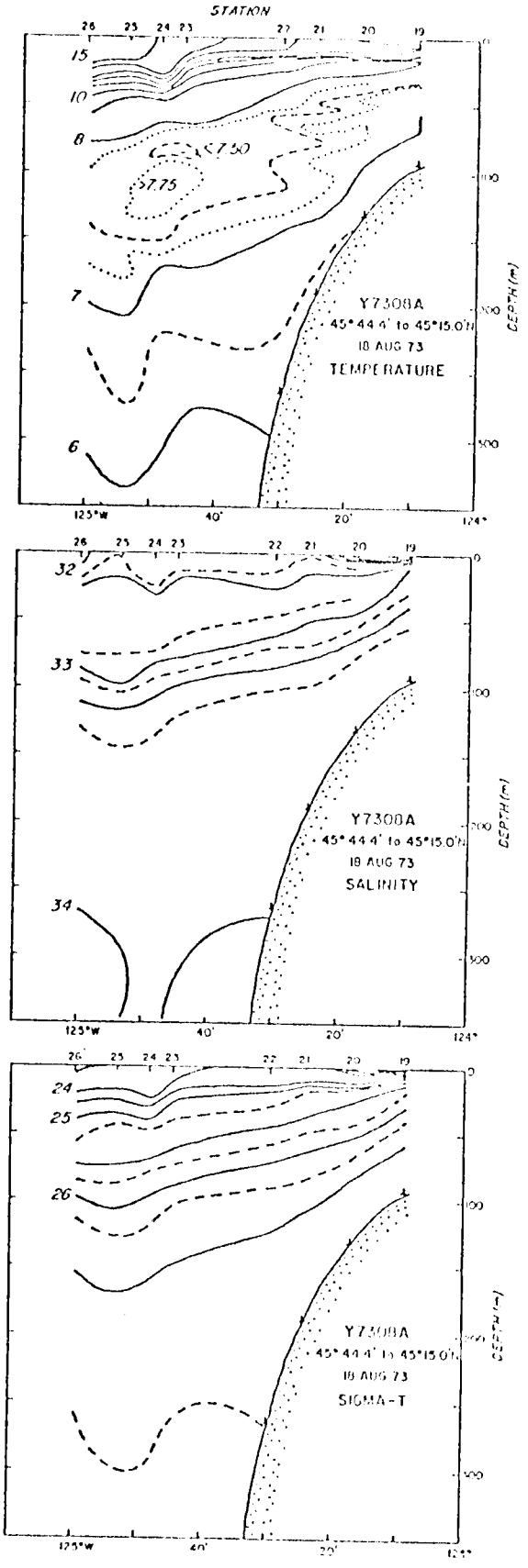
STATION
26 25 24 23 22 21 20 19
15
10
8
<7.50
7.75
7
6
Y7308A
45°44.4' to 45°15.0'N
18 AUG 73
TEMPERATURE
DEPTH (m)
125°W
40'
20'
124°
32
33
34
SALINITY
24
25
26
SIGMA-T

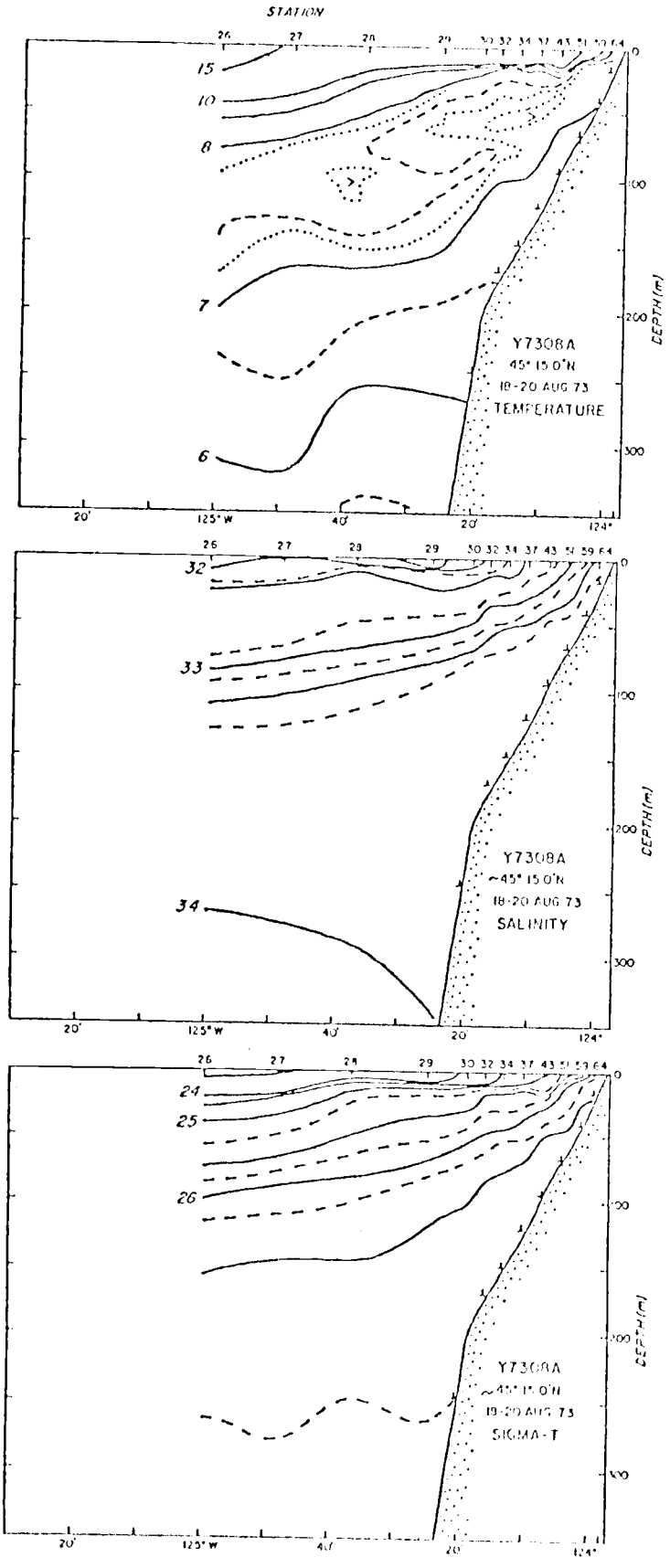
STATION
26 27 28 29 30 32 34 37 43 51 59 64
15
10
8
7
6
Y7308A
45° 15.0'N
18-20 AUG 73
TEMPERATURE
DEPTH(m)
0
100
200
300
20'
125° W
40'
20'
124°
32
33
34
SALINITY
24
25
26
SIGMA-T

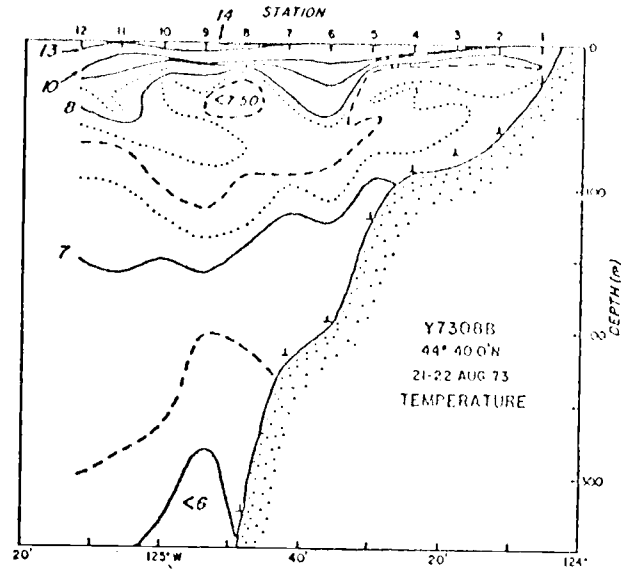
STATION
14
13
10
8
7
<6
<7.50
Y7308B
44° 40.0'N
21-22 AUG 73
TEMPERATURE
DEPTH (m)
125° W

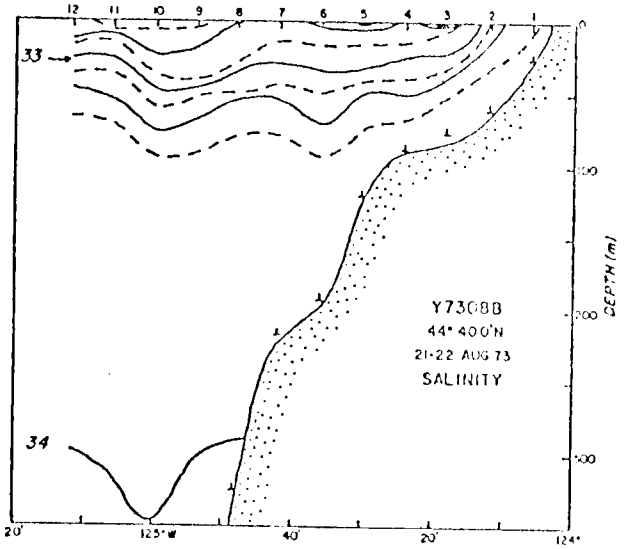
33
34
Y7308B
44° 40.0'N
21-22 AUG 73
SALINITY
DEPTH (m)
125° W

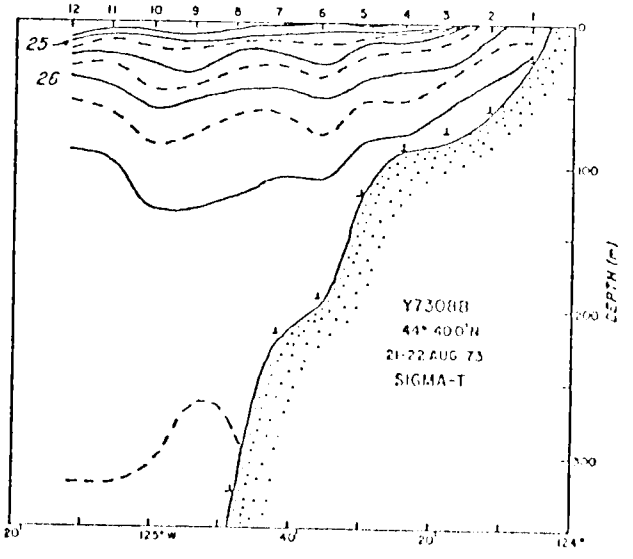
25
26
Y7308B
44° 40.0'N
21-22 AUG 73
SIGMA-T
DEPTH (m)
125° W

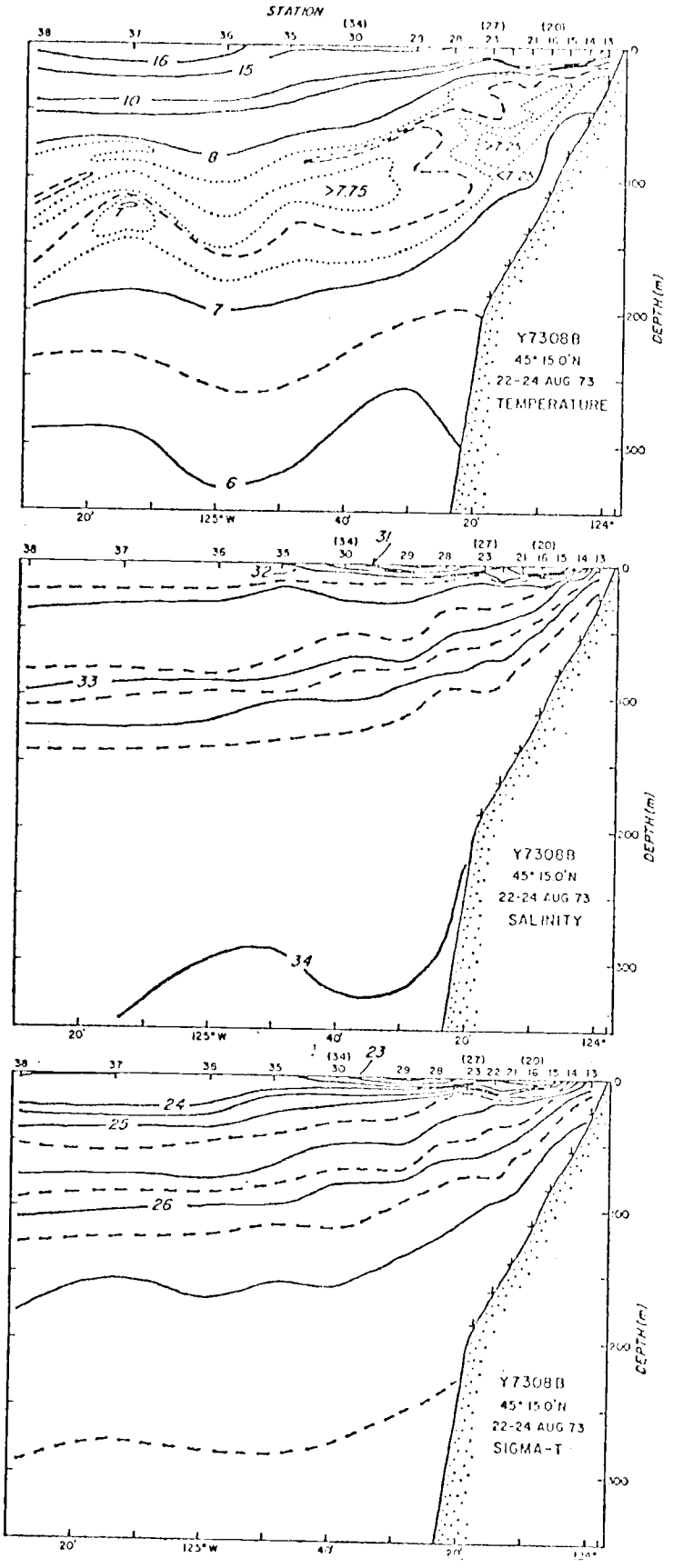
STATION
38 37 36 35 (34) 30 29 28 (27) 23 (20)
16
15
10
8
>7.75
7
6
Y7308B
45° 15.0'N
22-24 AUG 73
TEMPERATURE
DEPTH (m)
0
100
200
500
20'
125° W
40'
20'
124°
31
32
33
34
SALINITY
23
24
25
26
SIGMA-T